İ.BARAN

OPTIMIZATION OF VIBRATION CHARACTERISTICS OF A RADAR ANTENNA STRUCTURE

İSMET BARAN

FEBRUARY 2011

METU 2011

OPTIMIZATION OF VIBRATION CHARACTERISTICS OF A RADAR ANTENNA STRUCTURE

A THESIS SUBMITTED TO
THE GRADUATE SCHOOL OF NATURAL AND APPLIED SCIENCES
OF
MIDDLE EAST TECHNICAL UNIVERSITY

BY

İSMET BARAN

IN PARTIAL FULFILLMENT OF THE REQUIREMENTS
FOR
THE DEGREE OF MASTER OF SCIENCE
IN
MECHANICAL ENGINEERING

FEBRUARY 2011

Approval of the thesis:

OPTIMIZATION OF VIBRATION CHARACTERISTICS OF A RADAR ANTENNA STRUCTURE

Submitted by **İSMET BARAN** in partial fulfillment of the requirements for the degree of **Master of Science in Mechanical Engineering Department, Middle East Technical University** by,

Prof. Dr. Canan Özgen _____
Dean, Graduate School of **Natural and Applied Sciences**

Prof. Dr. Süha Oral _____
Head of Department, **Mechanical Engineering**

Asst. Prof. Dr. Gökhan O. Özgen _____
Supervisor, **Mechanical Engineering Dept., METU**

Asst. Prof. Dr. Ender Ciğeroğlu _____
Co-supervisor, **Mechanical Engineering Dept., METU**

Examining Committee Members:

Prof. Dr. Samim Ünlüsoy _____
Mechanical Engineering Dept., METU

Asst. Prof. Dr. Gökhan O. Özgen _____
Mechanical Engineering Dept., METU

Asst. Prof. Dr. Ergin Tönük _____
Mechanical Engineering Dept., METU

Asst. Prof. Dr. Ender Ciğeroğlu _____
Mechanical Engineering Dept., METU

Dr. Ümit Ceyhan _____
TUBITAK, SAGE

Date: 11.02.2011

I hereby declare that all information in this document has been obtained and presented in accordance with academic rules and ethical conduct. I also declare that, as required by these rules and conduct, I have fully cited and referenced all material and results that are not original to this work.

Name, Last Name : İsmet Baran

Signature :

ABSTRACT

OPTIMIZATION OF VIBRATION CHARACTERISTICS OF A RADAR ANTENNA STRUCTURE

Baran, İsmet
M.S. Department of Mechanical Engineering
Supervisor: Asst. Prof. Dr. Gökhan O. Özgen
Co-Supervisor: Asst. Prof. Dr. Ender Ciğeroğlu

February 2011, 145 Pages

Radar antenna structures especially array antennas which are integrated onto structures of aerial vehicles are subject to dynamic structural and aerodynamic loads. Due to occurrences of these dynamic loads there will be certain dynamic deformations which affect the antenna's performance in an adverse manner. The influence of deformations and vibrations are important on array antenna structures, since they cause a change in orientation of elements of the phased array antenna which affects the gain of the antenna negatively.

In this study, vibration characteristics of a particular radar antenna structure are optimized using topology and stiffener design optimization methods such that negative effects of mechanical vibrations on functional performance of radar antenna are minimized. Topology and stiffener design optimization techniques are performed separately by the use of ANSYS Finite Element (FE) software in order to modify the design of the radar antenna structure such that its critical natural frequencies in the range of 0-500 Hz are shifted out of the dominant peak sinusoid frequency range of the air platform. As a result of this, it will be possible to minimize the vibration response of the phased array elements in the frequency

range of 0-500 Hz; hence better antenna performance can be achieved. In addition to this, it will also be possible to minimize the broadband random vibration response of base excitation coming from air platform.

Keywords: Radar Antenna Structure, Vibration, Topology and Design Optimization, Stiffeners, Finite Element Method.

ÖZ

BİR RADAR ANTEN YAPISININ TİTREŞİM ÖZELLİKLERİNİN OPTİMİZASYONU

Baran, İsmet
Yüksek Lisans, Makine Mühendisliği Bölümü
Tez Yöneticisi: Yrd. Doç. Dr. Gökhan O. Özgen
Ortak Tez Yöneticisi: Yrd. Doç. Dr. Ender Ciğeroğlu

Şubat 2011, 145 sayfa

Hava araçlarına entegre edilen radar anten yapılarından özellikle dizi antenler dinamik yapısal ve aerodinamik yüklere maruz kalmaktadır. Bu yüklerin var olmasından ötürü antenin performansını olumsuz yönde etkileyen belirli dinamik yer değiştirmeler mevcuttur. Yer değiştirmeler ve titreşimler faz dizi anten elemanlarının oryantasyonunda değişimlere sebep olduğundan dolayı, ki bu da anten kazancını olumsuz yönde etkilemektedir, yer değiştirmelerin ve titreşimlerin dizi anten yapıları üzerindeki etkisi oldukça önemlidir.

Bu çalışmada belirli bir radar anten yapısının titreşim karakteristiği topolojik optimizasyon ve destek elemanı tasarım optimizasyonu teknikleri kullanılarak optimize edilmiştir şöyle ki mekanik titreşimlerin radar anteninin fonksiyonel performansına olan olumsuz etkileri minimize edilmiştir. Radar anten yapısının tasarımını değiştirmek için şöyle ki antenin 0-500 Hz aralığındaki kritik doğal frekansları hava platformunun yarattığı baskın harmonic frekans aralığı dışına ötelenecek şekilde topolojik optimizasyon ve destek elemanı tasarım optimizasyonu teknikleri ANSYS Sonlu Eleman (SE) yazılımı kullanılarak ayrı ayrı uygulanmaktadır. Bunun sonucunda, 0-500 Hz frekans aralığındaki faz dizi

elemanların titreşim cevabının minimize edilebilmesi mümkün olacaktır; böylece daha iyi anten performansı elde edilebilir. Buna ek olarak, hava platformundan gelen tabandan uyarma geniş bant rastgele titreşim cevabının da minimize edilmesi mümkün olacaktır.

Anahtar Kelimeler: Radar Anten Yapısı, Titreşim, Topoloji ve Tasarım Optimizasyonu, Destek Elemanı, Sonlu Eleman Yöntemi.

To My Family…

ACKNOWLEDGEMENTS

I would like to gratefully thank my supervisor Asst. Prof. Dr. Gökhan O. ÖZGEN and my co-supervisor Asst. Prof. Dr. Ender CİĞEROĞLU for their continuous support and perfect guidance from beginning to end of this thesis.

Asst. Prof. Dr. Gökhan O. ÖZGEN and Asst. Prof. Dr. Ender CİĞEROĞLU opened my mind for dynamic and vibration analysis and structural optimization of the radar antenna system.

I am also grateful for the support of 2nd Main Maintenance Center Command (Kayseri) and Department of Mechanical Engineering, METU.

I also would like to thank to TUBITAK for their support during this thesis.

I would like to specially thank my fiancee Didem DUYGULU for her never ending encouragement.

Finally I would like to thank to my mother for her vulnerable support and endless patience since the beginning of primary school till the end of master study.

TABLE OF CONTENTS

ABSTRACT iv

ÖZ vi

ACKNOWLEDGEMENTS ix

TABLE OF CONTENTS x

LIST OF TABLES xiv

LIST OF FIGURES xvi

LIST OF SYMBOLS AND ABBREVIATIONS xxi

CHAPTER

1. INTRODUCTION 1

2. LITERATURE SURVEY 3

2.1 RADAR ANTENNA STRUCTURES 3

2.1.1 Basic Operating Principles of Radar Antenna 4

2.1.2 Effects of Structural Vibrations on Antennas 9

2.1.3 Compensation of Structural Vibrations of Radar Antennas 14

2.2 HELICOPTER VIBRATION 16

2.2.1 Characterization of Helicopter Vibration 16

2.2.2 Vibration Exposure Levels 17

2.2.3 AH-64 (Late) Apache Helicopter 20

2.2.4 Design Criteria 23

2.3 OPTIMIZATION 24

2.3.1 Mathematical Formulation 24

2.3.2 Classification of Optimization 26

2.3.3 Topology Optimization 27

2.4 OPTIMIZATION METHODS PROVIDED BY ANSYS 29

2.4.1 Topology Optimization 29

2.4.2 Design (Parameter) Optimization 30

2.4.2.1 Sub Problem Approximation Method 30

2.4.2.2 First Order Method 31

2.5 THE USE OF STIFFENERS FOR STIFFENED PLATES 33

2.5.1 Vibration of Plates 33

2.5.2 Selection of Stiffeners 37

2.5.3 Modeling of Stiffeners 38

2.6 SIMILAR OPTIMIZATION STUDIES IN LITERATURE 39

3. VIBRATION CHARACTERISTICS OF THE RADAR ANTENNA 41

3.1 GEOMETRY OF THE RADAR ANTENNA 41

3.2 BOUNDARY CONDITIONS 45

3.3 FINITE ELEMENT MODEL (FEM) OF THE RADAR ANTENNA 46

3.3.1 Validation of Element Type and Size 46

3.4 MODAL ANALYSIS OF THE RADAR ANTENNA 54

3.5 RANDOM VIBRATION ANALYSIS OF THE RADAR ANTENNA 70

3.6 INTUITIVE DESIGN OF RADAR ANTENNA 74

4. OPTIMIZATION STUDIES 77

4.1 SELECTION OF DESIGN SPACE 77

4.2 CASE-1: TOPOLOGY OPTIMIZATION 80

4.2.1 Topology Optimization Parameters 80

4.2.2 Topology Optimization Results 82

4.2.3 Parameter Optimization on the Reinforcement Plates Designed Using Topology Optimization Results 95

4.2.4 Random Vibration Analysis of the Optimum Antenna Design 107

4.3 CASE-2: STIFFENER OPTIMIZATION 109

4.3.1 Stiffener Optimization Parameters 109

4.3.2 Stiffener Optimization Results 117

4.3.3 Random Vibration Analysis of the Optimum Antenna Design 123

4.4 CASE-3: TOPOLOGY AND STIFFENER OPTIMIZATION 124

4.4.1 Optimization Parameters 124

4.4.2 Optimization Results 125

4.4.3 Random Vibration Analysis of the Optimum Antenna Design 131

5. DISCUSSION AND CONCLUSIONS 132

5.1 OVERVIEW OF RESULTS 132

5.2 CONCLUSION 140

5.3 RECOMMENDATIONS FOR FUTURE STUDIES 140

REFERENCES 141

LIST OF TABLES

TABLES

Table 2.1 Helicopter vibration exposure [16]..... 19
Table 2.2 AH-64 (Late) main rotor source frequencies. 22
Table 3.1 Element comparison table. 48
Table 3.2 Model comparison table. 53
Table 3.3 Natural frequencies of original radar antenna structure. 54
Table 3.4 Calculated $\boldsymbol{k}$ values of the radar antenna structure(factor $\boldsymbol{k}$). 69
Table 3.5 Random vibration analysis results for original radar antenna structure (deformation in y-direction) 72
Table 3.6 Natural frequencies and corresponding $\boldsymbol{k}$ values of intuitively reinforced radar antenna structure. 76
Table 3.7 Random vibration analysis results for intuitively reinforced radar antenna structure (deformation in y-direction). 76
Table 4.1 Natural frequencies of radar antenna structure for different reinforced configurations and the corresponding weight of the radar antenna structures (CASE-1). (Hz)..... 91
Table 4.2 Calculated $\boldsymbol{k}$ Values of Different Configuration of the Radar Antenna Structures (CASE-1). 93
Table 4.3 Parameter (design) optimization results. 97
Table 4.4 Natural frequencies and $\boldsymbol{k}$ values of reinforced radar antenna structure after parameter (design) optimization is performed..... 97
Table 4.5 Random vibration analysis results for reinforced radar antenna structure (deformation in y-direction) 107
Table 4.6 Design variables for different radar antenna configuration and the corresponding weight of the antenna. 118
Table 4.7 Natural frequencies of stiffened radar antenna structure for different stiffener configurations (CASE-2). (Hz)..... 120

Table 4.8 Calculated $\boldsymbol{k}$ values of different stiffener configuration of the stiffened radar antenna structures. (CASE-2) 121
Table 4.9 Random vibration analysis results for stiffened radar antenna Structure ("DR2_C") (deformation in y-direction). 123
Table 4.10 Design variables for reinforced radar antenna configurations and the corresponding weight of the antennas. 126
Table 4.11 Natural frequencies of reinforced radar antenna structure for different stiffener configurations (CASE-3). (Hz) 128
Table 4.12 Calculated $\boldsymbol{k}$ values of different stiffener configuration of the reinforced radar antenna structures. (CASE-3) 129
Table 4.13 Random vibration analysis results for stiffened radar antenna structure ("Topo_Stiff_T") (deformation in y-direction). 131
Table 5.1 Natural frequencies of optimum configurations of radar antenna structures. (Hz) 136
Table 5.2 Calculated $\boldsymbol{k}$ values for optimum configurations of radar antenna structure. 138
Table 5.3 Random vibration results of optimum configurations in y-direction. 138

LIST OF FIGURES

FIGURES

Figure 2.1 The operating principle of a primary radar antenna structure. 5
Figure 2.2 The plot of antenna radiation pattern (electric field) having 5 elements (radiators) [1]. 7
Figure 2.3 Total electric field of the antenna pattern having five elements (radiator) [1]. 7
Figure 2.4 Antenna pattern in a polar-coordinate graph [1]. 8
Figure 2.5 Example model of a phased array antenna radiation pattern [1]. 10
Figure 2.6 Deformed and undeformed radiation pattern. 11
Figure 2.7 Effects of deformation of the plate where antenna elements are attached. (a) undeformed plate, (b) deformed plate. 12
Figure 2.8 Helicopter vibration [16]. 18
Figure 2.9 Helicopter vibration zones [16]. 18
Figure 2.10 Apache (AH-64) helicopter [45]. 20
Figure 2.11 General dimensions of Apache helicopter (AH-64) [48]. 21
Figure 2.12 AH-64 (Late) helicopter vibration exposure levels for externally integrated materials (not scaled *x*-axis). 23
Figure 2.13 Simply supported rectangular plate. 34
Figure 2.14 Stiffened plate 36
Figure 2.15 Smearing of a stiffened, flat plate 36
Figure 3.1 Isometric view of the radar antenna structure (top/front/right view). 42
Figure 3.2 Isometric view of the radar antenna structure (back/top/right view). 43
Figure 3.3 Isometric (top/front/right) view of the radar antenna structure (fin cover is invisible). 43
Figure 3.4 Isometric (back/bottom/right) view of the radar antenna structure (fin cover and back plate are invisible). 44

Figure 3.5 Isometric (back/bottom/left) view of the radar antenna structure (fin cover and back plate are invisible)..... 44
Figure 3.6 General dimensions of the radar antenna structure (all dimensions are in mm)..... 45
Figure 3.7 Simply supported rectangular plate used in element comparison..... 47
Figure 3.8 CASE1: 1 layer, 0.02m element size, 3D 20-Node SOLID95 element. 49
Figure 3.9 CASE2: 1 layer, 0.005m element size, 3D 20-Node SOLID95 element. 49
Figure 3.10 CASE3: 5 layer, 0.02m element size, 3D 20-Node SOLID95 element. 50
Figure 3.11 CASE4: 5 layer, 0.005m element size, 3D 20-Node SOLID95 element. 50
Figure 3.12 FEM of the radar antenna structure (left/front/top isometric view)..... 51
Figure 3.13 FEM of the radar antenna structure (right/bottom/back isometric view)..... 52
Figure 3.14 FEM of the radar antenna structure (back plate is invisible)..... 52
Figure 3.15 FEM of the radar antenna structure (back plate and fin cover are invisible)..... 53
Figure 3.16 Total displacement of 1st mode shape at 14.7 Hz..... 55
Figure 3.17 Total displacement of 2nd mode shape at 16.2 Hz..... 56
Figure 3.18 Total displacement of 3rd mode shape at 96.5 Hz..... 57
Figure 3.19 Total displacement of 4th mode shape at 148.1 Hz..... 58
Figure 3.20 Total displacement of 5th mode shape at 296.6 Hz..... 59
Figure 3.21 Total displacement of 6th mode shape at 300.4 Hz..... 60
Figure 3.22 Total displacement of 7th mode shape at 320 Hz..... 61
Figure 3.23 Total displacement of 8th mode shape at 322.5 Hz..... 62
Figure 3.24 Total displacement of 9th mode shape at 372.8 Hz..... 63
Figure 3.25 Total displacement of 10th mode shape at 409 Hz..... 64
Figure 3.26 AH-64 vibration exposure levels and natural frequencies of the radar antenna structure..... 66
Figure 3.27 Surfaces those phased array antenna elements are located..... 68
Figure 3.28 Random vibration input (AH-64 helicopter vibration profile) [16]..... 71

Figure 3.29 Directional displacement in *y*- direction for random input in *x*-direction (original radar antenna) 73
Figure 3.30 Directional displacement in *y*- direction for random input in *y*-direction (original radar antenna) 73
Figure 3.31 Directional displacement in *y*- direction for random input in *z*-direction (original radar antenna) 74
Figure 3.32 Intuitively reinforced radar antenna structure 75
Figure 4.1 von Mises mechanical strain (a-b) of the critical modes (1^{st} and 2^{nd} modes) (dimension in m) 79
Figure 4.2 Design spaces (DS1 in left and DS2 in right) that will be used for topology optimization (in blue colors) 81
Figure 4.3 Design spaces (DS3 in left and DS4 in right) that will be used for topology optimization (in blue colors) 82
Figure 4.4 Topology optimization results for volume reduction (30%, 50% and 75% respectively) in design space (DS1) to maximize the first natural frequency. 85
Figure 4.5 Topology optimization results for volume reduction (30%, 50% and 75% respectively) in design space (DS2) to maximize the first natural frequency. 86
Figure 4.6 Topology optimization results for volume reduction (30%, 50% and 75% respectively) in design space (DS3) to maximize the first natural frequency. 87
Figure 4.7 Topology optimization results based on volume reduction (30%, 50% and 75% respectively) in design space (DS4) to maximize the first natural frequency. 88
Figure 4.8 Reinforcement (blue color) according to the topology optimization results for volume reduction (30%, 50% and 75% respectively) in design space (DS1) to maximize the first natural frequency. 89
Figure 4.9 Reinforcement (blue color) according to the topology optimization results for volume reduction (30%, 50% and 75% respectively) in design space (DS2) to maximize the first natural frequency. 89

Figure 4.10 Reinforcement (blue color) according to the topology optimization results for volume reduction (30%, 50% and 75% respectively) in design space (DS3) to maximize the first natural frequency. 89
Figure 4.11 Reinforcement (blue color) according to the topology optimization results based on volume reduction (30% (a), 50% (b) and 75% (c)) in design space (DS4) to maximize the first natural frequency. 90
Figure 4.12 Natural frequencies of different reinforced radar antenna structures (CASE-1). 92
Figure 4.13 $\boldsymbol{k}$ values of mode shapes for different reinforced radar antenna structures (CASE-1). 94
Figure 4.14 Design variables of parameter optimization in ANSYS. 96
Figure 4.15 Final configuration of the radar antenna after design optimization (right/back/bottom isometric view, back plate is invisible). 98
Figure 4.16 Final configuration of the radar antenna after design optimization (left/back/top isometric view, back plate is invisible). 98
Figure 4.17 Total displacement of 1st mode shape at 146.7 Hz. 99
Figure 4.18 Total displacement of 2nd mode shape at 161.5 Hz. 100
Figure 4.19 Total displacement of 3rd mode shape at 172 Hz. 101
Figure 4.20 Total displacement of 4th mode shape at 296.4 Hz. 102
Figure 4.21 Total displacement of 5th mode shape at 322.5 Hz. 103
Figure 4.22 Total displacement of 6th mode shape at 328.1 Hz. 104
Figure 4.23 Total displacement of 7th mode shape at 374 Hz. 105
Figure 4.24 Total displacement of 8th mode shape at 408.3 Hz. 106
Figure 4.25 Directional deformation in *y*- direction for random input in *x* direction (reinforced radar antenna after design optimization). 108
Figure 4.26 Directional deformation in *y*- direction for random input in *y*- direction (reinforced radar antenna after design optimization). 108
Figure 4.27 Directional deformation in *y*- direction for random input in *z* direction (reinforced radar antenna after design optimization). 109
Figure 4.28 Feasible stiffener positioning regions (DS1 in left and DS2 in right) that will be used for stiffener optimization (in blue colors). 110
Figure 4.29 Orientation of stiffeners for DR1. 112
Figure 4.30 Orientation of stiffeners for DR2. 112

Figure 4.31 Configuration of bidirectional stiffened radar antenna structure ("DR1_C" (a) and "DR2_C" (b)) and orientation of closed form "C" Stiffener (c). 113
Figure 4.32 Design variables of closed form "C" type stiffener cross section..... 113
Figure 4.33 Configuration of bidirectional stiffened radar antenna structure ("DR1_T" (a) and "DR2_T" (b)) and orientation of "T" type stiffener (c). 114
Figure 4.34 Design variables of "T" type stiffener cross section. 114
Figure 4.35 Configuration of bidirectional stiffened radar antenna structure ("DR1_Box" (a) and "DR2_Box" (b)) and orientation of "Box" type stiffener (c). 115
Figure 4.36 Design variables of "Box" type stiffener cross section. 115
Figure 4.37 Configuration of bidirectional stiffened radar antenna structure ("DR1_Rect" (a) and "DR2_Rect" (b)) and orientation of "Rectangular" type stiffener (c). 116
Figure 4.38 Design variables of "Rectangular" type stiffener cross section. 116
Figure 4.39 Natural frequencies of different stiffened radar antenna structures (CASE-2). 119
Figure 4.40 $\boldsymbol{k}$ values of mode shapes for different stiffened radar antenna structures (CASE-2). 122
Figure 4.41 Reinforced radar antenna structure according to the topology optimization ("Topo_DS3 %50"). 125
Figure 4.42 Natural frequencies of reinforced radar antenna structures (CASE-3). 127
Figure 4.43 $\boldsymbol{k}$ values of mode shapes for stiffened radar antenna structures (CASE-3). 130
Figure 5.1 Natural frequencies of optimum configurations of radar antenna structure. 137
Figure 5.2 Calculated k values for optimum configurations of radar antenna structures. 139

LIST OF SYMBOLS AND ABBREVIATIONS

FE	: Finite Element
RF	: Radio Frequency
SAR	: Synthetic Aperture Radar
DGS	: Defected Ground Structure
MIL-STD	: Military Standard
F	: Objective function
$\{x\}$	: Design variables
$\{C\}$	: Equality constraints
$\{\Omega\}$	: Inequality constraints
λ_i	: i^{th} eigenfrequency
K	: Stiffness matrix
M	: Mass matrix
Φ_i	: Eigenvector associated with the i^{th} eigenvalue
N_{dof}	: Number of the degree of freedom
v_e	: Volume element of the element which has an element number e
ρ_e	: Pseudo density of the element which has an element number e
V	: Total volume

N	: Total element number
APDL	: ANSYS Parametric Design Language
SUMT	: Sequential Unconstrained Minimization Technique
a	: Length of the plate along x-axis
b	: Length of the plate along y-axis
D	: The flexural rigidity (bending stiffness) of a rectangular plate
E	: Young's modulus
υ	: Poisson's ratio
I	: Area moment of inertia
h	: Thickness of the plate
$\overline{m}$	: Plate mass per unit area
ω_{mn}	: Natural frequencies of simply supported rectangular plate
a_s	: Distance between the stiffeners in the x- direction
b_s	: Distance between the stiffeners in the y-direction
D_x	: The flexural rigidity of stiffened plate in the x-direction
D_y	: The flexural rigidity of stiffened plate in the y-direction
I_x	: Area moment of inertia along x-axis
I_y	: Area moment of inertia along y-axis
h_e	: Equivalent thickness
B	: Effective torsional rigidity

HDD :Hard Disk Drive

FEM : Finite Element Model

BC : Boundary condition

k : The ratio of displacement

y_{max} : Maximum displacement of i^{th} mode shape

y_{min} : Minimum displacement of i^{th} mode shape

d_{tot} : Maximum total displacement of i^{th} mode shape

PSD : Power Spectral Density

W : Random vibration level

Y_{max} : Maximum deformation *y*-direction

Y_{min} : Minimum deformation *y*-direction

DS : Design space

ρ_e : Pseudo density

t_i : Thickness of the reinforcement plates

CAD : Computer Aided Design

DR : Design region

s : Spacing between stiffeners parallel to the *y*-axis

s_1 : Spacing between stiffeners parallel to the and *x*-axis

w1 : Width of stiffener cross section

w2 : Height of stiffener cross section

CHAPTER 1

INTRODUCTION

The common sources of mechanical deformations and vibrations on aerospace structures are dynamic loads and in fact, dynamical load cycles can damage or cause a reduction in the service life of mechanical parts. The presence of static and dynamic loads may also have severe adverse effects on the performance of radar antenna structures installed on air platforms. Hence, deformation and vibration mechanisms of the antenna structure and its elements must be well studied and understood.

The objective of this thesis is to fine tune the dynamic characteristics of a certain radar antenna structure by making vibration and optimization analysis for minimizing the effects of structural vibrations of the antenna on its functional performance. This radar antenna is to be externally integrated to an Apache AH-64 (Late) helicopter platform. In order perform the intended the optimization study, first a finite element model of the radar antenna structure will be constructed. For the finite element model of the radar antenna structure which is mainly composed of plate-like structures, solid elements will be used. The verification of the constructed finite element model is done primarily by comparing modal frequencies of a generic simply supported plate (of similar size as the radar antenna) which is modeled using the same type of finite elements and similar element size with analytical solution of the same plate. After the verification of the finite element model, topology and stiffener parameter optimizations are performed on the same model using optimization capabilities of ANSYS FE software. Base the design of the radar antenna structure to modify such that its critical natural frequencies (which cause higher vibration responses on specific direction and have adverse effects on radar antenna's functional performance) are

tried to be shifted out of the vibration exposure range (0-500 Hz) of AH-64 (Late) helicopter platform. Moreover, in order to obtain better results, stiffener design optimization is performed on reinforced antenna configuration obtained from topology optimization study. As a result of this, advantages of both optimization methods are combined for further minimization of the unwanted vibratory response of the antenna structure.

The organization of this thesis is proceeding with literature survey which is devoted in Chapter 2. Vibration of helicopter platform and its effects on radar antenna structures are mentioned in this chapter. Moreover optimization techniques and the use of stiffeners in structural design of stiffened plates are investigated. Similar optimization studies in literature are also given in this chapter.

Finite element model of a radar antenna structure is obtained in Chapter 3 to understand the dynamic behavior of radar antenna system. For the confirmation of the element size and type, a verification study is performed, where finite element model of a simply supported plate is compared with the analytical solution available in the literature. Then modal and random vibration analyses are carried out for the whole assembly. In addition to that an intuitive design of radar antenna structure is developed in this chapter.

In order to minimize the adverse effects of mechanical vibrations coming from helicopter platform on to the radar antenna, optimization studies are conducted using ANSYS FE software in Chapter 4. Firstly topology optimization is performed to maximize the critical natural frequencies of the radar antenna. Next stiffener design optimization is carried out. Finally stiffener design optimization is performed on optimum topology optimization results in this chapter.

Summary of the results and conclusions are discussed in Chapter 5 with the outcomes of this thesis. Recommendations for future studies are also presented in this chapter.

CHAPTER 2

LITERATURE SURVEY

A detailed literature survey has been made as a part of this study. The aim of this survey was to find out the previous work done on this subject and to clarify the methodology of this study. Firstly, the radar antenna structures are explained including adverse effects of mechanical vibrations coming from air platforms on functional performance of antennas. Next, helicopter vibration, the theory of optimization methods used in this study and the use of stiffeners for stiffened plates are described, respectively. Finally similar optimization research work in the literature is exemplified.

2.1 RADAR ANTENNA STRUCTURES

A radar antenna is a microwave system that radiates or receives energy in the form of electromagnetic waves. Reciprocity which is an important property of radar antennas means that the different characteristics of the antenna are identical during transmitting and receiving an electromagnetic signal. Parabolic reflectors and phased arrays are the two basic constructions of radar antennas.

Generally antennas are divided into two categories, directional and omnidirectional. For a specific antenna position, directional antennas radiate radio frequency (RF) energy in patterns of lobes or beams that extend outward from the antenna in one direction. In contrast that RF energy is radiated by omnidirectional antennas in all directions simultaneously.

Radiation patterns can be plotted on a rectangular- or polar-coordinate graph. These patterns are a measurement of the energy leaving an antenna.

- Energy is equally radiated in all directions for an isotropic radiator.
- Energy is radiated directionally for an anisotropic radiator.
- The main lobe is the bore sight direction of the radiation pattern.
- Side lobes and the back lobe are unwanted areas of the radiation pattern [1].

2.1.1 Basic Operating Principles of Radar Antenna

The basic operating principle of a radar antenna structure is shown in Figure 2.1. Antenna is a device which picks up the reflected microwave signal from the target which is generated by the radar antenna to illuminate the target and the return is defined as the electromagnetic signal picked up by the receiving antenna. It should be noted that an effective transmitter generates the electromagnetic signal and then a highly sensitive receiver is picked up the signal. When the radar antenna radiates electromagnetic energy to targets, the reflected signal which is called scattering from all targets is formed in a wide number of directions. If the reflection is provided in opposite directions to the radiated energy, a “backscatter” is obtained.

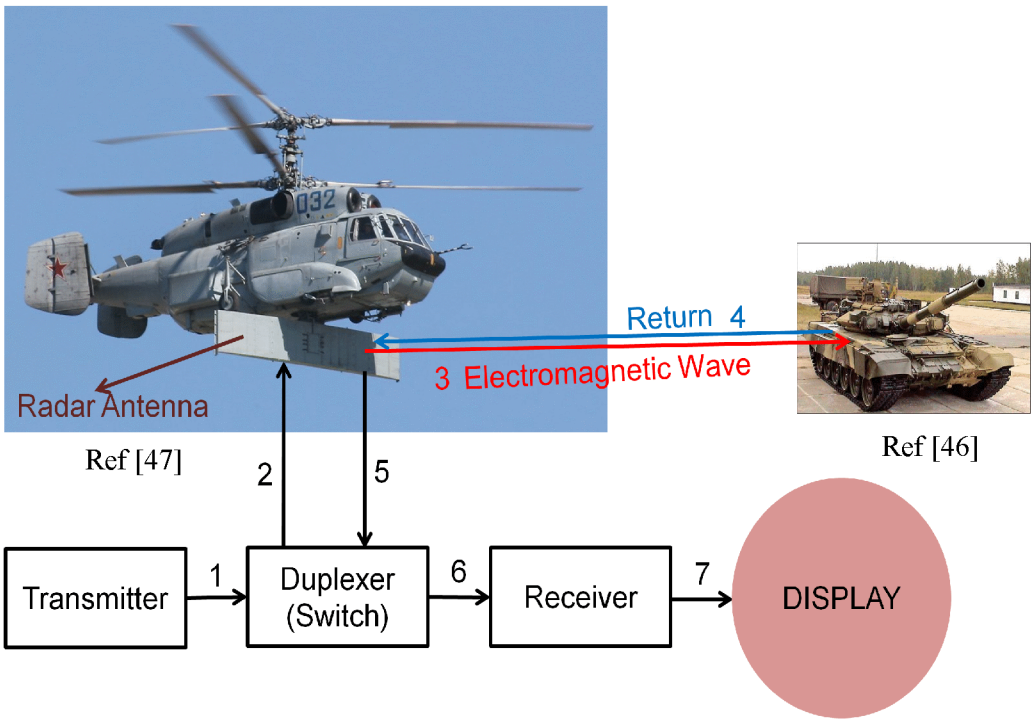

Figure 2.1 The operating principle of a primary radar antenna structure.

Several antenna beam definitions can be described as follows [2];

Transmitter:

Radar transmitter is used to obtain the high power RF signal radiated through the space.

Duplexer:

According to the transmitting or receiving process of the radar antenna, the duplexer alternately switches the antenna for proper condition. This is a required step for radar antenna in order not to make the receiver destroyed due to the high-power pulses of the transmitter.

eceiver:

The receivers is a device used as decoder for amplifying the received RF signals then it generates proper signals for the output.

Radar Antenna:

The radar antenna is used for transferring or receiving the generated energy to electromagnetic signals.

Indicator(Display):

The relative position of targets can be seen and easily understood by an observer as a graphic screen by the use of indicator (display).

Some important characteristics of radar antennas are given as follows:

Antenna Gain:

Antenna gain which is independent for transmitting or receiving processes is a significant characteristic of a given. For highly directional antennas, more electromagnetic energy is radiated in specific directions than in others. The gain can be defined as the ratio between the amount of energy radiated for directional antennas (anisotropic radiation) and the energy that would be radiated if the antenna were not directional (isotropic Radiation). The gain is same for transmitting and receiving operations of antennas [1], [3].

Antenna Pattern:

Generally in specific direction most radiators of antennas radiate large amount of energy which is indicated as anisotropic radiators. Radiation pattern generated in this direction can be traced by the use of standard methods such as marking the positions around a source so that specific pattern can easily be compared with another.

An electric field having a specific radiation pattern is formed by the energy radiated from an antenna. The radiated energy from an antenna can be plotted by the use of radiation pattern and the shape of this pattern depends on the type of antenna utilized. At a constant distance from the antenna, this radiated energy is measured at various angles. The plot of antenna radiation pattern (Electric field) having five elements (radiators) is illustrated in Figure 2.2.

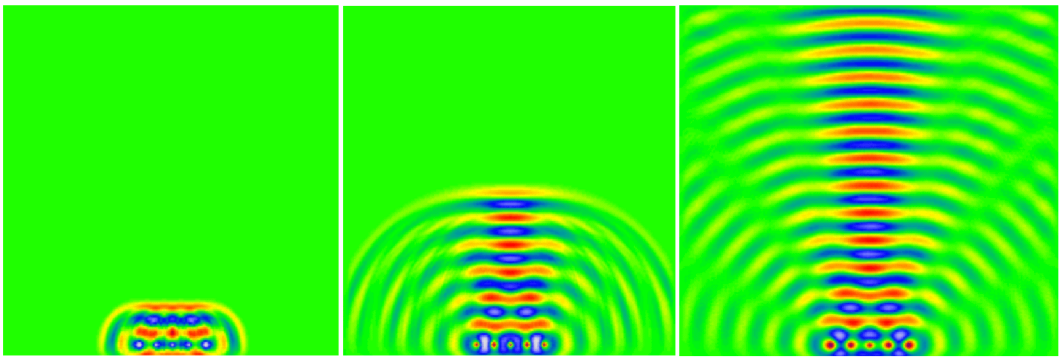

Figure 2.2 The plot of antenna radiation pattern (electric field) having 5 elements (radiators) [1].

In Figure 2.2, distribution of the radiated power (electromagnetic signal) in space is shown. These figures identify where power is being radiated or received (since they are reciprocal) and also they show how much reduction can be expected if the antenna is not aimed properly. The total electric field of this antenna pattern can also be seen in Figure 2.3.

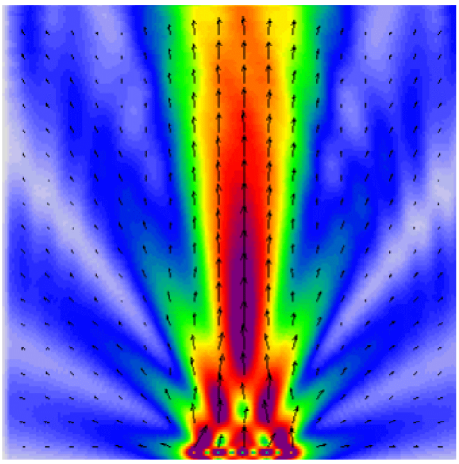

Figure 2.3 Total electric field of the antenna pattern having five elements (radiator) [1].

To plot this pattern, polar coordinate graphs which are preferable for identifying the radiation characteristics of antennas can be used. The polar-coordinate graph of the measured radiation is given in Figure 2.4.

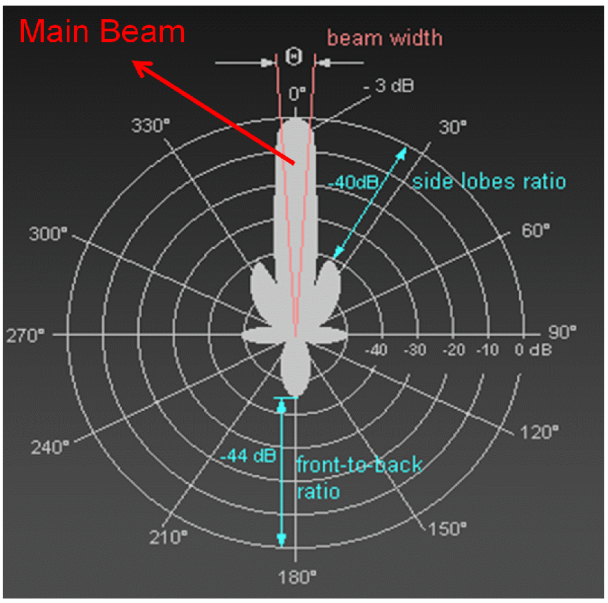

Figure 2.4 Antenna pattern in a polar-coordinate graph [1].

For optimum performance, these antenna plots help radar antennas to obtain a suitable positioning on all the desired signals. It can be observed that, the narrower the beam width, the greater the difficulty in properly aiming the antenna.

It is seen from Figure 2.4 that the main beam (or main lobe) is usually the region within a 3 dB range of the peak of the main beam around the direction in which the maximum radiation energy is obtained [1].

The side lobes are defined as smaller beams that are located away from the main beam directions. It is a fact that the undesired radiation obtained from these side lobes can never be completely eliminated and beside that for characterizing the radiation patterns the side lobe level (or side lobe ratio) is an important parameter used in radar antennas [1].

Beam Width:

Beam width is described as the angular range of the antenna pattern in which at least half of the maximum power is still emitted [4].

Phased Array Antenna:

A phased array antenna can calibrate the phase of electromagnetic signal by using radiating array elements which have phase shifter. In order to guide the patterns and beams of antenna in the desired direction, beams are formed by controlling the phase difference of the signal emitted from each radiating array element [5].

2.1.2 Effects of Structural Vibrations on Antennas

The presence of static and dynamic loads may have severe adverse effects on the performance of radar antenna structures installed on air platforms and other vehicles. Hence deformation and vibration mechanisms of the antenna structure and its elements must be identified. Particularly the cause of vibration and its effects on antenna systems are the topics that must be taken into consideration during the detailed design phase. The deformity of the antenna surface and also patch arrays may;

- Affect the antenna's radiation pattern,
- Cause bore sight errors, beam gain etc.,
- Increase side lobe levels [6].

Mechanical vibrations will cause deformation of the antenna supporting structure. As a consequence, the positions and orientations of the elements of the phased

array antenna change. The relative phases of the respective signals feeding the antennas will vary; hence, the antenna radiation pattern is affected: the main beam direction can change and the beam width and/or side lobe levels can increase. This can be imagined as a hemisphere which can be used to clarify the effects of changes in orientations of the antenna elements in Figure 2.5. A headlight is placed in the center of the hemisphere and illuminates the inner surface of the hemisphere. The observer (Number 1) located at the center of the hemisphere always sees the equal spot size (as a projection) in central line of sight with beam width $\boldsymbol{\theta}$. On the other hand another observer (Number 2) located at the margin of the hemisphere looks sloping on the illuminated area of the hemisphere. Therefore if the 2nd observer wants to see the equal spot size as the 1st observer sees, a larger area must be lit on the margin of the hemisphere from center. In this case beam width increases i.e. $\boldsymbol{\theta}' > \boldsymbol{\theta}$.

From this point of view it can be concluded that the headlight can be focused in central beam direction better and its “beam width” is lower and its “antenna gain” is better than at a large angle of the irradiation.

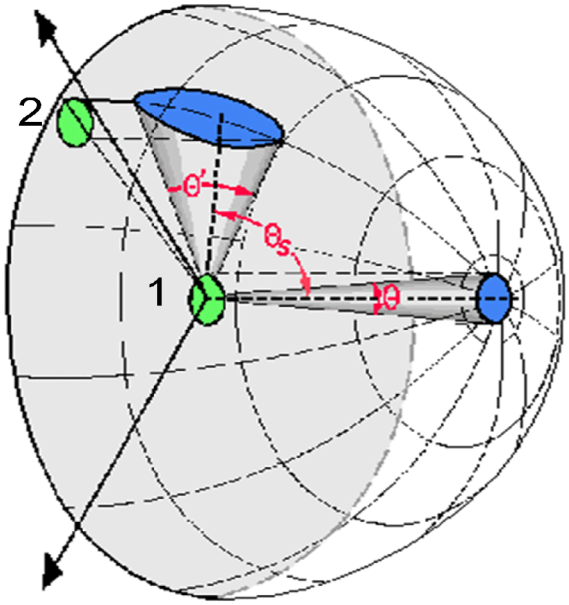

Figure 2.5 Example model of a phased array antenna radiation pattern [1].

Moreover the negative effect of changed position of the elements of the antenna due to structural vibrations can also be clarified in Figure 2.6.

In Figure 2.6, an antenna radiation pattern is considered. The original undeformed radiation pattern of the antenna is shown in blue color. Desired radiation pattern is occurred and main beam of this radiation covers the target i.e. the plane. Here the negative effects of side lobes are negligible. However under dynamic loads, deformations or when the structural vibration exposure level is high, the position of the main beam of the antenna pattern is deformed so that original antenna elements location is changed. Therefore the desired radiation pattern is also varied, which is shown in red colors in Figure 2.6.

It can be seen in Figure 2.7 that the plate where antenna elements are attached is deformed in normal direction (y-direction) and at the same time position of the antenna elements is changed automatically. Hence the main beam radiation becomes less important and the contribution of unwanted side lobes to the desired radiation pattern is increased. In addition the gain of the antenna is expected to decrease. As a consequence less effective power is transmitted or received by the antenna elements and there may be scan blindness such that the plane (Figure 2.6) or tank (Figure 2.7) may not be caught by the antenna.

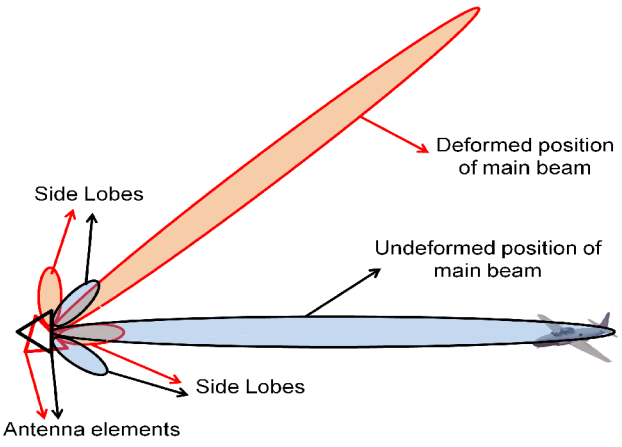

Figure 2.6 Deformed and undeformed radiation pattern.

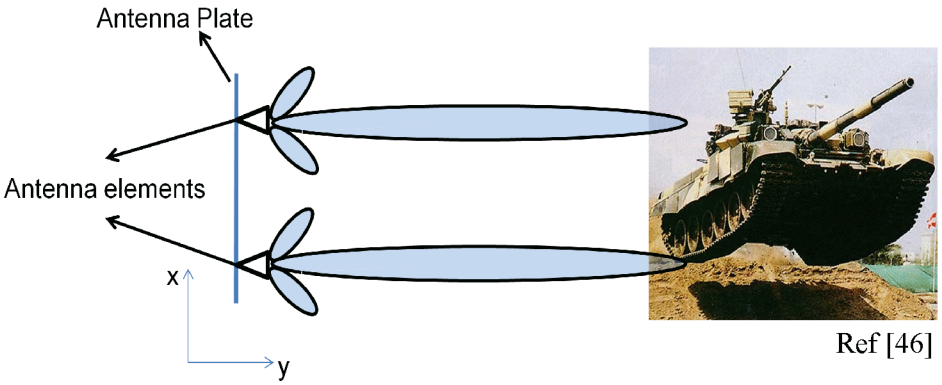

a)

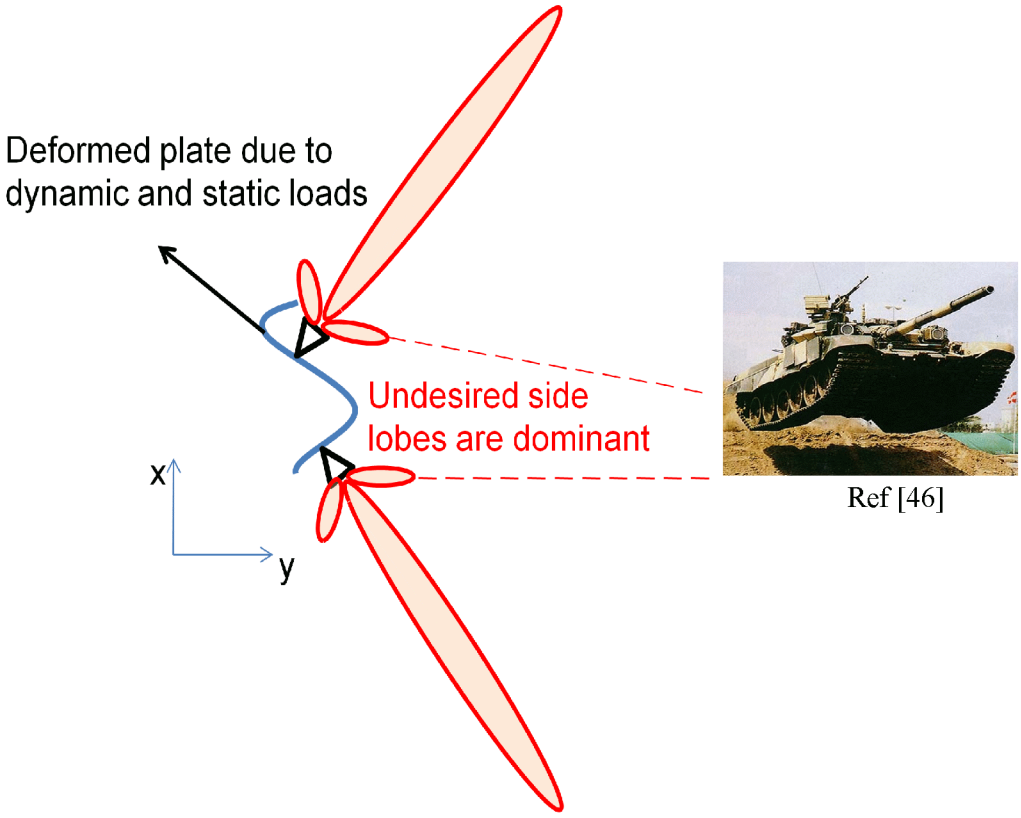

b)

Figure 2.7 Effects of deformation of the plate where antenna elements are attached. (a) undeformed plate, (b) deformed plate.

For investigating the effect of vibrations on the performance of a generic array radar antenna, a vibrating plate is considered as a typical test case in NATO Research Task Group. In this test setup eight embedded patch elements are mounted on array antenna in receiver mode. The effects of vibrations on this system are investigated for a radar aperture antenna and a generic interferometer array antenna [7]. It was observed that the direction of the main beam of the radar antenna becomes non stationary which is an undesirable situation considering the performance of the antenna.

In Ref. [8], the results of computer simulations of vibration effects on antenna elements were summarized for discussing the problem of maintaining a high-performance phased array radar antenna. Deformation of antenna structure and failure of antenna elements due to mechanical vibrations were also emphasized in order to discuss the performance assessment of the radar antenna.

The effects of vibration and rotation on millimeter wave synthetic aperture radar (SAR) are shown in Ref. [9] theoretically and simulated by real data. It was explained that mechanical vibrations and rotations of radar targets cause phase changes in received radar signal.

The importance of calibrating the position errors of an antenna element due to aperture vibrations were emphasized in Ref. [10]. The estimated position information of eight element array was substituted into beam forming process relative to the reference sources to compensate the deformed pattern of the antenna array due to vibration.

Array antenna, which is commonly a group of antenna elements, is used to obtain high directivity, low side lobes, particular radiation pattern characteristics. The most important stage for the design of an array antenna is the selection of elements and array geometry, and then the determination of the element excitations required for achieving a particular performance comes [11].

In phased array antennas the structural vibrations may lead to scan blindness of the antenna, where no effective power is transmitted or received by the array elements [12]. Due to the deformation of the structure of the antenna, mutual coupling

occurs between the elements of array system which leads to scan blindness. In this case, the characteristics of the pattern of the antenna are changed and the array cannot transmit energy in desired directions [13]. Scan blindness must be considered in phased array design because it limits the scan range of the antenna and lowers the efficiency of antenna [14]. In addition to this an un-optimized design of an array antenna may lead to scan blindness. According to Ref [15], it is efficient to use defected ground structure (DGS) on a linear microstrip scanning array antenna to remove the blindness angle.

2.1.3 Compensation of Structural Vibrations of Radar Antennas

In literature there are different tools for modeling and design of radar antenna structures against unwanted vibrations in order to maintain proper working conditions. One of them is the passive compensation of static deformations and vibrations based on the estimation of the position of the antenna (patch) elements which is used for generating the radar signal. Besides, there are numerical analyses of antenna array geometries with deformations and results of which are related to the antenna parameters such as beam width, side lobe level, pointing error etc.

Different structural vibration modes at different natural frequencies may occur depending on the mechanical properties of the radar antenna structure and actual loads acting on the antenna. Moreover, the vibration amplitude of the antenna surface also depends on local and global mode shapes of the radar antenna structure.

Negative effects of structural vibrations and deformations on antenna surface and patch elements may be prevented by [7];

- Structural modifications such as reinforcement,
- Active or passive damping control,
- Active shape control of global or local deformation,
- Signal processing methods.

A simple and straightforward way to prevent adverse effects of structural vibrations on antenna elements is shifting the critical natural frequencies and mode shapes, which affect the performance of the radar antenna negatively, out of the frequency range in which vibration levels due to transmitted vibrations of platform (radar antenna structure is integrated) to the antenna are effective.

For instance, the vibration exposure of the radar antenna structure which is integrated to a helicopter platform becomes effective in the frequency range of 0-500 Hz according to Military Standard 810G (MIL-STD-810G) [16]. Especially sinusoidal peaks produced by rotating components of the helicopter platform dominate the vibrations coming from helicopter. Details of estimating vibration levels of different helicopter platform are defined in military standards (MIL-STD-810G). Vibrations which are out of the frequency range 0-500 Hz have a lower displacement level and also these vibrations can be successfully filtered by vibration isolation systems generally used in integration of the radar system to the helicopter platform.

If natural frequencies and mode shapes of the radar antenna structure are kept out of the frequency range where dominant sinusoids occur, performance drop of the antenna due to transmitted vibrations can be reduced since frequency response of structure decreases as the excitation frequency gets away from the natural frequencies. To achieve such a condition, the design of the radar antenna structure can be modified by the use of optimization techniques such as topology optimization or stiffener reinforcement.

In order to increase the stiffness to weight ratio of the radar antenna system, especially for the plate on which antenna elements are installed, stiffeners can be used. This improves the stiffness of the radar antenna structure and also the natural frequencies of the antenna can be increased.

In this thesis, design of a phased array radar antenna structure is modified by using stiffener reinforcement and topology optimization techniques.

2.2 HELICOPTER VIBRATION

2.2.1 Characterization of Helicopter Vibration

In the military standard MIL-STD-810G [16], helicopter vibration is characterized by dominant peaks superimposed on a broadband background, as stated in Figure 2.8. The major rotating components (main rotor, tail rotor, engine, gearboxes, shafting, etc.) produce the peaks which are sinusoids. These peaks occur at the rotational speed (frequency) of each component and corresponding harmonics of these speeds. On the other hand the broadband background also includes random vibrations which are caused by sources such as aerodynamic flow or potential worst case environments.

According to the different types of helicopter, vibration levels and spectrum shapes vary widely and they depend on strength and position of materials and also the geometry and stiffness of the structure.

To identify the design criteria the broadband background is expressed as random vibration. However, in real life conditions it is not easy to define and specify the random vibration or lower sinusoidal components.

On the other hand the dominant sinusoids are generated by rotating components of the helicopter such as;

- primarily the main rotor(s),
- tail rotor,
- engine(s),
- drive shafts,
- and gear meshing [16].

The normal operating speeds of these components are generally constant, varying less than five percent.

2.2.2 Vibration Exposure levels

The vibration exposure levels for components integrated to helicopters should be derived from field measurements. However, when measured data are not available, levels can be derived from Table 2.1, Figure 2.8 and Figure 2.9. These levels are specified considering the worst case environment conditions and have been aggressively compressed in time [16].

In order to determine the vibration exposure levels, helicopter is divided into zones as shown in Figure 2.9. To calculate the values of A1, A2, A3, and A4 (Figure 2.8) the related source frequencies of helicopter components should be used for all component locations shown in Figure 2.9. For instance, for a component located in the horizontal projection of the tail rotor disc, the source frequencies of the tail rotor must be used and for a component located on or in close to drive train components such as gearboxes and drive shafts, the source frequencies of that drive train component (i.e., gear mesh frequencies, shaft rotational speeds) must be used for calculating the values of A1, A2, A3, and A4 [16]. For regions other than these locations indicated above, the source frequencies of the main rotor must be used. Fundamental main and tail rotor source frequencies of several helicopters are given in Table 2.1, from which convenient values can be selected.

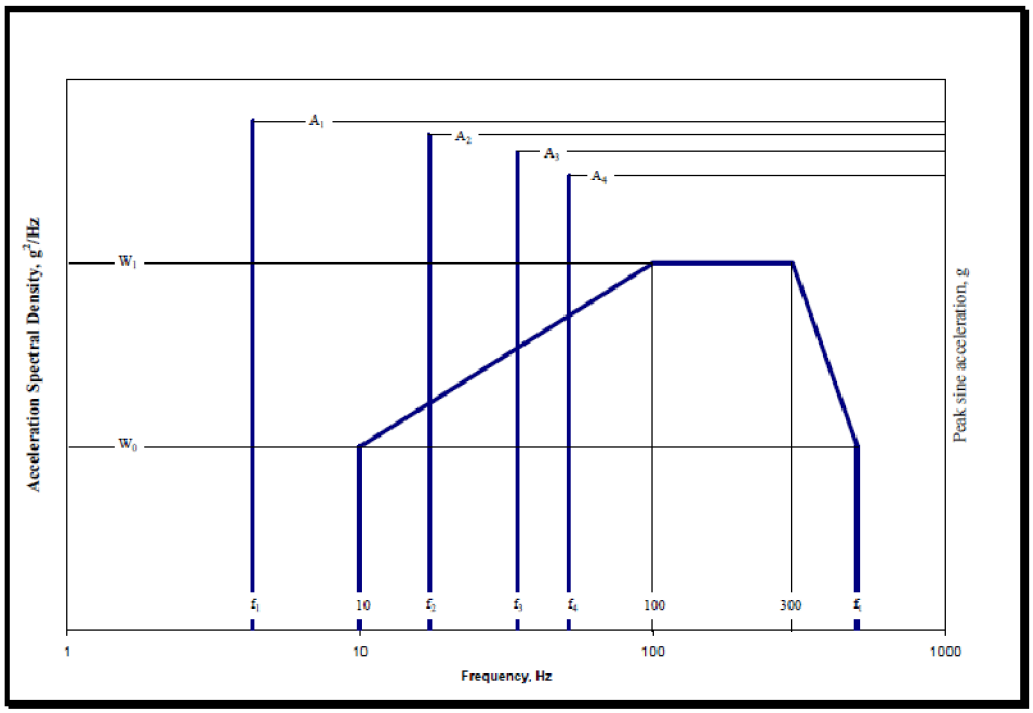

Figure 2.8 Helicopter vibration [16].

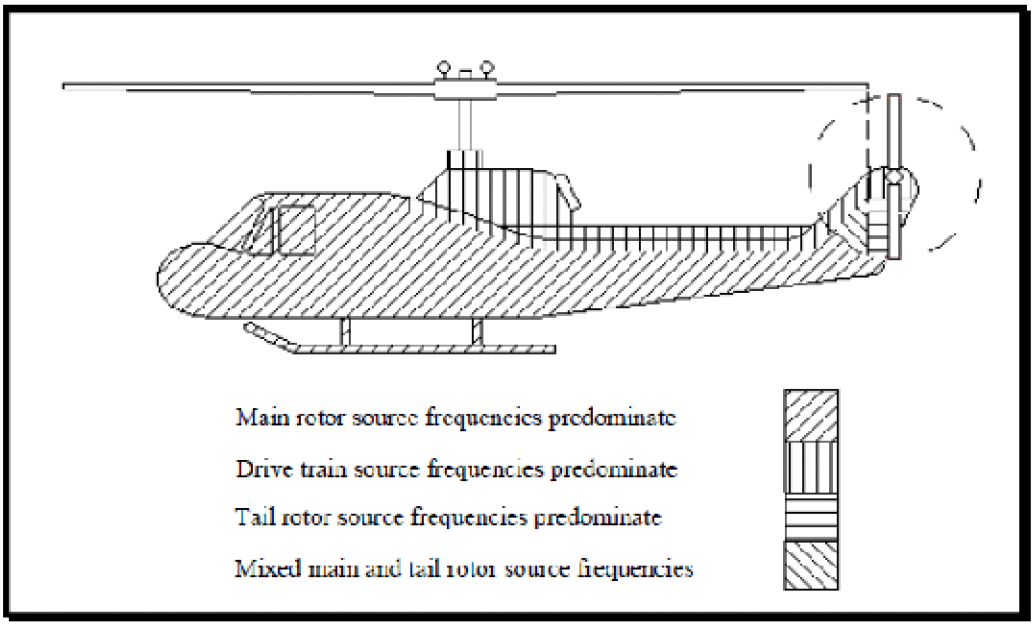

Figure 2.9 Helicopter vibration zones [16].

Table 2.1 Helicopter vibration exposure [16]

MATERIEL	RANDOM LEVELS	SOURCE FREQUENCY (f_x) RANGE (Hz)	PEAK ACCELERATION (A_x) at f_x (GRAVITY UNITS (g))
General	$W_0 = 0.0010\ g^2/Hz$ $W_1 = 0.010\ g^2/Hz$ $f_t = 500$ Hz	3 to 10 10 to 25 25 to 40 40 to 50 50 to 500	$0.70/(10.70 - f_x)$ $0.10 \times f_x$ 2.50 $6.50 - 0.10 \times f_x$ 1.50
Instrument Panel	$W_0 = 0.0010\ g^2/Hz$ $W_1 = 0.010\ g^2/Hz$ $f_t = 500$ Hz	3 to ≤ 10 >10 to 25 25 to 40 40 to 50 50 to 500	$0.70/(10.70 - f_x)$ $0.070 \times f_x$ 1.750 $4.550 - 0.070 \times f_x$ 1. 050
External Stores	$W_0 = 0.0020\ g^2/Hz$ $W_1 = 0.020\ g^2/Hz$ $f_t = 500$ Hz	3 to ≤ 10 >10 to 25 25 to 40 40 to 50 50 to 500	$0.70/(10.70 - f_x)$ $0.150 \times f_x$ 3.750 $9.750 - 0.150 \times f_x$ 2.250
On/Near Drive System Elements	$W_0 = 0.0020\ g^2/Hz$ $W_1 = 0.020\ g^2/Hz$ $f_t = 2000$ Hz	5 to ≤ 50 > 50 to 2000	$0.10 \times f_x$ $5.0 + 0.010 \times f_x$

Main or Tail Rotor Frequencies (Hz) Determine 1P and 1T from the Specific Helicopter or from the table (below).			**Drive Train Component Rotation** Frequency (Hz) Determine 1S from Specific Helicopter and Component.	
$f_1 = 1P$	$f_1 = 1T$	fundamental	$f_1 = 1S$	fundamental
$f_2 = n \times 1P$	$f_2 = m \times 1T$	blade passage	$f_2 = 2 \times 1S$	1st harmonic
$f_3 = 2 \times n \times 1P$	$f_3 = 2 \times m \times 1T$	1st harmonic	$f_3 = 3 \times 1S$	2nd harmonic
$f_4 = 3 \times n \times 1P$	$f_4 = 3 \times m \times 1T$	2nd harmonic	$f_4 = 4 \times 1S$	3rd harmonic

Helicopter	MAIN ROTOR		TAIL ROTOR	
	Rotation Speed 1P (Hz)	Number of Blades n	Rotation Speed 1T (Hz)	Number of Blades m
AH-1	5.40	2	27.7	2
AH-6J	7.95	5	47.3	2
AH-6M	7.92	6	44.4	4
AH-64 (early)	4.82	4	23.4	4
AH-64 (late)	4.86	4	23.6	4
CH-47D	3.75	3	2 main rotors and no tail rotor	
MH-6H	7.80	5	47.5	2
OH-6A	8.10	4	51.8	2
OH-58ÅC	5.90	2	43.8	2
OH-58D	6.60	4	39.7	2
UH-1	5.40	2	27.7	2
UH-60	4.30	4	19.8	4

2.2.3 AH-64 (Late) Apache Helicopter

In this study, in order to perform the optimization methods Apache (AH-64) helicopter is selected. This helicopter has a four-blade main rotor and a four-blade tail rotor that is shown in Figure 2.10 and Figure 2.11. The crew sits in tandem, with the pilot sitting behind and above the copilot/gunner.

Figure 2.10 Apache (AH-64) helicopter [45].

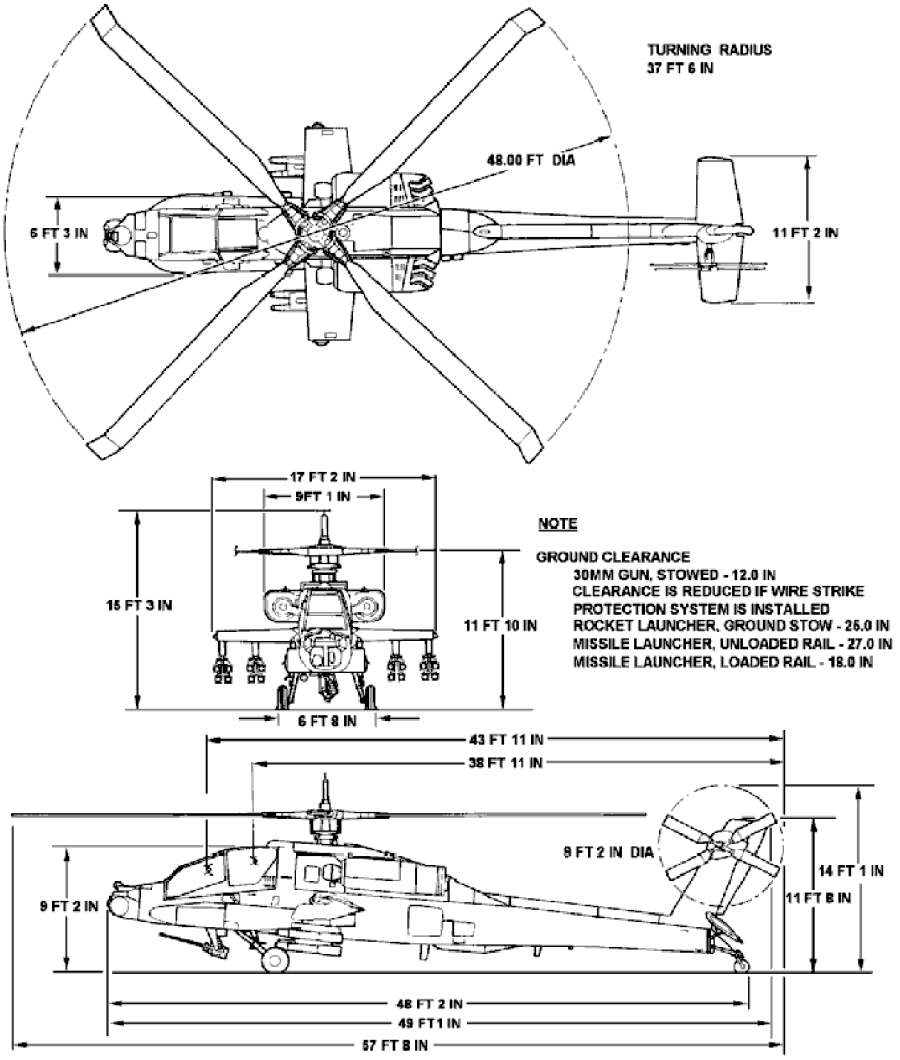

Figure 2.11 General dimensions of Apache helicopter (AH-64) [48].

Specified radar antenna structure is integrated to the AH-64 (Late) helicopter externally and its location is in the range (zone) that main rotor source frequencies are dominant.

AH-64 (Late) helicopter vibration exposure frequencies and corresponding levels for externally integrated components are evaluated according to the Figure 2.8, Table 2.1 and Figure 2.9 and shown in Figure 2.12. The dominant sinusoids which are present due to main rotor occur at frequencies f_1, f_2, f_3 and f_4 and these are illustrated as red lines in Figure 2.12 and also they are given in Table 2.2. On the other hand, levels of random vibrations which are due to aerodynamic flow and loads are also illustrated as blue colors in Figure 2.12.

The broadband vibration exposure level is between 0-500 Hz. The amplitudes and frequencies of broadband harmonic and random vibrations are determined from Table 2.1 for AH-64 (Late) helicopter.

Table 2.2 AH-64 (Late) main rotor source frequencies.

Rotation Speed 1P		4.86 Hz
Number of Blades (n)		4
Fundamental	f_1	4.86 Hz
Blade Passage	f_2	19.44 Hz
1st Harmonic	f_3	38.88 Hz
2nd Harmonic	f_4	58.32 Hz

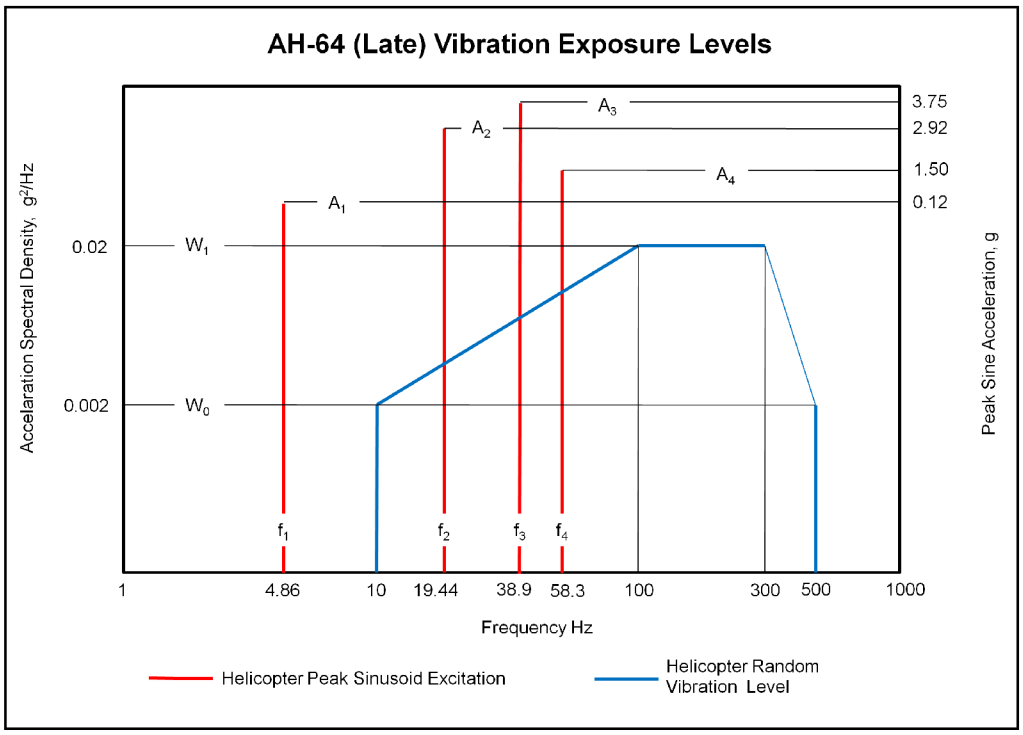

Figure 2.12 AH-64 (Late) helicopter vibration exposure levels for externally integrated materials (not scaled *x*-axis).

2.2.4 Design Criteria

An obvious requirement for helicopter component design is to avoid a match or near match between natural frequencies of components (integrated to the helicopter externally) and the dominant sinusoids of the helicopter based excitations. At least 5% of a minimum clearance between operating frequency of air platform and resonant frequency of components installed to platform is recommended in the military standard MIL-STD-810G [16]. It should be noted that the source frequencies and corresponding amplitudes of helicopters are varied for specific type and model of helicopters. In addition to that the random vibration response of the radar antenna due to base excitation coming from the helicopter platform should be minimized.

Stiffness of the base plate where antenna elements are attached is an important parameter in order radar antenna to have a suitable functional performance. Therefore stiffeners can be suitable for this action because they are efficient for enhancing the stiffness of the radar antenna with a very small increase in mass

2.3 OPTIMIZATION

Achieving maximum structural performance in the design of a certain mechanical system has always been an important problem. With the aid of computer programs, simulations of many various designs can be performed to reach an optimum solution without actually building them. In engineering applications this can be done by adjusting the parameters to optimize the performance of initial designs. Structural optimization can be defined as finding values of the variables that optimize the objective function.

Recently, optimization techniques which are being used in a wide spectrum of industries have reached to an important level in engineering applications.

2.3.1. Mathematical Formulation

From a mathematical point of view, optimization can be defined as the process of finding the conditions that give the maximum or minimum value of a function. For optimizing a system as opposed to a function, first objective or objectives must be identified. The measure of the performance of a system or a design is determined as an objective which is known as the objective function that. This is the criterion which provides an optimized design when expressed as a function of the design variables.

The objective function depends on certain parameters of the system which are called design variables. The goal of the optimization process is to find values of the design variables that optimize the objective. In addition to the objective function, there may also be additional functional requirements and restrictions that

must be satisfied to produce an acceptable design. These are called design constraints. Generally design variables are restricted, or constrained.

The general mathematical form of an optimization problem can be shown as follows:

Minimize or Maximize

$$F = F(x_1, x_2, x_3 \ldots\ldots x_n) \tag{2.1}$$

Subjected

$$\begin{aligned} C_1 &= C_1(x_1, x_2, x_3 \ldots\ldots x_n) = 0, \\ C_2 &= C_2(x_1, x_2, x_3 \ldots\ldots x_n) = 0, \\ &\vdots \\ C_n &= C_n(x_1, x_2, x_3 \ldots\ldots x_n) = 0, \end{aligned}$$

and

$$\begin{aligned} \Omega_1 &= \Omega_1(x_1, x_2, x_3 \ldots\ldots x_n) \geq 0, \\ \Omega_2 &= \Omega_2(x_1, x_2, x_3 \ldots\ldots x_n) \geq 0, \\ &\vdots \\ \Omega_n &= \Omega_n(x_1, x_2, x_3 \ldots\ldots x_n) \geq 0, \end{aligned}$$

where

$\boldsymbol{F}$ is the objective function, $\boldsymbol{x_1, x_2, x_3 \ldots\ldots x_n}$ are the design variables, $\boldsymbol{C_1, C_2, C_3 \ldots\ldots C_n}$ are equality constraints and $\boldsymbol{\Omega_1, \Omega_2, \Omega_3 \ldots\ldots \Omega_n}$ are inequality constraints.

The selection of the type of optimization algorithm or search method depends on user and the problem itself.

2.3.2 Classification of Optimization

Optimization problems can be classified with respect to different aspects of the application. Generally classification of optimization problems is analyzed in three groups [17]:

1. *Constrained vs. Unconstrained*: Constrained optimization problems have some defined constraints which have to be satisfied while optimizing the objective. When there is no condition to be satisfied in the defined problem, the problem can be defined as an unconstrained optimization problem. This type of optimization is sometimes obtained as reconstruction of constrained optimization problems, in which the constraints are replaced by penalization terms added or barrier functions imported to objective function that have the effect of eliminating constraint violations.

2. *Stochastic vs. Deterministic:* In some optimization problems, the model cannot be fully specified due to unknown functional parameters at the time of formulation of the design problem. In order to obtain a solution that reaches the assumed criteria of goal (objective), *Stochastic optimization* algorithms use these unknown quantifications. On the contrary, in *deterministic optimization* problems the parameters defined in the model are completely known.

3. *Single Objective vs. Multi Objective:* Multi objective optimization problems have more than one objective function that multiple objective functions are optimized simultaneously.

2.3.3 Topology Optimization

Topology optimization is used to find an initial structural configuration that meets a predefined criterion. This type of optimization sometimes gives a design that can be completely new and innovative. Structural optimization tools and computer simulations have gained the paramount importance in industrial applications as a result of innovative designs, reduced weight and cost effective products. Especially, in aircraft platforms and automobile industries, topology optimization has become an integral part of the product design process.

Nowadays material distribution methods are typically based on mathematical programming together with finite element models for analysis. This indicates that there is a similarity between material distribution methods and methods developed for sizing optimization, but complexity arises related to the special form of the design parameterization for topology. Moreover special attention should be taken for topology optimization with a large-scale setting when formulating the design problems to be solved [19].

In order to achieve a predefined set of performance goals within a given design space and under determined set of loads and boundary conditions, material layout is optimized with a mathematical approach. Hence, engineers are utilizing topology optimization to find the best concept design that meets the design requirements. Finite element methods are used for modeling and performing the topology optimization applications.

At conceptual design stage of a system or process, topology optimization is used to give an initial idea for prescribed design that is then calibrated for performance and the point of view of manufacturability. As a consequence of this the costly design revisions and iterations that are time consuming can be reduced. Therefore design performance is improved while the design progression time and overall cost of design processes are decreased. Topology optimization problem can be defined as through the following:

Design space: Permissible volume used in optimization process within which the design can exist is defined as design space. While specifying this space, it certain

variables are needed to be considered such as conditions of packing and assembly, human and tool accessibility etc. On the other hand, parts or materials in the defined model which cannot be changed during the optimization process is specified as non-design regions.

Design constraints: Design constraints are the design variables or restrictions that cannot be broken. If the design constraints are violated, an infeasible design will be obtained.

Objective function: This is defined as the aim of the optimization study which can generally be specified as minimization or maximization of performance criteria.

Mathematical formulation of topology optimization is in the following form in element matrices and this can also be used for vibration approach [20]:

$$F = \max or\ min(\lambda_i) \tag{2.2}$$

Subjected to

$$\left(K - \lambda_i M\right)\Phi_i = 0, i = 1,2,\ldots\ldots,N_{dof} \tag{2.3}$$

$$\sum_{e=1}^{N} v_e \rho_e \le V, 0 < \rho_e < 1, e = 1,2,\ldots\ldots,N \tag{2.4}$$

Where, $\boldsymbol{F}$ is the objective function which is the maximization of ith eigenfrequency (ith natural frequency), $\boldsymbol{\lambda_i}$ is the ith eigenfrequency, $\boldsymbol{K}$ is the stiffness matrix of the system, $\boldsymbol{M}$ is the mass matrix of the system, $\boldsymbol{\Phi_i}$ is the mass normalized eigenvector associated with the ith eigenvalue, $\boldsymbol{N_{dof}}$ is the number of the degree of freedom of the system, $\boldsymbol{v_e}$ is the volume element of the element which has an element number $\boldsymbol{e}$, $\boldsymbol{\rho_e}$ is the pseudo density of the element which has an element number $\boldsymbol{e}$, $\boldsymbol{V}$ is the total volume of the system and $\boldsymbol{N}$ is the total element number.

The derivative of Equation 2.3 with respect to the pseudo density $\boldsymbol{\rho_e}$ is

$$[\frac{\partial K}{\partial \rho_e} - \lambda_i \frac{\partial M}{\partial \rho_e} - \frac{\partial \lambda_i}{\partial \rho_e} M]\Phi_i = 0 \tag{2.5}$$

The sensitivities of a single modal eigenvalue can be found as multiplying Equation 2.5 by the transpose of mass normalized eigenvector, $\boldsymbol{\Phi_i}$:

$$\frac{\partial \lambda_i}{\partial \rho_e} = \Phi_i^T [\frac{\partial K}{\partial \rho_e} - \lambda_i \frac{\partial M}{\partial \rho_e}]\Phi_i \tag{2.6}$$

The *pseudodensity* for each element varies from 0 to 1 where

- $\rho_e \sim 0$ represents material to be removed;
- $\rho_e \sim 1$ represents material that should be kept after topology optimization is done [21]

2.4 OPTIMIZATION METHODS PROVIDED BY ANSYS

In ANSYS, optimization types are mainly divided into two groups. Design (parameter) optimization is the first one which works entirely with the ANSYS Parametric Design Language (APDL) and is contained within its own module. Design optimization is entirely controlled by user therefore it is possible to fine tune the APDL functions or parameters by the use of regular optimization methods in ANSYS. The second optimization type is the topology optimization which is a form of shape optimization that is sometimes known as layout optimization is the literature.

2.4.1 Topology Optimization

The aim of topology optimization is to find the best use of material for a system such that an objective criterion which is the maximization of minimization of a

global stiffness or natural frequency value subjected to previously defined constraints (i.e., volume reduction in design space) is satisfied. Topology optimization module of ANSYS includes preprocessing (/PREP), solution (/SOLUTION), and post processing (/POST1) structures and the use of APDL is not required. Independent design variables which are defined explicitly and used in design (parameter) optimization tool of ANSYS are not required for topology optimization. However in topology optimization the material distribution function is utilized as design variable (parameter) within a design space.

In order to perform a topology optimization in ANSYS, definition of the problem including material properties, finite element model, boundary conditions etc., an objective function and design constraints denoted as state variables in ANSYS must be specified considering the predefined performance criteria.

2.4.2 Design (Parameter) Optimization

Design optimization module works as an integral part of the ANSYS software to reach to an optimal design (best design) and the use of APDL is a necessary stage in the optimization process. Some of the optimum design examples are minimum weight or maximum frequency; in heat transfer, the minimum temperature; or in magnetic motor design, the maximum peak torque. However, this is not sufficient to achieve the goal so predefined design constraints such that volume, deformation, maximum stress etc. must also be taken into account.

In design optimization three types of variables are needed to characterize the design process: design variables, design constraints (state variables), and the objective function. In ANSYS APDL, these variables are defined explicitly in the form of scalar parameters. There are two methods provided by design optimization tool in ANSYS. The first one is the "Sub-problem Approximation Method" and the other one is the "First Order Method".

2.4.2.1 Sub Problem Approximation Method

Sub-problem approximation method is defined as an advanced, zero order technique. For this type of optimization the derivatives of dependent variables which are objective function and design constraints are not required, only the values of them are used. The frame of this method is constituted by two important topics:

- the use of approximations for the objective function and constraints,
- the conversion of the constrained optimization problem to an unconstrained problem by using penalty functions [18,22].

The first step of this technique is constructing the approximate values of the dependent variables (objective function and constrained variables). This is performed by ANSYS automatically according to the choice of the user. Typical approximation forms for dependent variables are the linear fit, quadratic fit and quadratic plus cross terms. By default in ANSYS quadratic plus cross terms is used for objective function and the quadratic fit is used for constrained variables [23].

If the design constraints are defined by explicit functions in specific simple forms, are explicit functions of the variables and have certain simple forms, the independent parameters (variables) may be transformed into a form such that automatically the design constraints are fulfilled. Therefore an unconstrained optimization problem may be obtained from converting constrained one by performing modification on parameters. For numerical solutions penalty function techniques are used to transform the formulation of constrained optimization problems into an alternative one such that constrained optimization problem becomes an unconstrained one. In order to achieve the objective function each iterations performing in design optimization tool of ANSYS uses Sequential Unconstrained Minimization Technique (SUMT) that every minimization process is applied on the approximated penalized function called the sub-problem until the convergence of the optimization is succeeded or termination is obtained.

Because the sub-problem approximation method is based on approximation of the dependent variables, a certain design data set must be prepared. Therefore this method generates design set as random. The advantages of this method are that it is a generalized approach and it reaches to a minimum fast.

2.4.2.2 First Order Method

Unlike sub-problem approximation method, the derivatives of the dependent variables (objective function and constrained variables) are used for first order method. There are two important concepts related with this method:

- The use of derivatives of the dependent variables,
- The transformation of the constrained optimization problem to an unconstrained one by using penalty functions,
- The use of decent search technique.

The first step is the transformation of the constrained problem into an unconstrained one by applying proper penalty functions on design variables, constrained variables and objective function [18]. Then the derivatives of objective function and constrained variable penalty function are formed. This is performed according to the search direction in design space (design variables). In this procedure various steepest decent and conjugate direction searches are performed for each iteration step until the convergence is reached. The step size of these searches and the forward difference applied to design variables can be specified by using the module provided by ANSYS but typically the default values for these two inputs are sufficient.

The most important point here is that each of these iterations are composed of sub-iterations which include individual search direction and derivative calculations meaning in the first order method, several analyses loops are performed in each parameter optimization iterations. Therefore, it takes longer than sub-problem approximation problem method and it is usually seen to be computationally more demanding. The advantage of this method is the accuracy of the optimization and

it solves the actual finite element representations (not an approximation) within the given tolerance.

Sometimes it is possible for this method to reach an infeasible solution. In that case the result is probably the local minimum due to derivative terms. In this case it is generally useful to perform a sub-problem approximation method to compare the results with the first order method [23].

2.5 THE USE OF STIFFENERS FOR STIFFENED PLATES

The buckling and vibration characteristics of stiffened plates are of considerable importance to mechanical and structural engineers and also the use of stiffeners improves the static and dynamic characteristics of the base structure.

Stiffeners improve the load carrying capacity of structures and the benefit of stiffening lies in achieving lightweight and robust design of structures. For this purpose, they have wide use in structural engineering domain. Especially, stiffened plates are used in critical and sensitive structures such as in aircrafts, ship hulls and box girders in which safety and a perfect design is crucial.

2.5.1 Vibration of Plates

In literature, many researchers have paid much attention to the dynamic behavior of stiffened shells and plates [25-32].

A coarse but fast method to model dynamics of stiffened plates is to smear the stiffeners to the base plate. The theory of free flexural vibration of rectangular plates and smeared stiffened plates with an effective tensional rigidity has been summarized by Szilard [24].

In mathematical physics it is considered that the undamped free flexural vibrations of rectangular plates are basically considered as boundary value problems. The plate seen in Figure 2.13 is simply supported from all its edges i.e. only the

displacement in z-direction is fixed ($z=0$) along all edges. The length of the plate is $\boldsymbol{a}$ along the x-axis and $\boldsymbol{b}$ along the y-axis as shown in Figure 2.13.

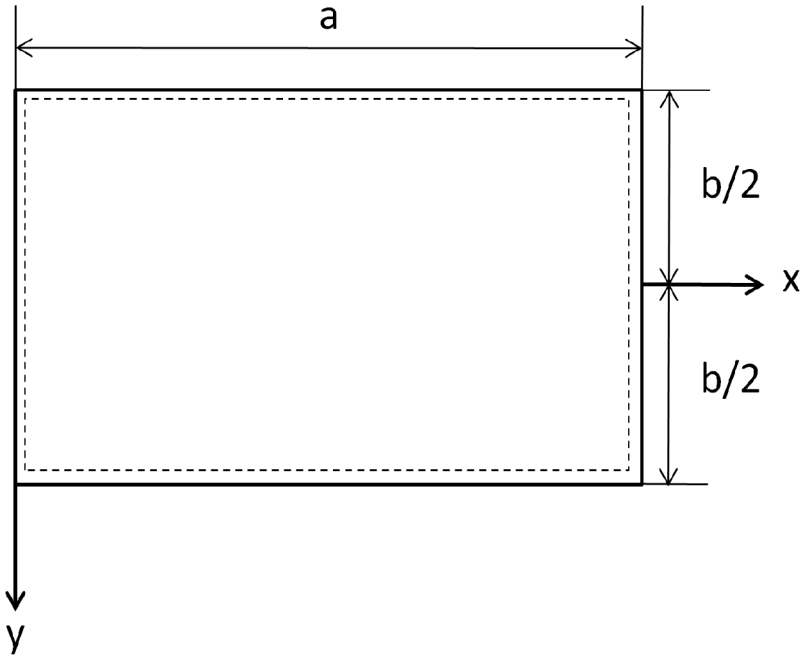

Figure 2.13 Simply supported rectangular plate.

The flexural rigidity (bending stiffness) of a rectangular plate, $\boldsymbol{D}$, can be computed by the product of the Young's modulus, $\boldsymbol{E}$, of the material and the area moment of inertia of the plate ($\boldsymbol{I_{plate}}$). The thickness of the plate is $\boldsymbol{h}$ and $\boldsymbol{\upsilon}$ is the Poisson's ratio of the plate and then the flexural rigidity (bending stiffness) of a rectangular plate is

$$D = EI_{plate} \tag{2.7}$$

where

$$I_{plate} = \frac{h^3}{12(1-\upsilon^2)} \tag{2.8}$$

The equation for the natural frequencies of simply supported rectangular plate is given as

$$\omega_{mn} = \frac{\pi^2 \left[\frac{m^2}{a^2} + \frac{n^2}{b^2} \right] \sqrt{\frac{D}{\bar{m}}}}{2\pi} \tag{2.9}$$

where $\bar{m}$ is the plate mass per unit area [24].

It has long been recognized that the lower modes of vibration of stiffened plates may be estimated by "smearing" the mass and stiffening effects of the stiffeners over the surface of the plate. Smearing process means that the density and stiffness characteristics of the removed material are transferred to remaining material of the model as seen in Figure 2.14. The theories are latest summarized by Szilard [24] and also mentioned by Vantsel and Krauthammer [33] and Timoshenko [34]. The results in this section are mainly based on these theories.

The natural frequencies of a stiffened plate are determined in the following way. The plate is simply supported along all edges, and has the length dimension a in the x-direction and b in the y-direction (Figure 2.14). Other dimensions of the plate are also shown in Figure 2.14, a_s is the distance between the stiffeners in the x-direction, b_s is the distance between the stiffeners in the y-direction and h is the thickness of the plate.

The flexural rigidity (bending stiffness) of stiffened plate in the x-direction, D_x, can be computed by the product of the Young's modulus, E, of the material and the area moment of inertia of plate and stiffeners (I) taken with respect to the middle axis of the smeared plate with a thickness h_e (Figure 2.15) in the x-direction [34]. Here, the stiffeners in the y- direction have nearly no effect on the bending stiffness in the x-direction. Therefore, only stiffeners in the x-direction are taken into account in I_x. Similarly, the bending stiffness in the y-direction, D_y, can be determined from the same equations using b_s instead of a_s.

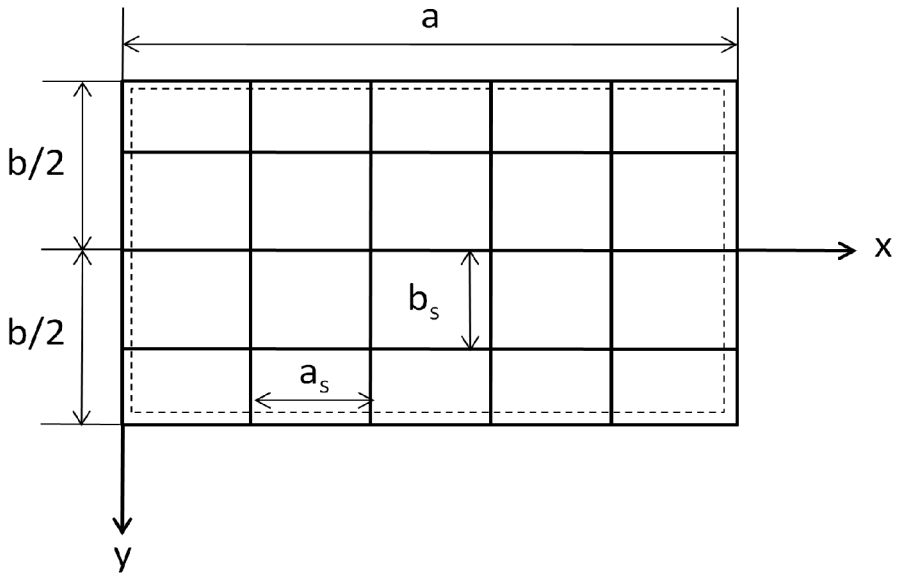

Figure 2.14 Stiffened plate

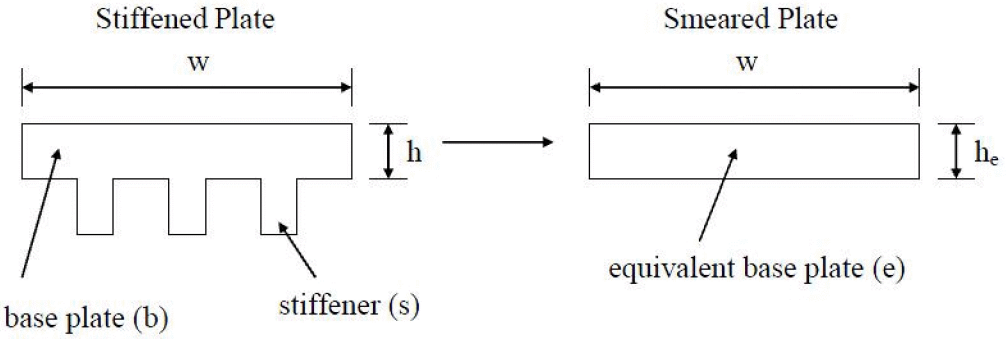

Figure 2.15 Smearing of a stiffened, flat plate

Then the bending stiffness of the stiffened plate in *x*-direction is

$$D_x = E(I_{plate} + \frac{I_x}{a_s}) \tag{2.10}$$

where

$$I_{plate} = \frac{h^3}{12(1-\upsilon^2)} + (\frac{h_e - h}{2})^2 \cdot h \tag{2.11}$$

The equation for the natural frequencies of a simply supported orthotropic plate is [24]:

$$\omega_{mn} = \frac{1}{2\pi}\sqrt{\frac{1}{m}}\sqrt{D_x(\frac{m\pi}{a})^4 + 2B(\frac{m\pi}{a})^2(\frac{n\pi}{b})^2 + D_y(\frac{n\pi}{b})^4} \tag{2.12}$$

where

$$B = \frac{1}{2}[\upsilon(D_x + D_y) + 2(1-\upsilon)\sqrt{D_x D_y}] \tag{2.13}$$

is the effective torsional rigidity of the plate [24].

2.5.2 Selection of Stiffeners

Stiffeners can be divided into two main groups according to their shapes. The first one is for closed section, like "Hat" or "Bead" section. The second group is for those with open section like "T", "I" or "L" sections. Structural behaviors of hat and bead type sections are very similar. Closed sections shows better structural properties for shear load than open sections. Some problems observed with this type of sections are the difficulties in manufacturing.

For open section stiffeners, only those with one axis of symmetry are selected in order to avoid the interaction of torsion failure with other types.

Structural requirements for stiffener selection are necessary and important at the design stage. There should be no coupling between in plane and out of plane deformations. Stiffener laminate shall be symmetric and balanced. Moreover, from the point of view of production, it is desirable to build the stiffener section from one or two flat laminates, which can be folded in "T" or "C" shapes [35].

2.5.3 Modeling of Stiffeners

Stiffened structures are considered as an orthotropic plate models which are formed in a simpler design by smearing the characteristics of the stiffeners over the surface of the plate. However serious restrictions came from the simplicity of approximation must be taken into account while modeling the stiffened plates. In order to obtain an orthotropic model which represents the plate precisely, stiffeners should be light, identical, closely and equally spaced, and the orientation of stiffeners should be orthogonal. If these conditions are not satisfied or in addition to this if the wavelength of vibration of the smeared plate is smaller than the spacing of the stiffeners the plate cannot be modeled accurately [36].

Finite element method is definitely the most precise and versatile for modeling stiffened plates among various numerical techniques available in literature since it can overcome any complicated or arbitrary geometry, material anisotropy and nonhomogenity.

Generally for stiffened structures, a convenient stiffener model is constructed using shell or beam elements. In Refs. [25], [28] and [37], dynamic behavior of stiffeners is modeled by finite elements as beam element. In Ref. [26] "C" type eccentric stiffeners are modeled as beam elements using MSC Nastran software to obtain dynamic and acoustic response of bidirectional stiffened plates. In Ref. [30] in order to obtain an optimum stiffener layout reducing the vibration and noise of gearbox housing, beam elements are used for modeling rib stiffeners. In Ref. [38] free vibration analysis of a stiffened laminated plate is studied and stiffeners are modeled by using layered shell elements and in Ref. [39] stiffeners are modeled by

SHELL43 element by using ANSYS software to clarify numerical and experimental investigations on the compression behavior of stiffened plates.

2.6 SIMILAR OPTIMIZATION STUDIES IN LITERATURE

In this section, similar optimization works in literature related with performed study within the scope of this thesis are investigated.

A real automotive component was optimized using topology optimization method within the ANSYS software in Ref. [40]. The optimization process was based on the maximization of the total potential energy with a volume constraint which depends on the imposed static (displacement, stress, stiffness) and dynamic (natural frequency) constraints.

In Ref. [41] compressor mounting bracket, propeller shaft and fuel tank used in automotive industry were optimized structurally and topologically using Altair OptiStruct software which is a finite element based structural analysis and optimization software. For compressor mounting bracket the objective function is minimizing the volume of bracket under static loading. For propeller shaft and fuel tank the aim is to maximize the fundamental natural frequency within identified design space of the components. After topology optimization is performed the fundamental natural frequencies of the shaft and tank were increased by 2% and 20% respectively.

In Ref. [42] the layout of the copper tube in an air conditioner was optimized structurally. The goal of this work was to avoid resonance in the air conditioner. For this topology optimization problem, Altair OptiStruct was used to optimize the layout of the copper tube with the objective of maximizing the natural frequency. The first and second natural frequencies of the tube were increased approximately by 100%.

Beam-type stiffeners were used in Ref. [43] in order to increase the natural frequencies of a hard disk drive (HDD) cover structure. Stiffener layout optimization problem was performed to maximize natural frequencies of the cover structure and it was stated that the proposed technique used for this work can also

be applicable to complex real engineering structures. After optimized stiffener reinforcement is done, the fundamental natural frequency of HDD was increased by nearly 15% according to the original design.

In Ref [44] the sound level of a horizontal vibrating screen machine, which is used for processing clean coal, was decreased by adding rib stiffeners made from steel channel with two different cross-sections (C and T). The optimization of layout of the stiffeners and the effects of orienting the stiffeners horizontally and vertically were investigated.

CHAPTER 3

VIBRATION CHARACTERISTICS OF THE RADAR ANTENNA

In this chapter the details of a radar antenna structure on which the optimization study is performed are given and the vibration characteristics of original configuration of this antenna are investigated. A verification study is carried out, where finite element model of a simply supported plate is compared with the analytical solution. In addition to this vibration characteristics of an intuitive design of radar antenna structure are examined.

In order to determine the effects of vibration transmitted by the helicopter platform onto a certain radar antenna system, dynamic characteristics of the radar antenna (natural frequencies, corresponding mode shapes etc.) which should be found over the interested frequency range (0-500 Hz) are investigated. By using these parameters, displacement of the system under vibration should be specified for vibration exposure levels of helicopter platform.

In this thesis ANSYS is used to construct the finite element model of the radar antenna and analyze its dynamic characteristics.

3.1 GEOMETRY OF THE RADAR ANTENNA

In this thesis a generic radar antenna structure design is used. The geometry of this radar antenna is given in Figure 3.1 through Figure 3.5. Radar antenna structure is mainly made up of aluminum, with elastic modulus of 70 GPa, a Poisson's ratio of 0.3 and density of 2700 kg/m^3. Total mass of the original radar antenna can be

calculated from the solid computer model as 16.6 kg and the total volume is calculated as 0.00614 m^3. Antenna elements (patches) are located inside the rectangular boxes which are fixed on the 3 mm thick plate as shown in Figure 3.1. The general dimensions of the generic radar antenna structure used in this thesis are given in Figure 3.6.

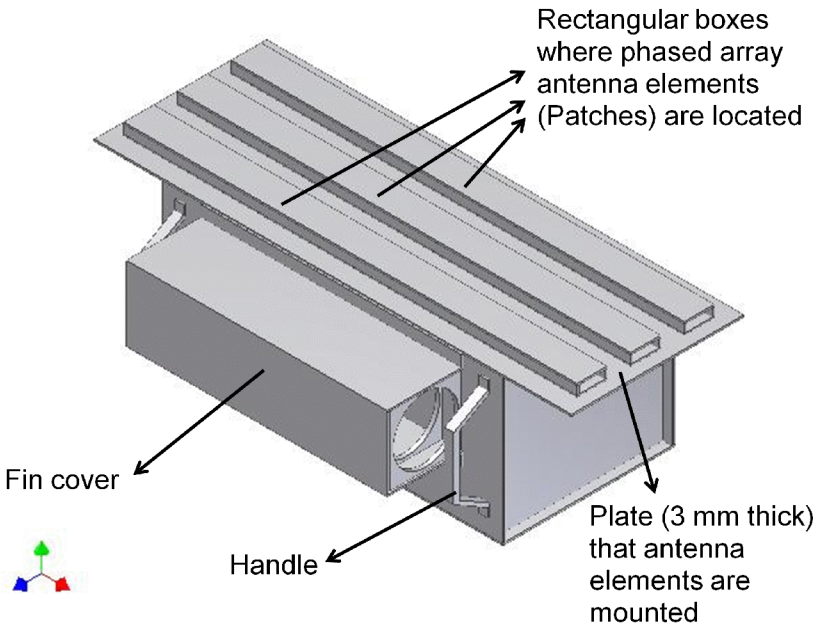

Figure 3.1 Isometric view of the radar antenna structure (top/front/right view).

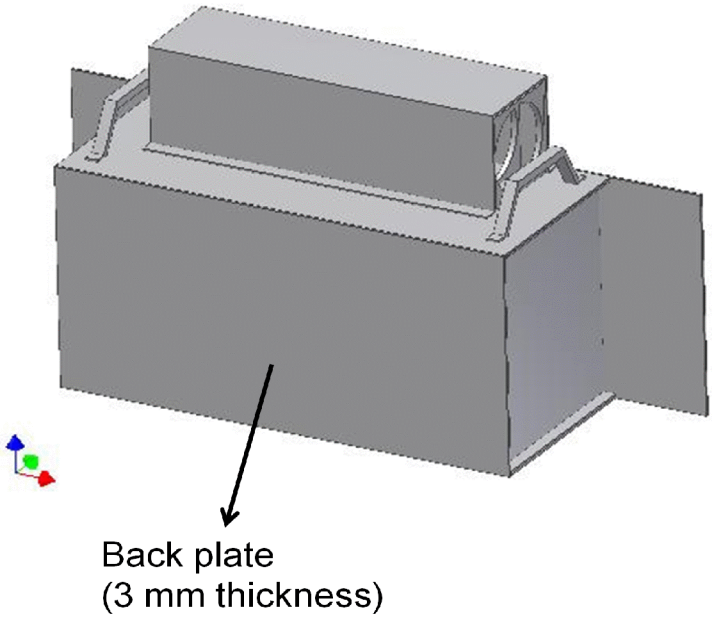

Figure 3.2 Isometric view of the radar antenna structure (back/top/right view).

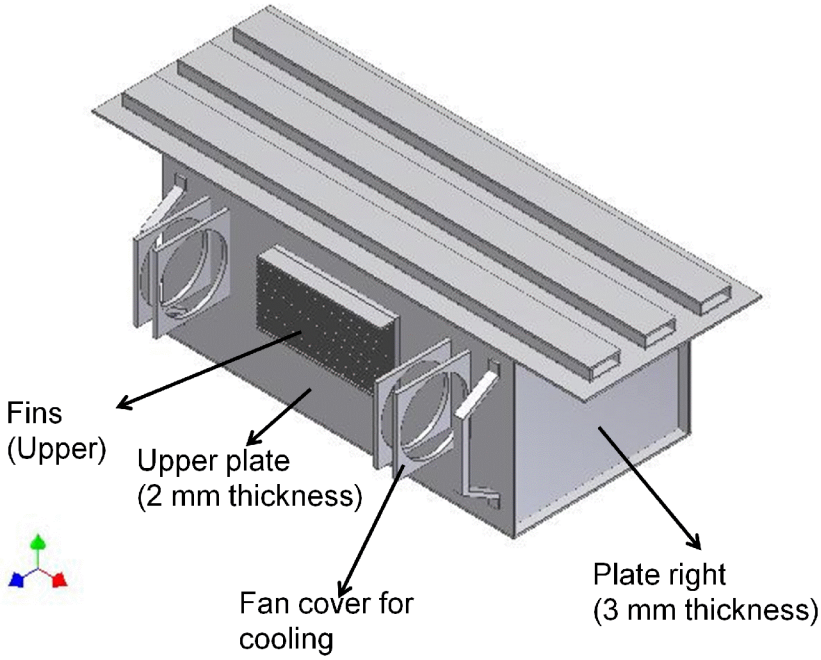

Figure 3.3 Isometric (top/front/right) view of the radar antenna structure (fin cover is invisible).

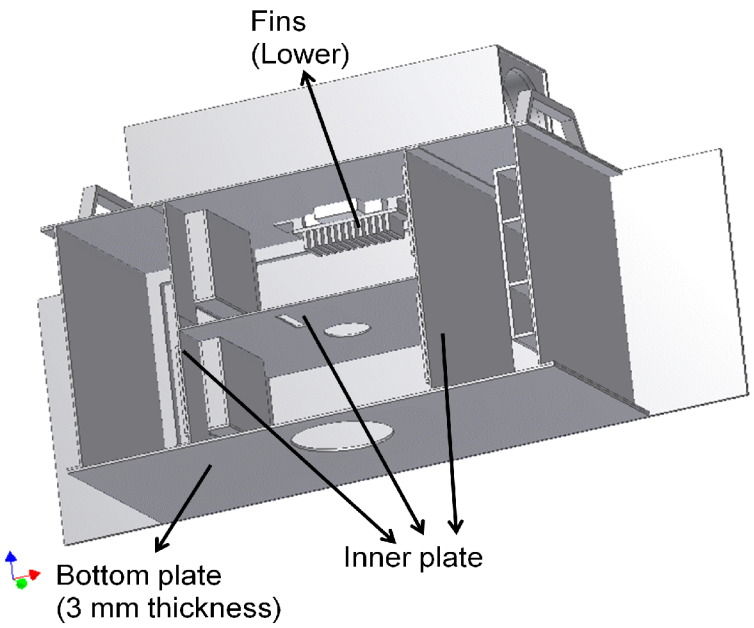

Figure 3.4 Isometric (back/bottom/right) view of the radar antenna structure (fin cover and back plate are invisible).

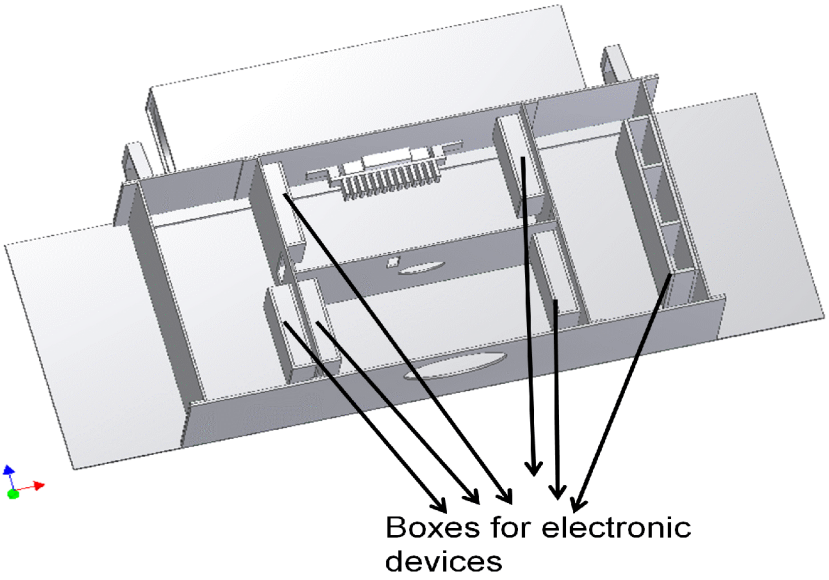

Figure 3.5 Isometric (back/bottom/left) view of the radar antenna structure (fin cover and back plate are invisible).

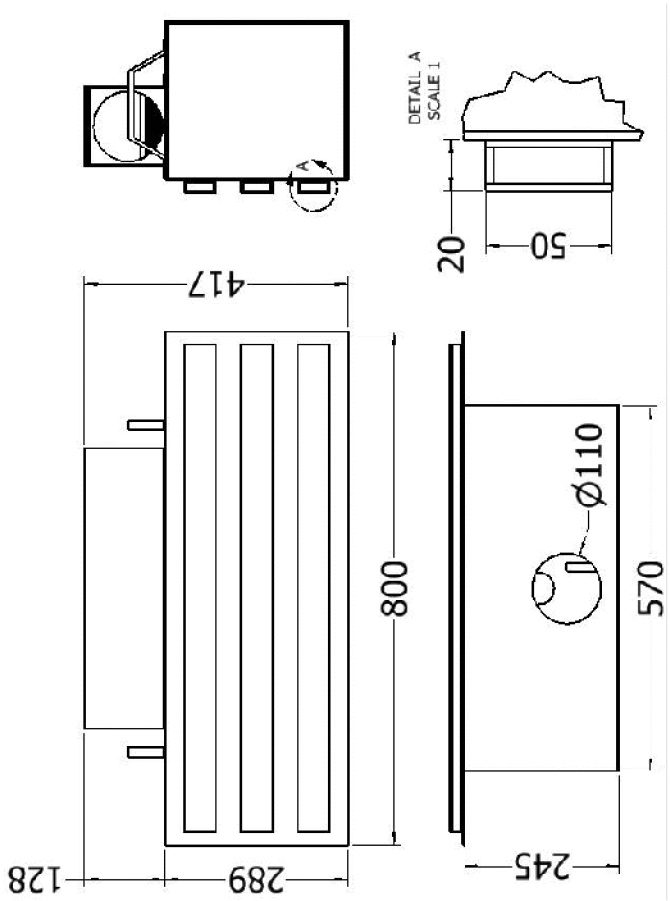

Figure 3.6 General dimensions of the radar antenna structure (all dimensions are in mm).

3.2 BOUNDARY CONDITIONS

All degrees of freedoms on the surface of shaft connection, which is defined by the hole that exists on the bottom plate (see Figure 3.4), is fixed as the boundary condition (BC) of the radar antenna structure.

3.3 FINITE ELEMENT MODEL (FEM) OF THE RADAR ANTENNA

The geometry of the radar antenna structure is automatically imported into ANSYS finite element software. In ANSYS, geometry of the antenna is meshed and material property of the antenna is defined.

3.3.1 Validation of Element Type and Size

In order to decide on the right type of element and right element size for the final FE model of the radar antenna structure, a simple validation study is performed using a simply supported plate of similar dimensions compared to the plates that form the original antenna structure. Analytical expressions of the modal frequencies of a simply supported rectangular plate were defined in Chapter 2. FE model validation is performed by comparing modal frequency results obtained in ANSYS with the analytical results. Two types of solid elements are used in the validation cases. Element sizes are also varied in order to observe any disagreements with the analytical solution. Results of all cases are compared with previously defined analytical solution of the simply supported plate.

For simply supported rectangular plate (displacement in z direction is fixed for all edges of the plate in Figure 3.7) $\boldsymbol{a}$ is selected as 570 mm, $\boldsymbol{b}$ is selected as 289 mm and $\boldsymbol{h}$ (thickness) is selected as 3 mm because these dimensions are same as back plate dimensions in the geometry of the radar antenna structure. According to this model analytical solution is done and the results are given in Table 3.1.

In ANSYS, simply supported rectangular plate is modeled as three dimensional SOLID95 and SOLID45 elements which have 20 nodes including midside nodes and 8 nodes, respectively. Also all edges of the plate are fixed only in z-direction to achieve the simply supported boundary condition. A total of eight cases are analyzed in ANSYS which are explained in Figures 3.8-3.11. In Figures 3.8-3.11, only the SOLID95 element configurations (first four cases) are given. Other four cases have the same mesh and only the element type is changed i.e. SOLID45

element type is used for the last four cases. Results of these 8 cases are given in Table 3.1 which also includes the analytical solution to the modal frequencies.

Looking at the results shown in Table 3.1, it can be concluded that for the cases where SOLID45 element type is used solution is obtained faster compared to the cases where SOLID95 element type is used. The reason for difference in solution time is obvious since SOLID45 element does not have midside nodes. On the other hand for both element types, the use of layered element configuration in thickness direction increases the solution time. The results of layered element configuration cases for SOLID95 (CASE-3 and CASE-4) are similar with the results of CASE-1 and analytical solution. However in CASE-7, although layered element configuration is used for SOLID45 element, the modal analysis results are not converged to the analytical solution as in CASE-5 since the element size is not small enough. Studying the results it can be concluded that the most efficient element configuration for the modeling of this plate is CASE-1 since the modal analysis results converge to the analytical solution in a short time. Therefore, in order to decrease the computation time of the modal and optimization analysis configuration of CASE-1 is used in this study.

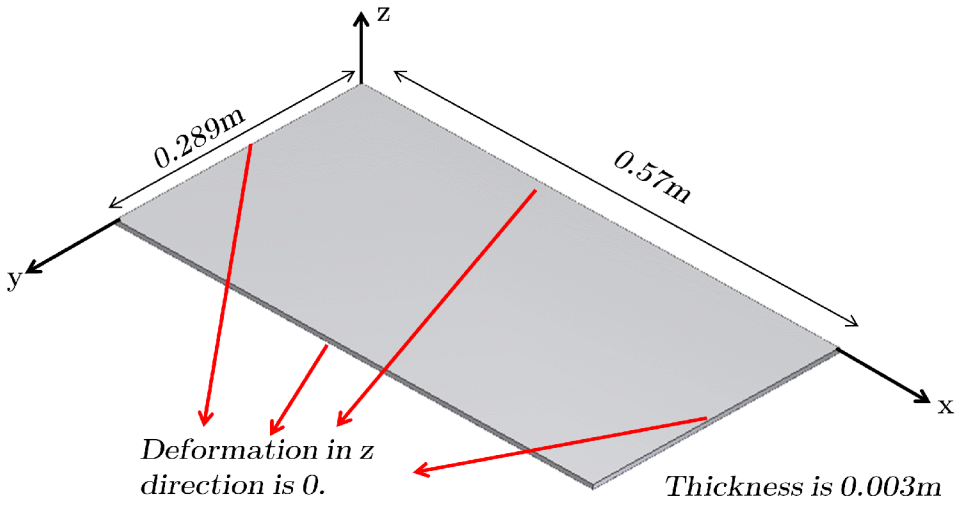

Figure 3.7 Simply supported rectangular plate used in element comparison.

Table 3.1 Element comparison table.

	ANALYTICAL SOLUTION	CASE 1	CASE 2	CASE 3	CASE 4	CASE 5	CASE 6	CASE 7	CASE 8
Element		3-D 20-Node SOLID95	3-D 20-Node SOLID95	3-D 20-Node SOLID95	3-D 20-Node SOLID95	3-D 8-Node SOLID45	3-D 8-Node SOLID45	3-D 8-Node SOLID45	3-D 8-Node SOLID45
Element Size (m)		0,02	0,005	0,02	0,005	0,02	0,005	0,02	0,005
Number of Layer		1	1	5	5	1	1	5	5
Number of equation		9364	139721	28778	242159	2704	40022	7584	63366
Time Duration (sec)		4	408	49	4177	2	25	6	151
Number of Elements		435	6612	2030	17400	435	6612	2030	17400
Number of Nodes		3268	47147	10080	82057	960	13570	2700	21594
1st Nat. Freq (Hz)	109.29	109.29	109.07	109.3	109.06	110.33	109.18	110.49	109.19
2nd Nat. Freq (Hz)	176.33	176.22	175.79	176.19	175.78	179.56	176.05	179.92	176.15
3rd Nat. Freq (Hz)	288.07	288.23	287.26	288.16	287.28	296.3	287.73	297.07	288.2
4th Nat. Freq (Hz)	370.09	371.8	369.62	372.05	369.59	379.98	370.21	381.89	370.23
5th Nat. Freq (Hz)	437.13	438.25	436.02	438.42	435.96	454.51	436.87	457.12	437.02
6th Nat. Freq (Hz)	444.51	445.84	443.39	445.66	443.52	462.58	444.27	464.11	445.76
7th Nat. Freq (Hz)	548.88	549.48	546.93	549.53	546.87	579.97	548.19	583.84	548.74
8th Nat. Freq (Hz)	645.64	649.77	644.08	649.36	644.48	681.32	645.73	684.12	649.39
9th Nat. Freq (Hz)	705.32	706.08	702.46	705.96	702.44	758.46	704.34	764.27	705.9

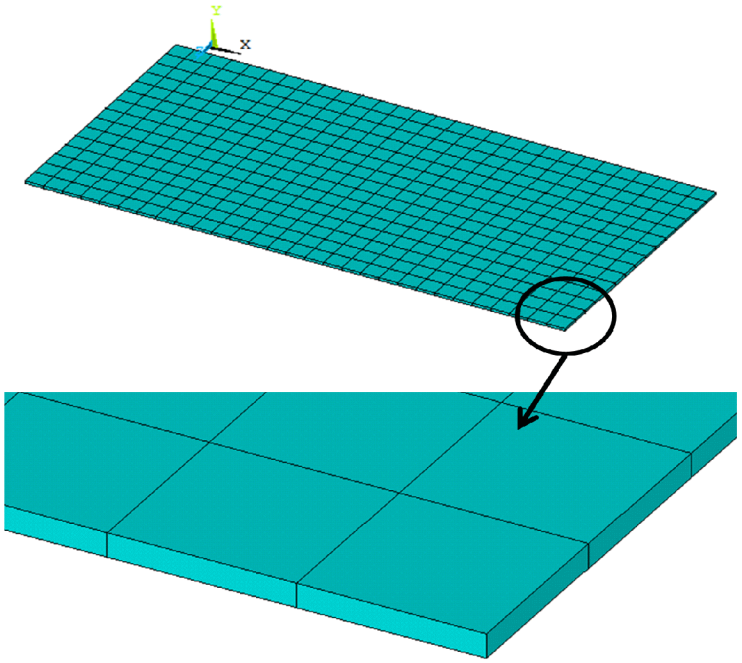

Figure 3.8 CASE1: 1 layer, 0.02m element size, 3D 20-Node SOLID95 element.

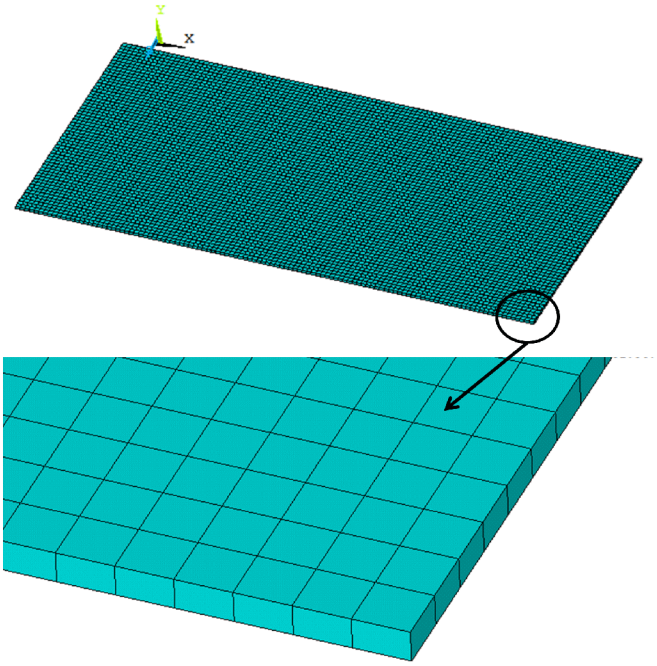

Figure 3.9 CASE2: 1 layer, 0.005m element size, 3D 20-Node SOLID95 element.

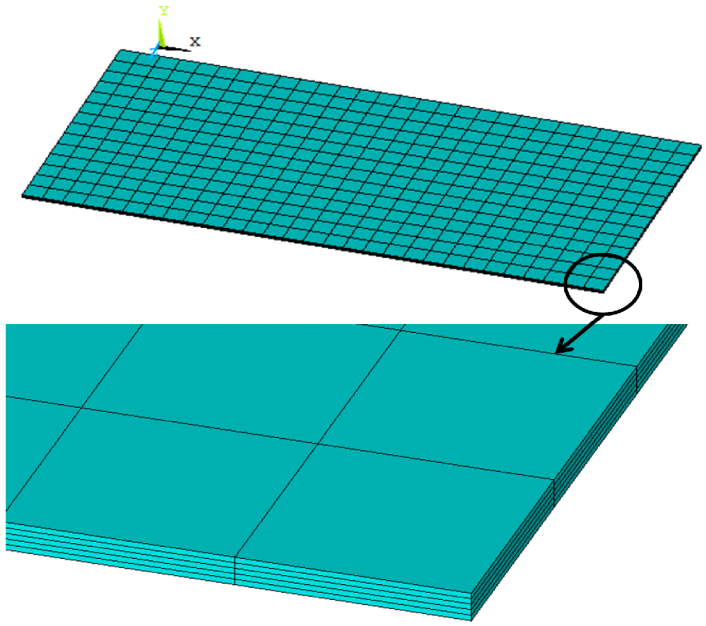

Figure 3.10 CASE3: 5 layer, 0.02m element size, 3D 20-Node SOLID95 element.

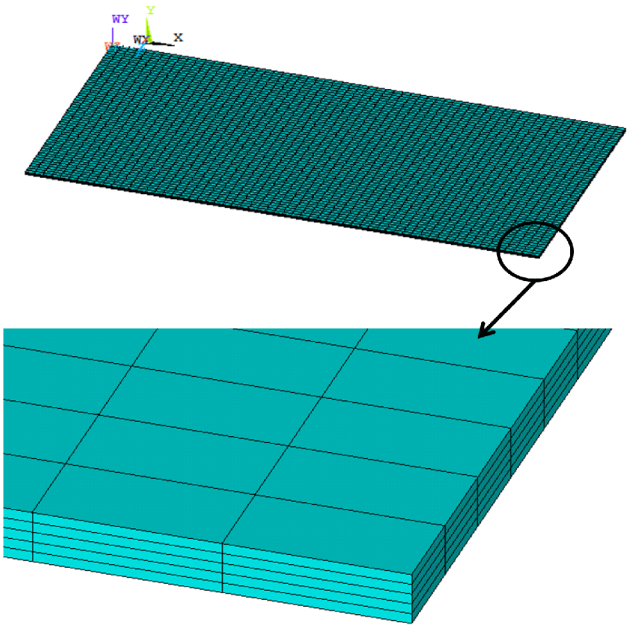

Figure 3.11 CASE4: 5 layer, 0.005m element size, 3D 20-Node SOLID95 element.

Based on the conclusions derived from the validation and accuracy study performed on a simply supported plate the FE model of the radar antenna structure is modeled by using SOLID95 elements. Constructed FE mesh of the radar antenna structure can be seen in Figure 3.12 through Figure 3.15. This model contains 24448 element and 54934 nodes.

In order to check the convergence characteristics of the current finite element model, a second FE model which has 56614 elements and 197264 nodes is constructed using the same type of elements. Modal analysis is performed for these two models for the same boundary conditions specified in Section 3.2. The results are given in Table 3.2 and it is seen that natural frequencies of the current model are very close to the refined model. Therefore, the first model with 24448 of SOLID95 elements and 54934 nodes has been found to be satisfactory in the optimization studies to be performed which will require only dynamic analysis of the radar antenna structure (modal and harmonic analysis).

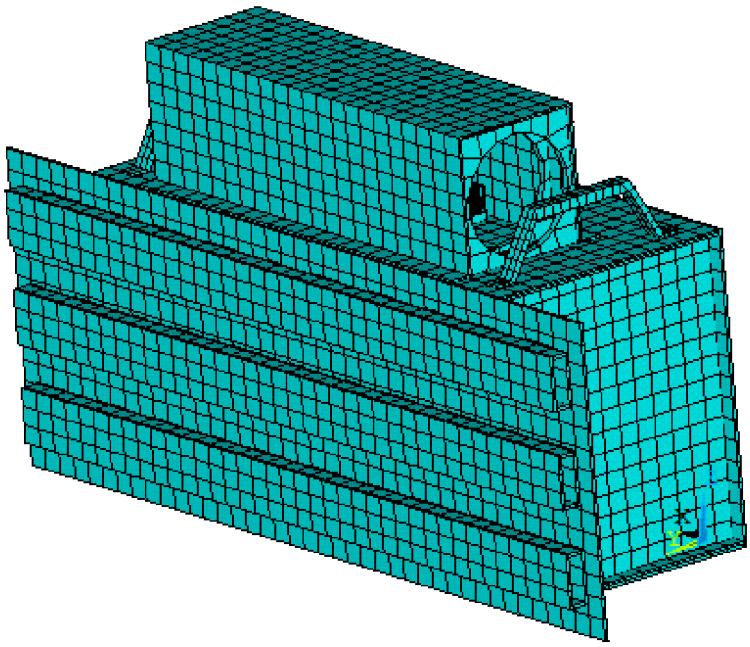

Figure 3.12 FEM of the radar antenna structure (left/front/top isometric view).

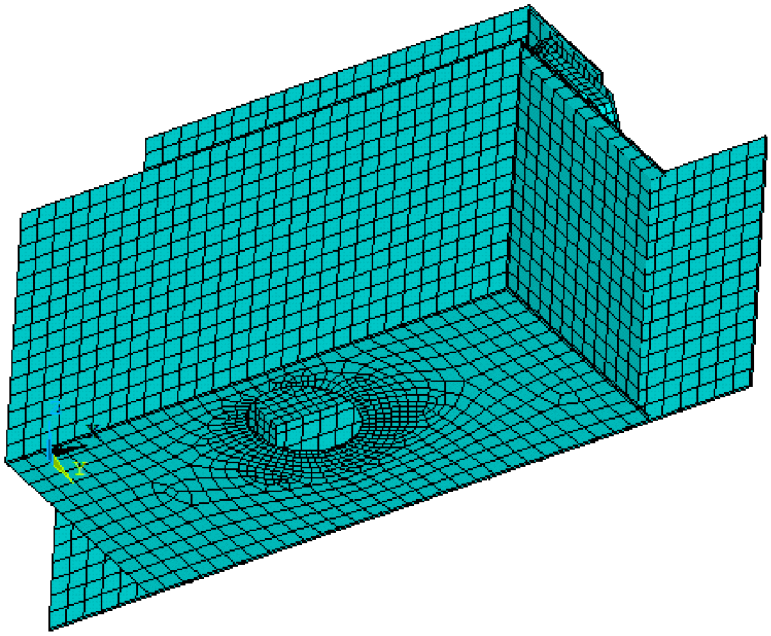

Figure 3.13 FEM of the radar antenna structure (right/bottom/back isometric view).

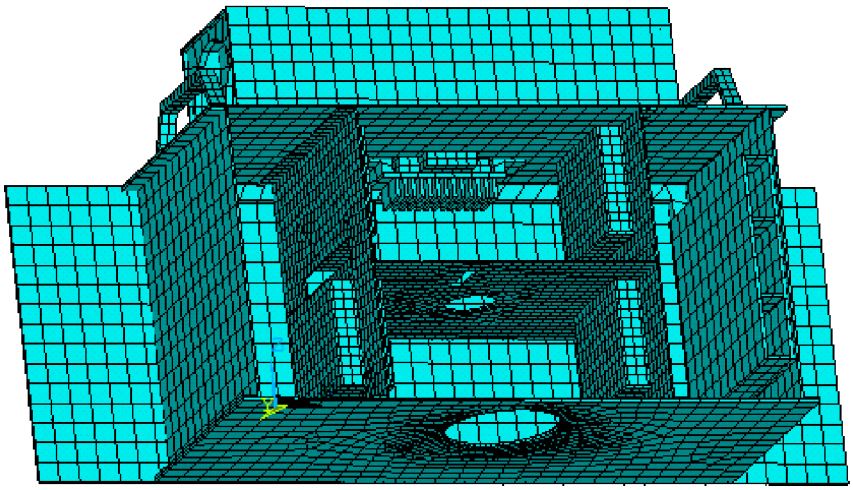

Figure 3.14 FEM of the radar antenna structure (back plate is invisible).

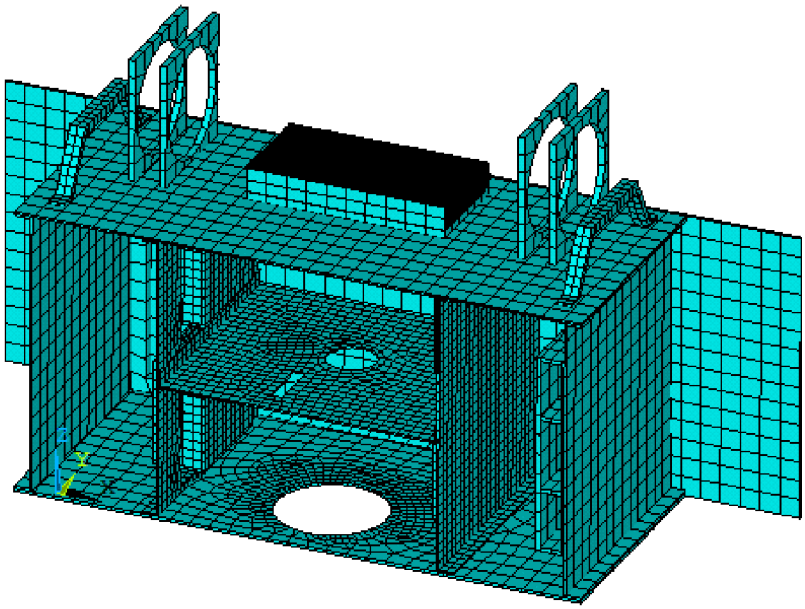

Figure 3.15 FEM of the radar antenna structure (back plate and fin cover are invisible).

Table 3.2 Model comparison table.

	Current Model	**Fine Model**	
Number of equations	163873	569452	
Time Duration (sec)	665	10960	
Number of Elements	24448	56614	
Number of Nodes	54934	197264	
			CHANGE (%)
1st Nat. Freq (Hz)	14.7	14.83	-0.88
2nd Nat. Freq (Hz)	16.2	15.9	1.89
3rd Nat. Freq (Hz)	96.5	93.5	3.21
4th Nat. Freq (Hz)	148.1	147.9	0.14
5th Nat. Freq (Hz)	296.6	295.9	0.24
6th Nat. Freq (Hz)	300.4	298.2	0.74
7th Nat. Freq (Hz)	320	308.9	3.60
8th Nat. Freq (Hz)	322.5	315.4	2.25
9th Nat. Freq (Hz)	372.8	371.2	0.45
10th Nat. Freq (Hz)	409	396	3.29

3.4 MODAL ANALYSIS OF RADAR ANTENNA

In order to identify the vibration characteristics of the radar antenna that is assumed to be externally installed on the AH-64 helicopter platform, mode shapes that fall between 0-500 Hz as stated before will be taken into account. Natural frequencies obtained in ANSYS of the radar antenna structure with previously defined BC's, are given in Table 3.3. Mode shapes obtained in the same ANSYS analysis are shown in Figures 3.16 through 3.25. It can be easily seen that the first two mode shapes are global while the others have some local vibration patterns.

Table 3.3 Natural frequencies of original radar antenna structure.

Mode Shape	**1**	**2**	**3**	**4**	**5**	**6**	**7**	**8**	**9**	**10**
Frequency (Hz)	14.7	16.2	96.5	148.1	296.6	300.4	320	322.5	372.8	409

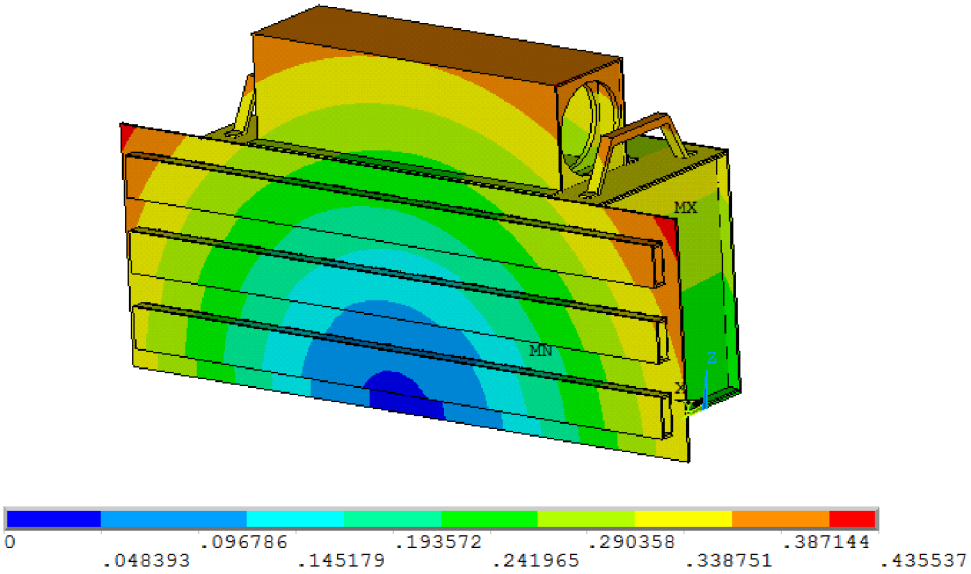

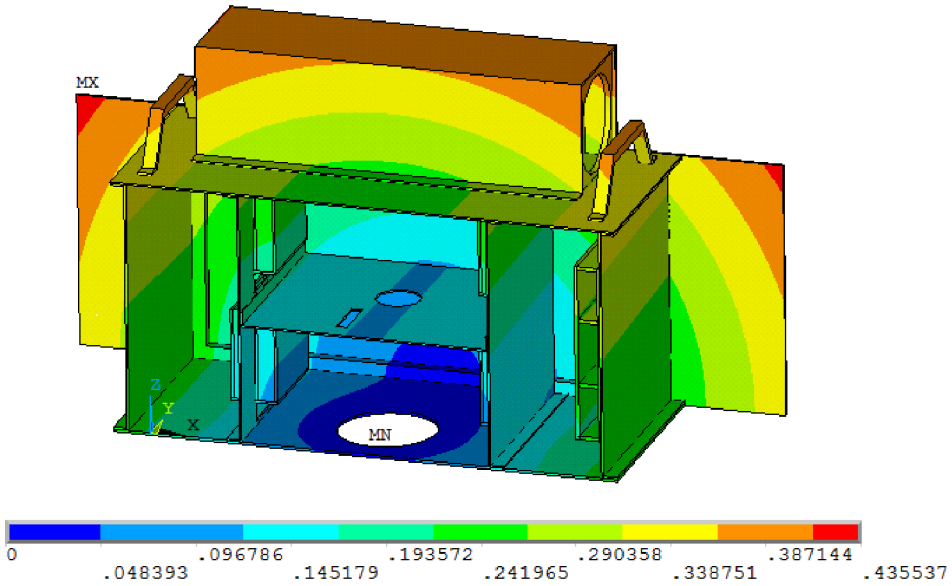

Figure 3.16 Total displacement of 1st mode shape at 14.7 Hz.

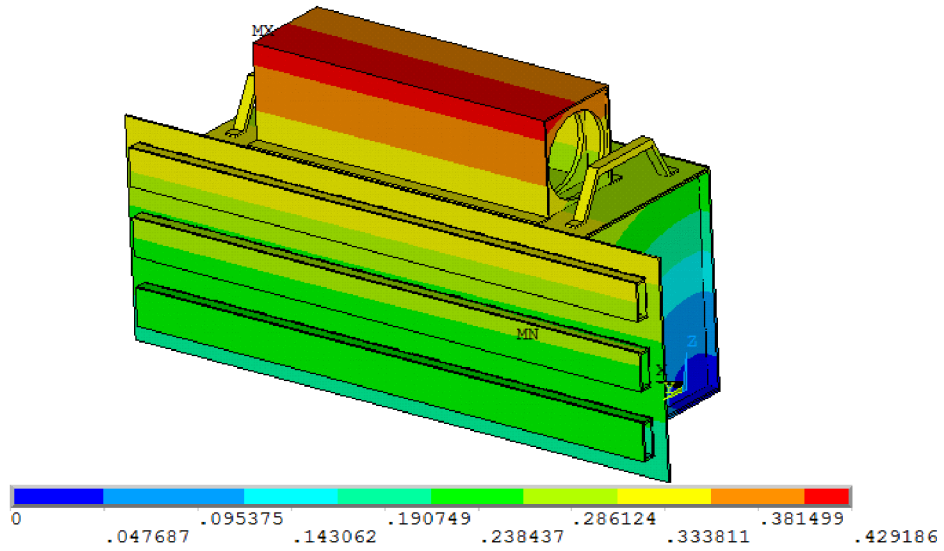

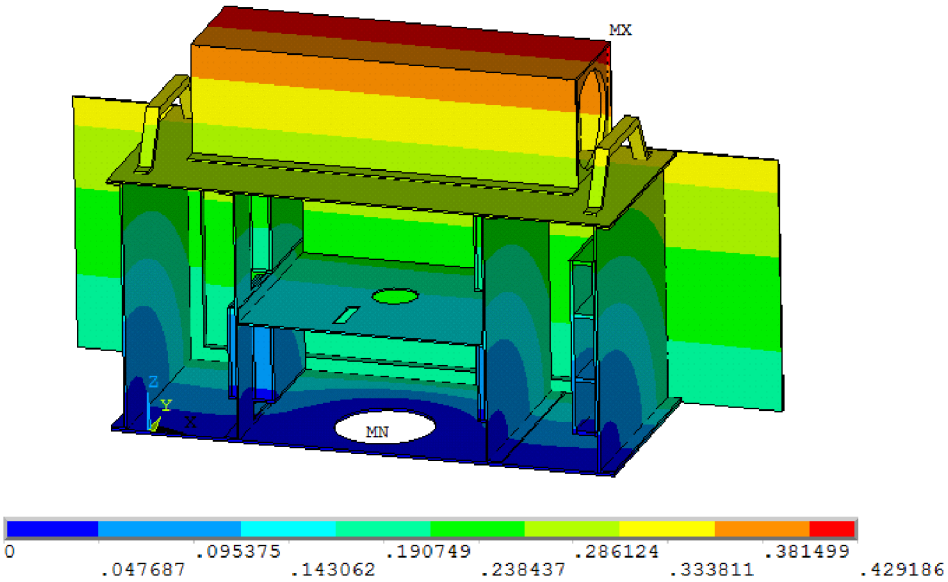

Figure 3.17 Total displacement of 2nd mode shape at 16.2 Hz.

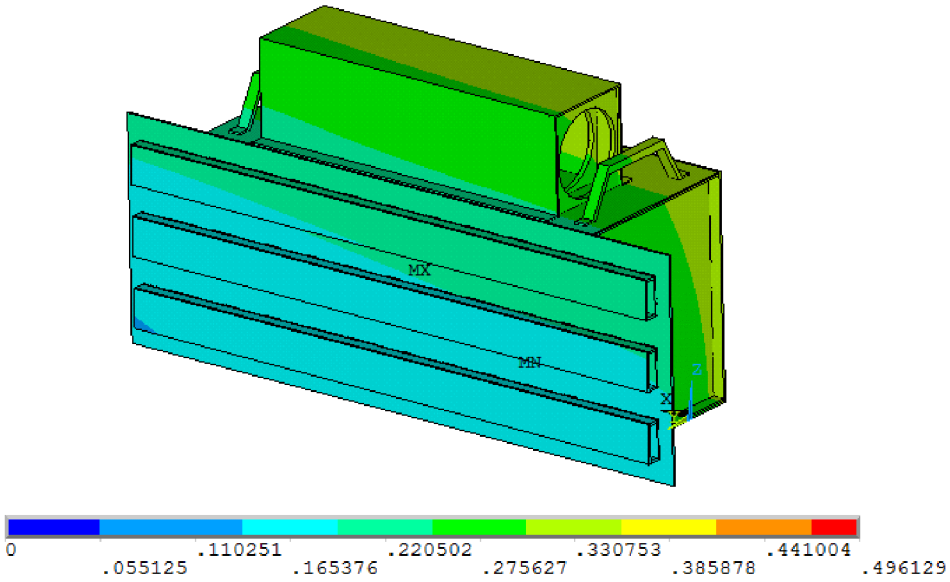

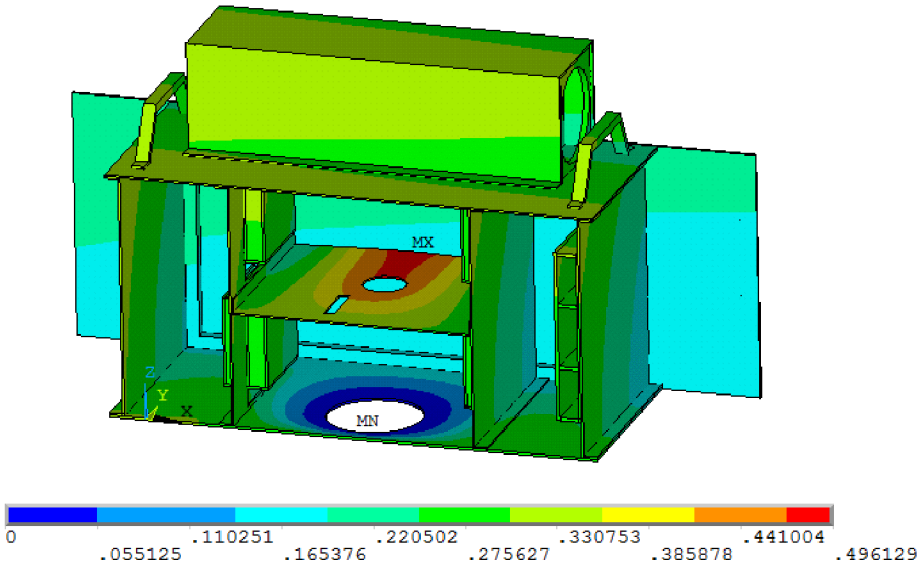

Figure 3.18 Total displacement of 3rd mode shape at 96.5 Hz.

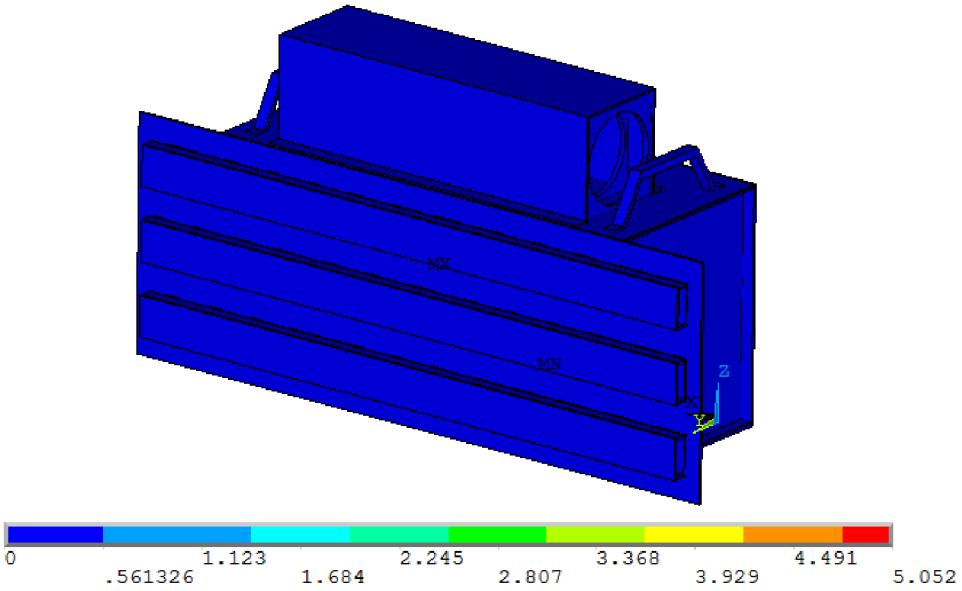

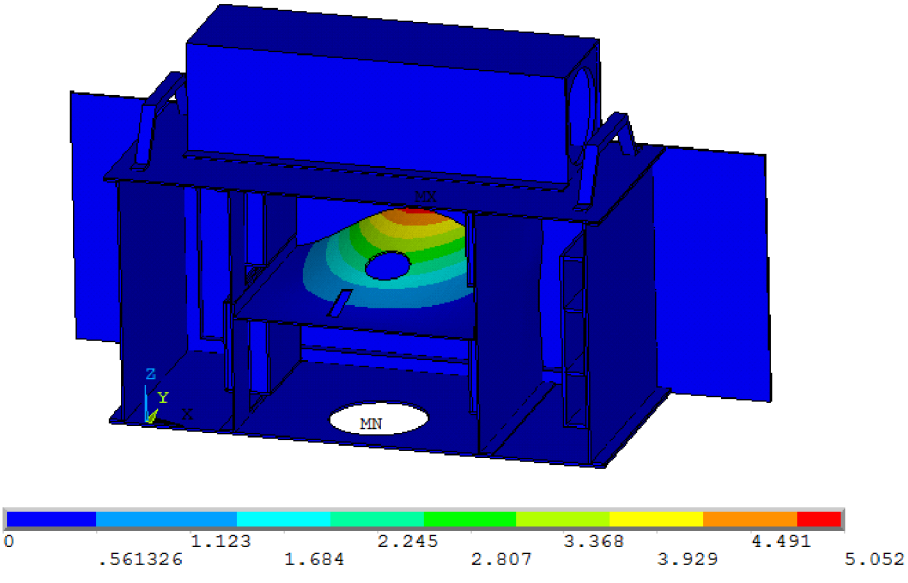

Figure 3.19 Total displacement of 4th mode shape at 148.1 Hz.

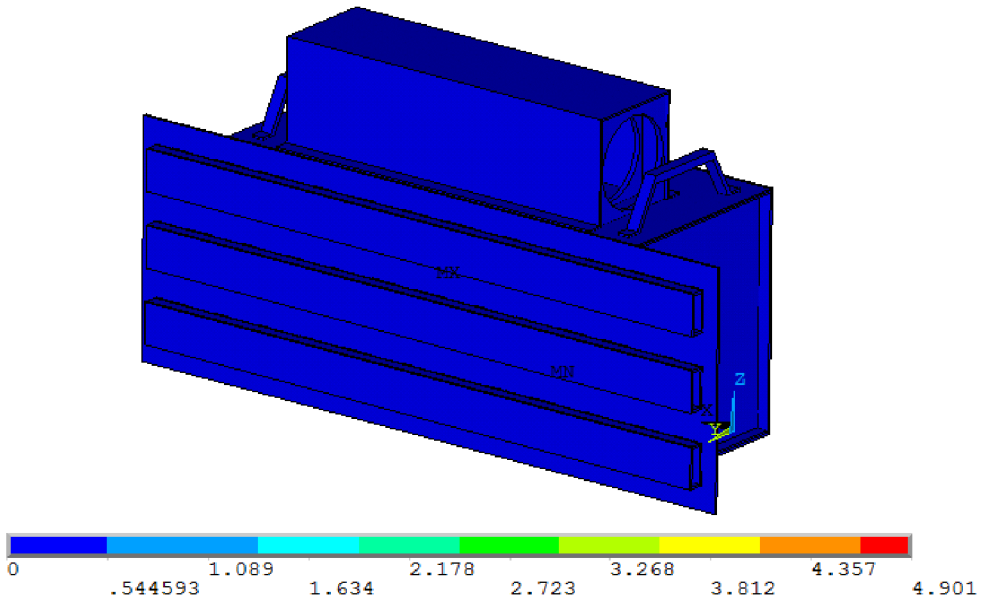

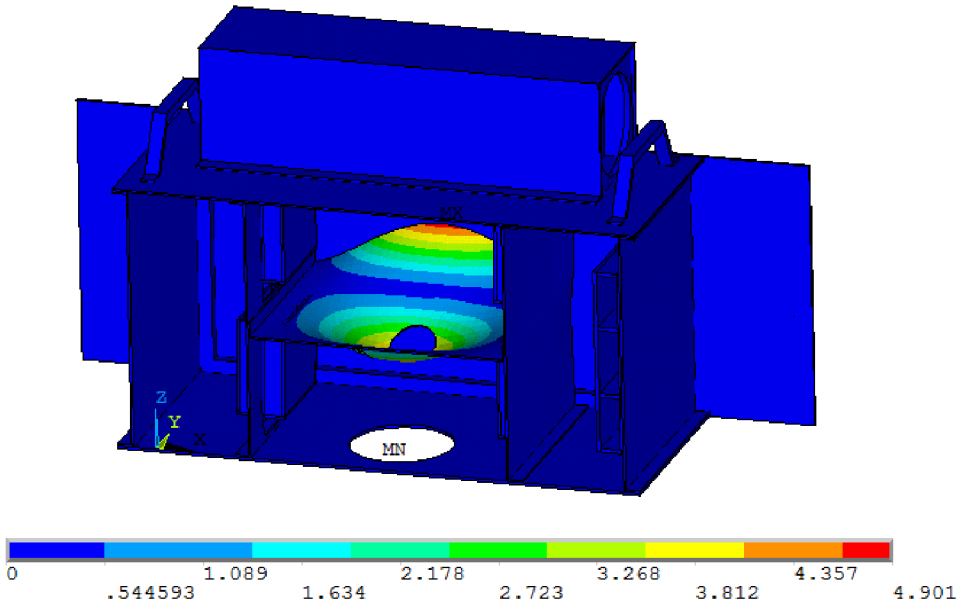

Figure 3.20 Total displacement of 5th mode shape at 296.6 Hz.

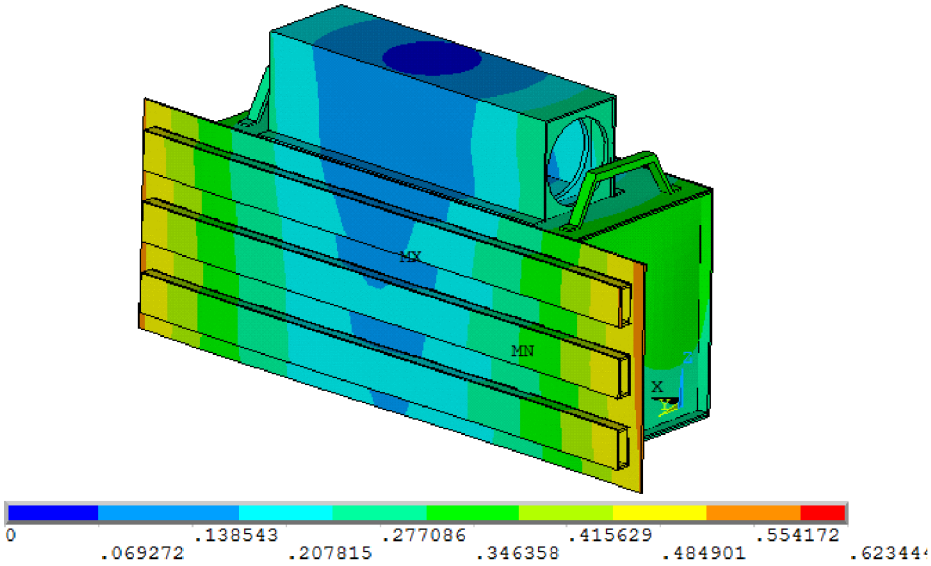

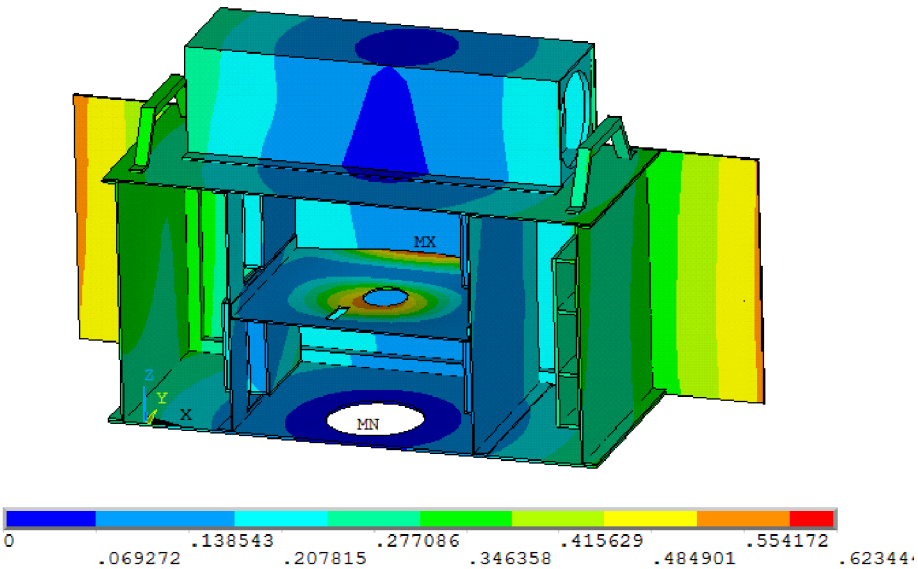

Figure 3.21 Total displacement of 6th mode shape at 300.4 Hz.

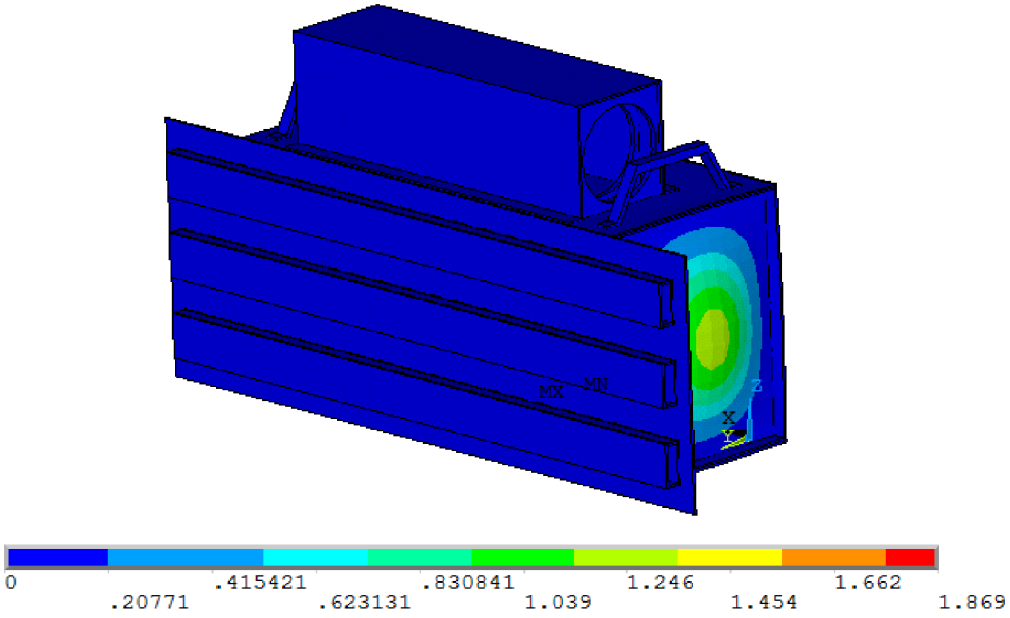

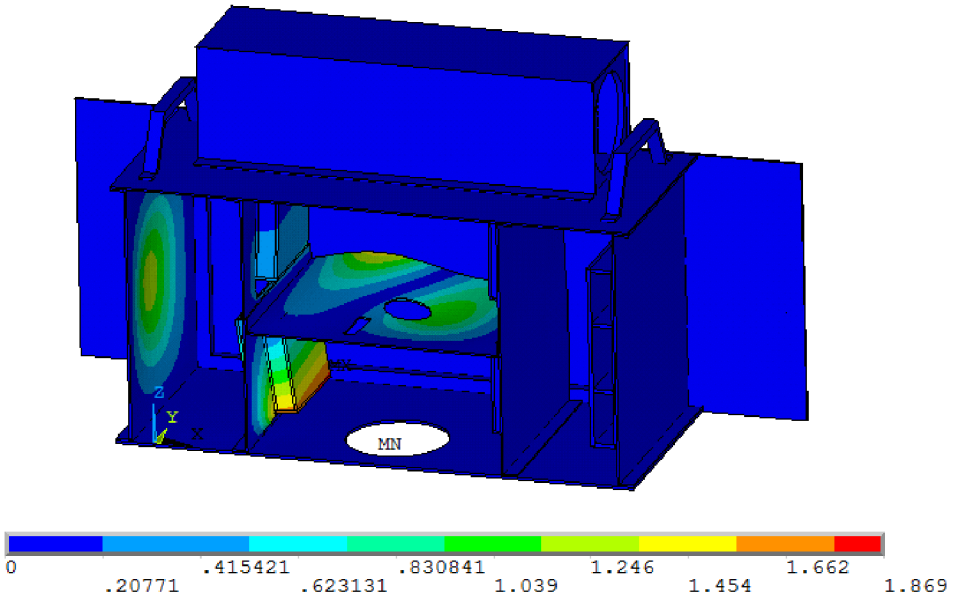

Figure 3.22 Total displacement of 7th mode shape at 320 Hz.

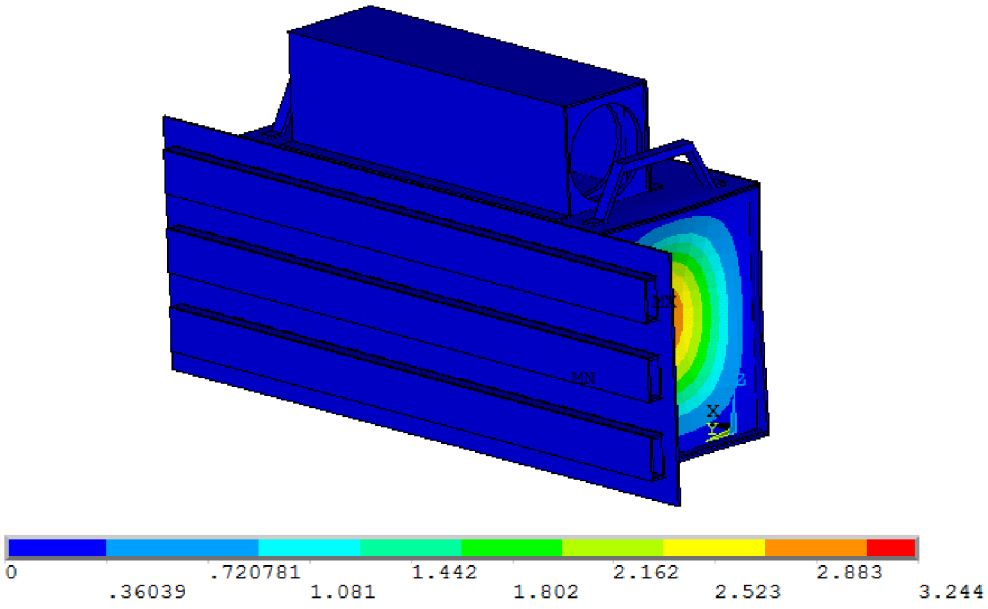

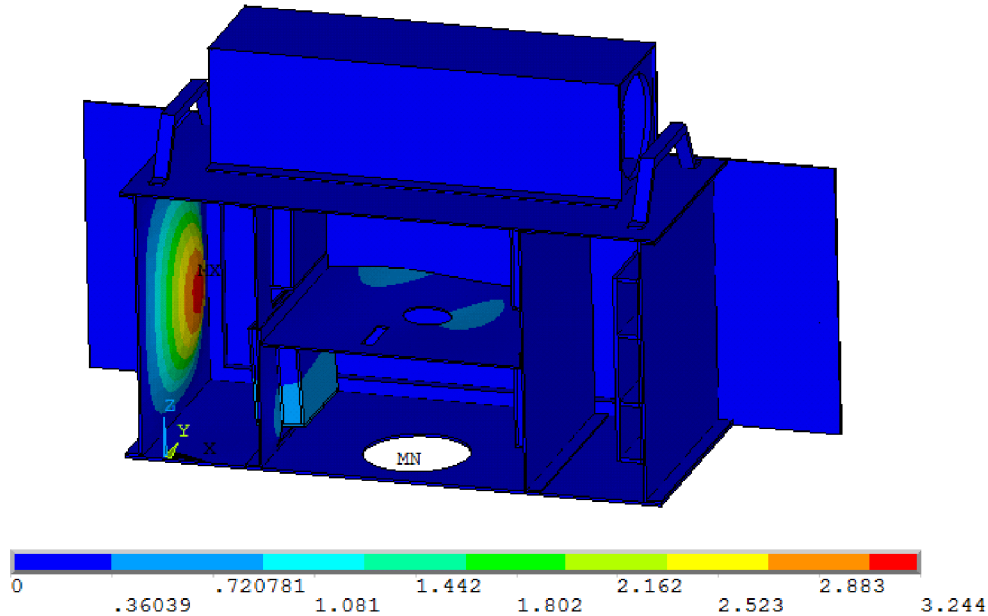

Figure 3.23 Total displacement of 8th mode shape at 322.5 Hz.

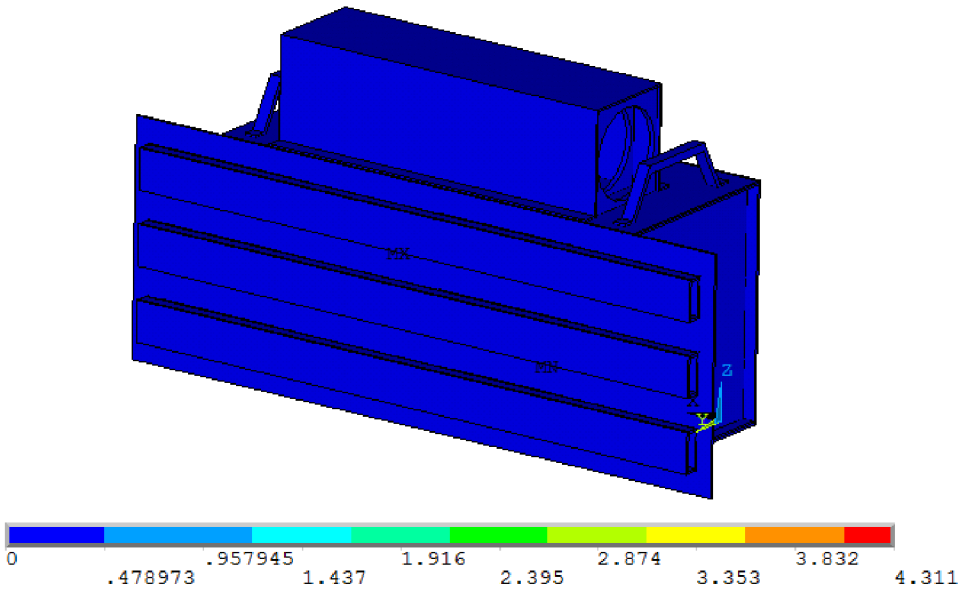

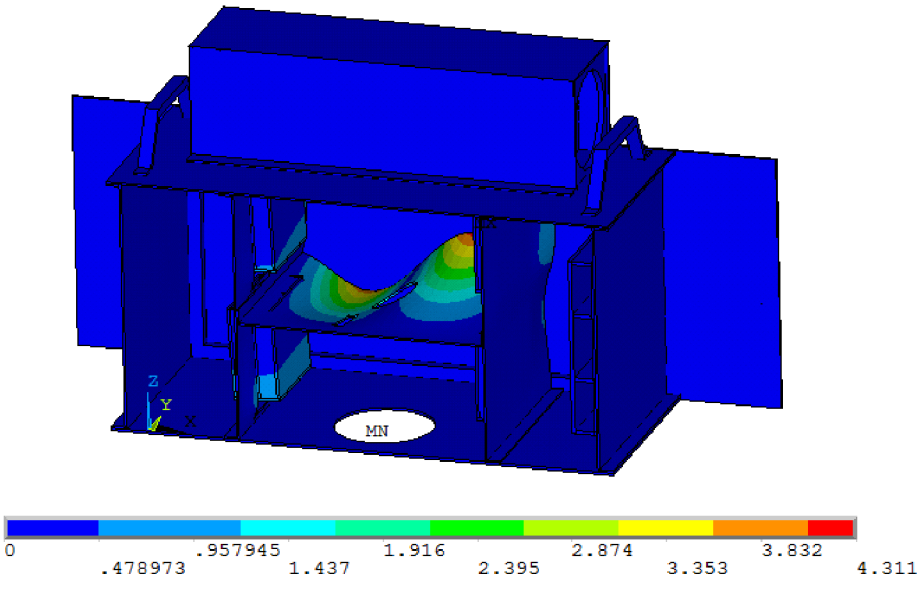

Figure 3.24 Total displacement of 9th mode shape at 372.8 Hz.

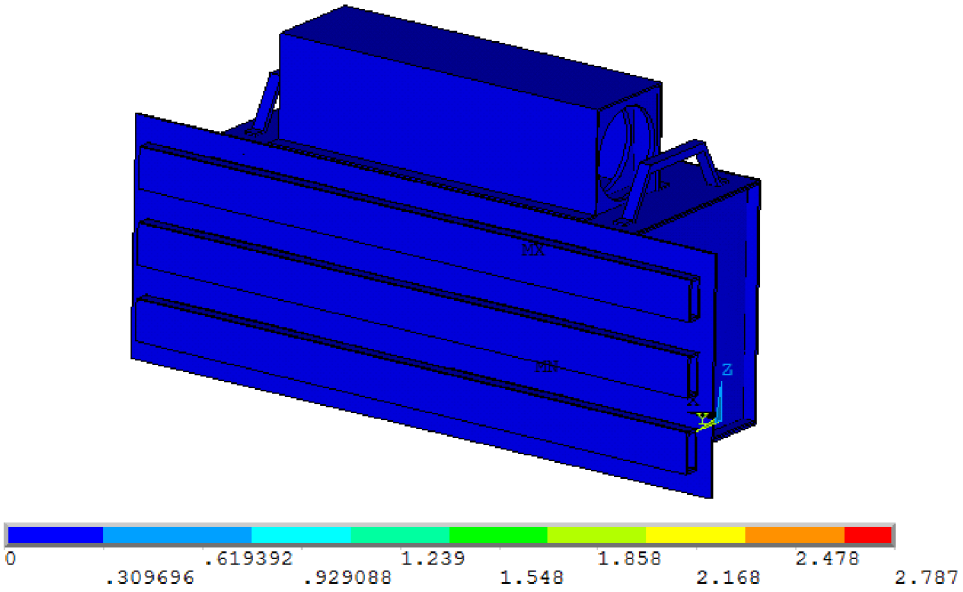

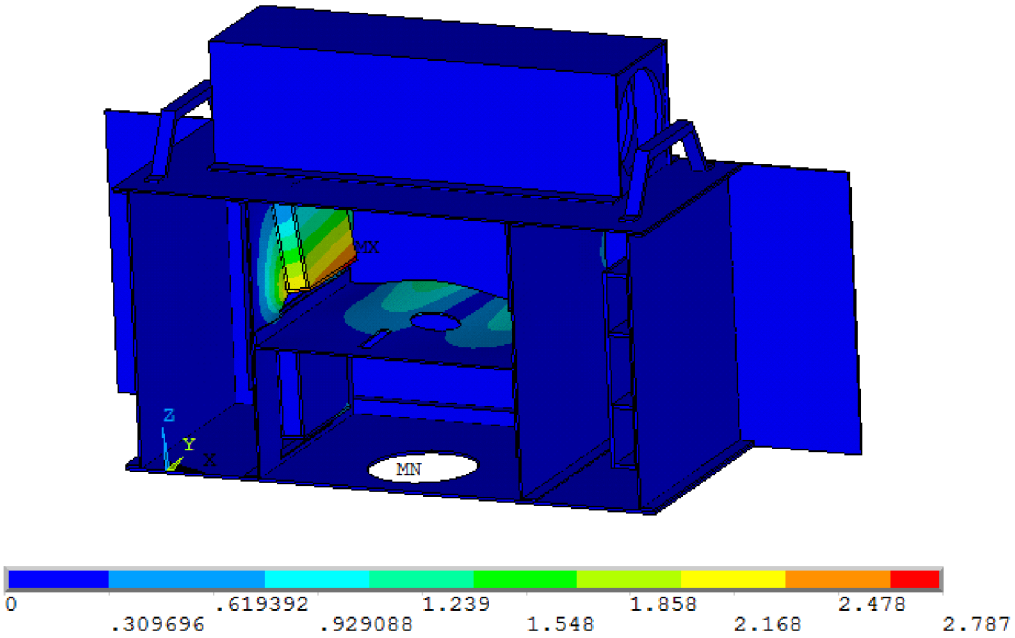

Figure 3.25 Total displacement of 10th mode shape at 409 Hz.

When vibrations of the helicopter platform, especially dominant sinusoids of the rotating components match the natural frequencies of the radar antenna there will be excessive deformations in the radar antenna structure. These dynamic deformations change the positions and orientations of the elements of the phased array antenna which will have serious negative effects on performance of the radar. The natural frequencies of the radar antenna and Apache AH-64 helicopter vibration exposure levels (power spectrum plots) are both given in Figure 3.26. Green lines indicate the natural frequencies of the radar antenna, red lines are the dominant sinusoids of the AH-64 helicopter, and blue spectrum represents the random vibration level which are taken from MIL-STD 810G. It is seen from Figure 3.26 that the first and the second natural frequencies of the radar antenna do not match with any of the dominant sinusoids of the AH-64 helicopter vibration exposure profile. However these two natural frequencies are very close to the second sinusoidal excitation frequency of the helicopter platform. The two modal frequencies also lie in the random vibration exposure frequency range. Other natural frequencies are out of the dominant sinusoid range (approximately 0-60 Hz) however they fall into the random vibration exposure frequency range too.

According to the design guidelines given in MIL-STD 810G for components to be installed onto helicopter platforms, an important requirement is to avoid a match or near match between resonant frequencies of installed components and dominant sinusoids of the rotating elements of the helicopter platform. From that point of view, according to Figure 3.26 it is obvious that the first and the second resonant frequencies of the radar antenna (the lowest resonant frequencies) are the most critical ones for installment the radar antenna structure onto an AH-64 helicopter platform.

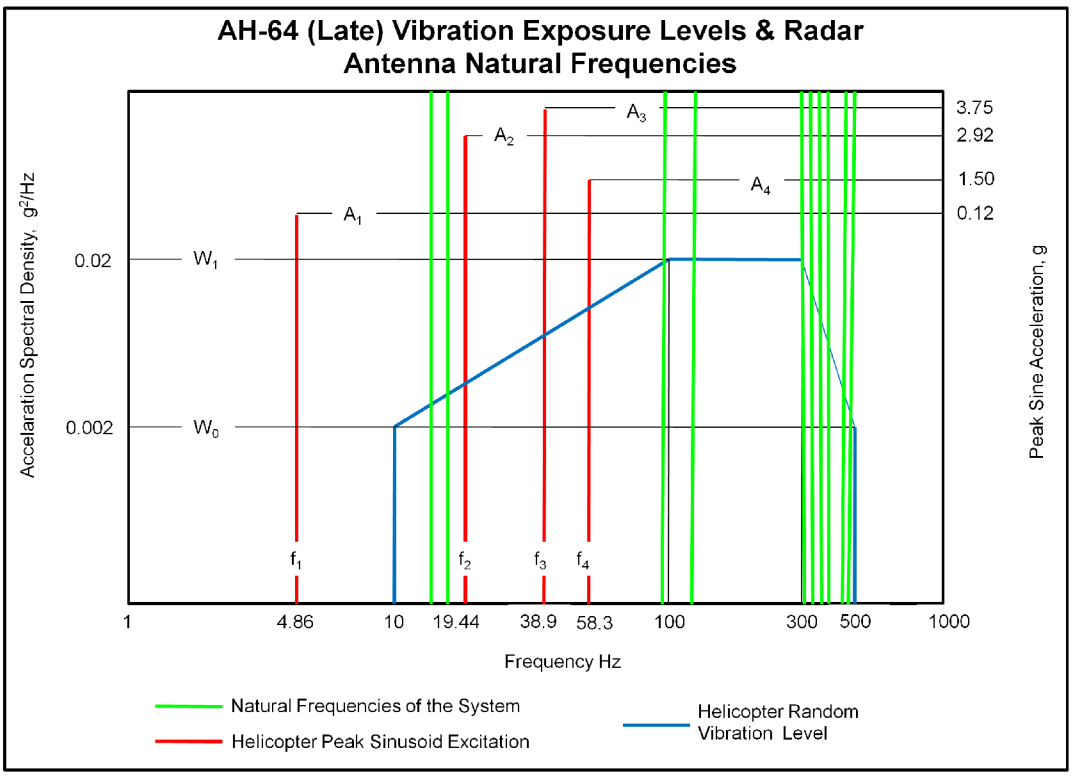

Figure 3.26 AH-64 vibration exposure levels and natural frequencies of the radar antenna structure.

For the radar antenna structure studied in this thesis, the main components of the mechanical vibration response which have adverse effects on antenna performance (on antenna gain) are the bending vibrations along *y*-axis which is the direction normal to the surface (Green Surface in Figure 3.27) where phased array antenna elements are located inside the box profile. Because of this fact, *y*-direction displacements of the points on the green surfaces can be considered as critical. Hence in addition to the critical natural frequencies of the radar antenna which are near match with the dominant source frequencies of the main rotor, the modal vibration response in *y*-direction of the points laying on green surfaces should be investigated.

Based on the discussions above, the ratio between difference of maximum and minimum displacement of a certain mode shape in the direction normal to the phased array antenna elements which is the *y*-direction at the locations where they are mounted and absolute value of maximum total displacement of a certain mode shape of the whole antenna structure can be determined. This will be useful for evaluating how important are deformation of the surfaces on which antenna elements and how critical the natural frequency that is being considered. For this purpose Table 3.4 is prepared which presents numerical values for the described displacement ratio which is the factor $\boldsymbol{k}$ calculated as follows,

$$k_i = \left[\frac{(y_{\max} - y_{\min})}{|d_{tot}|} \right]_i \tag{3.1}$$

where $\boldsymbol{y_{max}}$ and $\boldsymbol{y_{min}}$ are the maximum and minimum displacement of ith mode shape in the direction normal to the phased array antenna elements (*y*-direction), respectively and $\boldsymbol{d_{tot}}$ is the maximum total displacement of ith mode shape of the whole antenna system. By the use of factor $\boldsymbol{k}$, bending vibrations in the direction normal to green surface (Figure 3.27) can be investigated and their contributions to the displacement energy of the corresponding mode shape of the antenna can also be examined. Only, resonant frequencies in the range of 0-500 Hz are considered for factor $\boldsymbol{k}$ calculations.

From Table 3.4, the second, third and sixth mode shapes are critical according to the factor $\boldsymbol{k}$. It is seen that maximum value for $\boldsymbol{k}$ is 1.54 for the 6th mode shape and therefore in this mode, the bending vibrations of green surface (Figure 3.27) are much more dominant than the 2nd and 3rd modes. However the 6th natural frequency (300.4Hz) and also the 3rd natural frequency (96.5Hz) are far away from dominant sinusoid excitation range of the helicopter platform (0-60 Hz). Hence 2nd mode shape can be considered as critical for non-reinforced (original) radar antenna structure according to the factor $\boldsymbol{k}$ in Table 3.4.

It should be noted that depending on structure of the radar antenna and boundary conditions, the values of $\boldsymbol{k}$ and also the critical natural frequencies (first and second natural frequencies) of this antenna system can be changed.

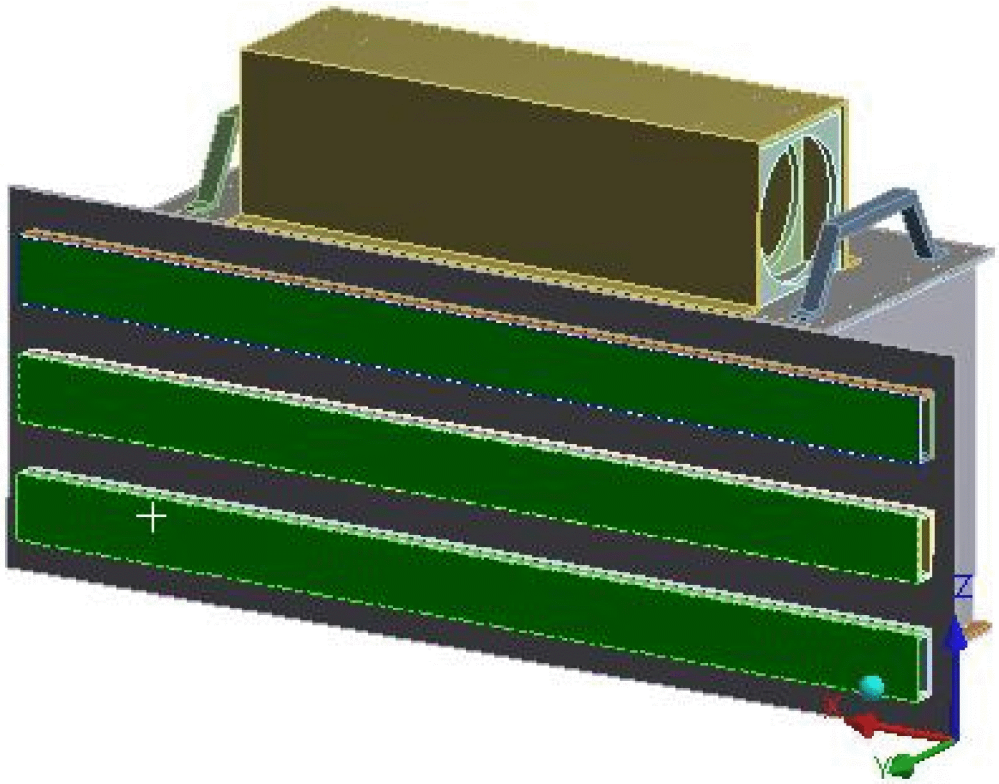

Figure 3.27 Surfaces those phased array antenna elements are located.

Table 3.4 Calculated k values of the radar antenna structure(factor k).

	Mode Shape 1	**Mode Shape 2**	**Mode Shape 3**	**Mode Shape 4**	**Mode Shape 5**	**Mode Shape 6**	**Mode Shape 7**	**Mode Shape 8**	**Mode Shape 9**	**Mode Shape 10**
y_{max}	0.0001	0.240	0.147	-0.001	0.061	0.490	0.064	0.020	0.023	0.0001
y_{min}	-0.006	0.026	0.015	-0.011	-0.047	-0.470	-0.056	-0.027	-0.025	-0.006
$\|d_{tot}\|$	0.436	0.429	0.496	5.052	4.900	0.623	1.869	3.244	4.311	2.787
k	0.014	0.500	0.266	0.002	0.022	1.540	0.065	0.015	0.011	0.002

3.5 RANDOM VIBRATION ANALYSIS OF RADAR ANTENNA

Generally military components are installed on platforms externally, such as helicopters, aircrafts or tanks. After the installation these components are exposed to environmental conditions and sources such as aerodynamic flow and random vibration exposure which is one of the most important environmental conditions. Therefore, in order to find response of the system under these conditions, random vibration analysis should be conducted.

ANSYS software enables user to determine the response of structures to vibration loads that are random in nature. In a random vibration analysis in ANSYS, the results such as displacements, acceleration, stresses etc. are statistical since the inputs are statistical in nature. In general it is assumed that the random vibration input data has a normal (Gaussian) distribution statistically [16].

In random vibration analysis option of ANSYS, inputs are applied to the system in the form of Power Spectral Density (PSD) functions which is a table of spectral values vs. frequency that captures the frequency content. The PSD captures the frequency and mean square amplitude content of the time history of load. The square root of the area under a PSD curve represents the root mean square (rms) value of the excitation. To perform a random vibration analysis in ANSYS the natural frequencies and corresponding mode shapes are also needed [23].

In this thesis study, PSD of the helicopter platform excitation given in MIL-STD 810G is used as the input for random vibration analysis. The platform excitation is defined as the acceleration PSD (in g^2 units) .The important point of this analysis is that the base excitation of platform is applied in the specified direction to all entities (nodes) that have a fixed support boundary condition. As explained before, radar antenna structure is installed on the AH-64 helicopter platform externally. Therefore the frequency range of interest (base excitation) is 10-500 Hz and random vibration level $\boldsymbol{W_0}$ is 0.002 g^2/Hz and $\boldsymbol{W_1}$ is 0.02 g^2/Hz, as shown in Figure 3.28. This random vibration input is applied to the surface of shaft connection defined as a fixed support boundary condition in Section 3.2 in each

axis (*x*-*y*-*z*) separately, than the output displacements (directional deformation normal to the green surface in Figure 3.27) are obtained for *y*-axis.

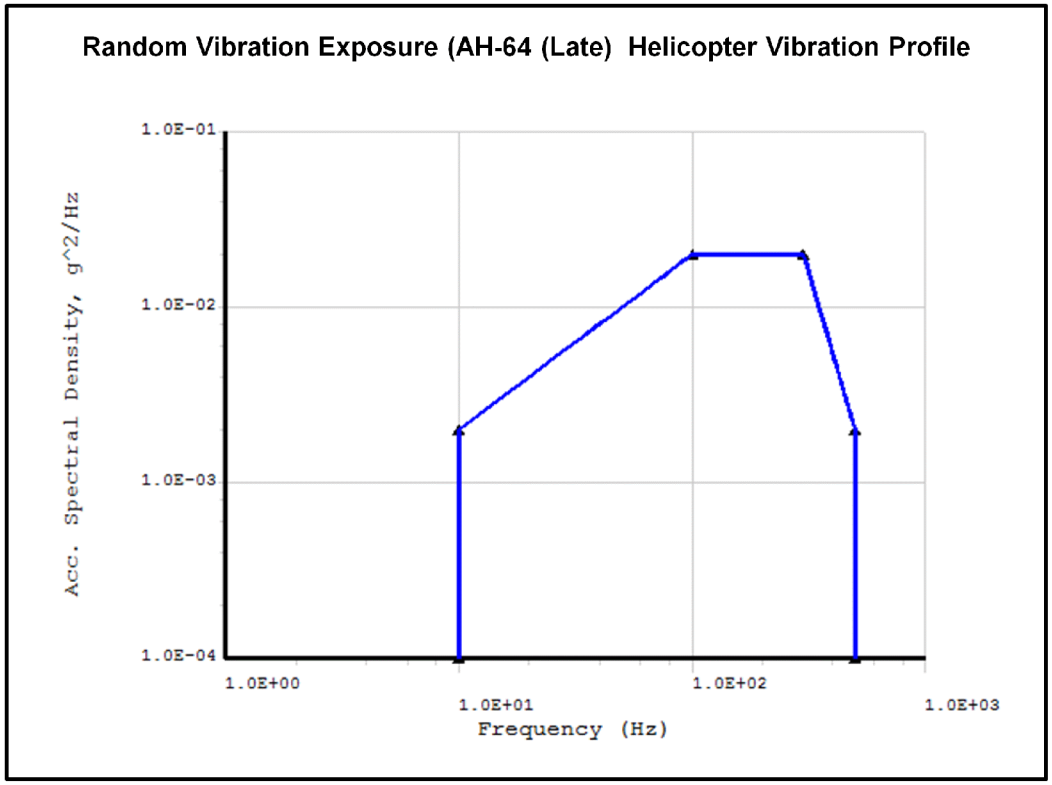

Figure 3.28 Random vibration input (AH-64 helicopter vibration profile) [16].

Since deformation in *y*-direction of the surfaces, on which the patch arrays are attached is critical, $(\boldsymbol{Y_{max} - Y_{min}})$ values (the difference between the maximum and the minimum deformation values of patch integrated surfaces in *y*-direction) should be investigated after random vibration analysis performed for each direction of platform (base) excitation. ANSYS results for PSD base excitation in each direction are given in Table 3.5 and Figures 3.29 through Figure 3.31 for surfaces (Green Surfaces in Figure 3.27) where phased array antenna elements are

attached. As expected, according to Table 3.5 the maximum value of ($\boldsymbol{Y_{max} - Y_{min}}$) is observed when the random vibration input is in *y*-direction and it is equal to $1.04 \cdot 10^{-3}$ m.

Table 3.5 Random vibration analysis results for original radar antenna structure (deformation in *y*-direction)

	Random Vibration Input in *x*-Direction	**Random Vibration Input in *y*-Direction**	**Random Vibration Input in *z*-Direction**
$\boldsymbol{Y_{max}}$ **(m)**	$7.52 \cdot 10^{-5}$	$1.16 \cdot 10^{-3}$	$8.92 \cdot 10^{-4}$
$\boldsymbol{Y_{min}}$ **(m)**	$6.50 \cdot 10^{-6}$	$1.23 \cdot 10^{-4}$	$9.55 \cdot 10^{-5}$
$\boldsymbol{Y_{max} - Y_{min}}$ **(m)**	$6.87 \cdot 10^{-5}$	$1.04 \cdot 10^{-3}$	$7.97 \cdot 10^{-4}$

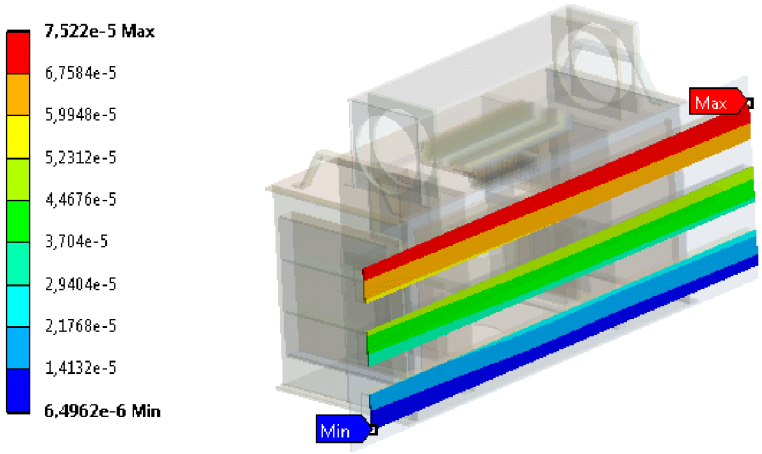

Figure 3.29 Directional displacement in *y*- direction for random input in *x*-direction (original radar antenna)

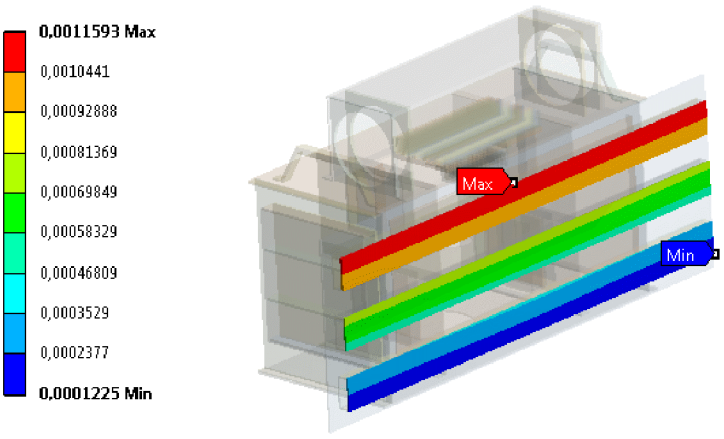

Figure 3.30 Directional displacement in *y*- direction for random input in *y*-direction (original radar antenna)

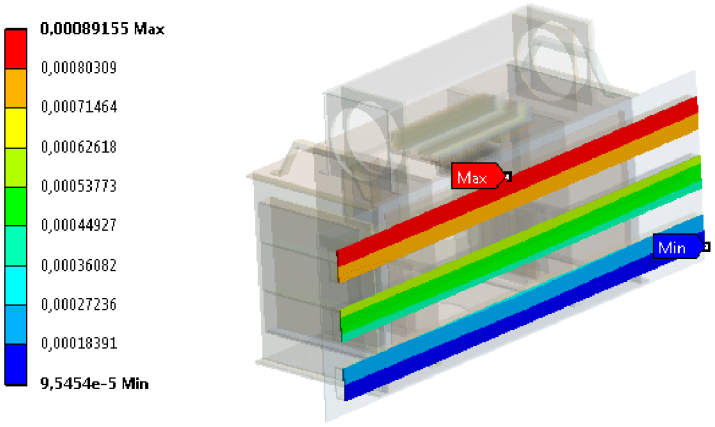

Figure 3.31 Directional displacement in *y*- direction for random input in *z*-direction (original radar antenna)

3.6 INTUITIVE DESIGN OF RADAR ANTENNA

Intuitively an initial material reinforcement design has been used to improve vibration characteristics of the original radar antenna structure. The geometry and location of this reinforcement is shown in Figure 3.32. In ANSYS, this reinforcement plate is modeled with SOLID95 elements with an element size 0.02 m. Total weight of the radar antenna structure with the reinforcement is 17 kg and the weight increase compared to the original radar antenna structure is 2.4%.

For this configuration the natural frequencies and corresponding $\boldsymbol{k}$ values are given in Table 3.6. It is seen that the first two natural frequencies are increased by approximately 100% - 200% but they are still in the dominant sinusoid range (0-60 Hz) of the helicopter platform which means that this configuration can still be affected adversely from helicopter vibration. Beside, some of other natural frequencies (3^{rd} – 8^{th} ones) are also increased and some of them remain as unchanged (9^{th} and 10^{th} ones).

For this intuitive reinforcement configuration, the k value of original radar antenna structure is decreased evidently for 6th mode shape (highest for the original configuration). In contrast, $\boldsymbol{k}$ value of 8th mode shape is increased considerably. Other changes in $\boldsymbol{k}$ values can be seen in Table 3.6.

The random vibration analysis results of intuitively reinforced configuration that is subjected to platform vibrations defined in Figure 3.32 and the improvements compared with the original radar antenna are given in Table 3.7. It is seen from Table 3.7 that the value of $(\boldsymbol{Y_{max} - Y_{min}})$ gets its maximum value of $3.71 \cdot 10^{-4}$ m) for random vibration input in y-direction and this shows that the value obtained for the original radar antenna structure is decreased by 64%. In addition to that the value of $(\boldsymbol{Y_{max} - Y_{min}})$ for random vibration input in z-direction decreases by 62% compared with the values obtained for the original radar antenna, on the other hand, for random vibration input in x-direction, $(\boldsymbol{Y_{max} - Y_{min}})$ increases by 68%.

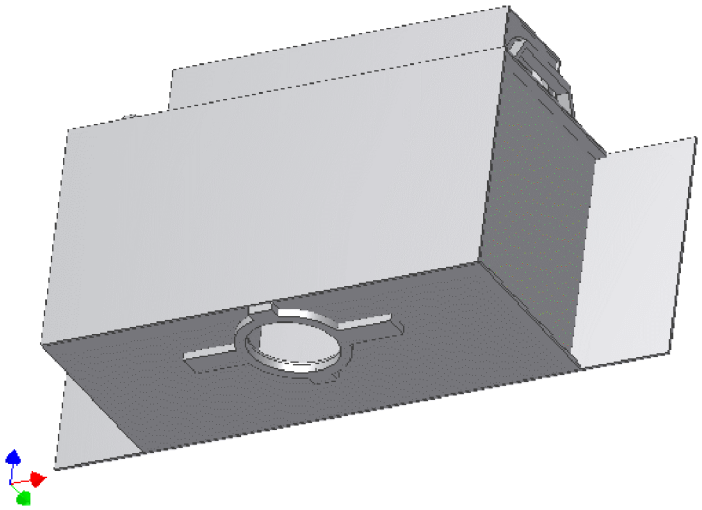

Figure 3.32 Intuitively reinforced radar antenna structure.

Table 3.6 Natural frequencies and corresponding k values of intuitively reinforced radar antenna structure.

Mode Shape	**1**	**2**	**3**	**4**	**5**	**6**	**7**	**8**	**9**	**10**
Frequency (Hz)	33.5	49	147.2	288.2	303.3	321	322.6	350	373.2	409
k	0.483	0.078	0.003	0.029	0.027	0.258	0.016	1.752	0.028	0.003

Table 3.7 Random vibration analysis results for intuitively reinforced radar antenna structure (deformation in y-direction).

	Random Vibration Input in x-Direction	**Random Vibration Input in y-Direction**	**Random Vibration Input in z-Direction**
Y_{max} **(m)**	$1.31 \cdot 10^{-4}$	$4.15 \cdot 10^{-4}$	$3.40 \cdot 10^{-4}$
Y_{min} **(m)**	$1.59 \cdot 10^{-5}$	$4.43 \cdot 10^{-5}$	$3.70 \cdot 10^{-5}$
$Y_{max} - Y_{min}$ **(m)**	$1.15 \cdot 10^{-4}$	$3.71 \cdot 10^{-4}$	$3.03 \cdot 10^{-4}$
Improvement (%)	-68	64	62

CHAPTER 4

OPTIMIZATION STUDIES

In this study topology optimization and stiffener parameter optimization techniques are employed by using ANSYS software to modify the design of the radar antenna structure such that critical natural frequencies are shifted out of the base vibration exposure range (0-500 Hz) of AH-64 helicopter platform.

Firstly topology (Case-1) and stiffener (Case-2) optimizations are performed separately. Then a combination of these two techniques (Case-3) is carried out and finally all the optimization results are studied to find the optimum design solution such that the adverse affects of helicopter platform on the vibration characteristics of the radar antenna structure are eliminated.

4.1 SELECTION OF DESIGN SPACE

For topology optimization, design space is the region for which optimization of the material distribution (optimization of pseudo densities, ρ_e) is done and this region can also be considered as a design area for stiffener parameter optimization. In other words design space is the allowable volume or area within or on which the design modifications can be performed.

While choosing this design space certain constraints related with design should be taken into account. Two of the important constrains are the maximum weight of the material that will be added to the original radar antenna structure and the permissible locations of the reinforcements. Regions or space in the model that

cannot be modified during the course of the optimization are considered as non-design regions.

Investigating the modal mechanical strain distribution of the radar antenna structure in its original non-reinforced configuration is a way to identify the most effective design space to be used in topology optimization and stiffener parameter optimization. It makes sense to reinforce regions that are subject to the most deformation energy for a particular vibration mode. Mechanical strain can be utilized as a relative measure of strain energy. Regarding this purpose von Mises mechanical strain of the critical modes of interest (first and second modes) of the original radar antenna defined in Chapter-3 are examined in ANSYS and they are also shown in Figure 4.1. In Figure 4.1 it is seen that the maximum strain occurs on bottom plate of the antenna. Therefore material and stiffener reinforcement should be done on the bottom plate of the antenna. It should be kept in mind that inner parts of the radar antenna cannot be modified or reinforced by additional material or stiffener because electronic devices and units are located in the inner part of the radar antenna structure that restricts any change or modification inside the system. Due to these design constraints design space can be only be selected amongst the outer region of the radar antenna structure except for the bottom plate. The inner side of the bottom plate can be utilized for design space since the use of middle region of the inner part of the bottom plate does not affect the configuration of the electronic devices inside the radar antenna structure.

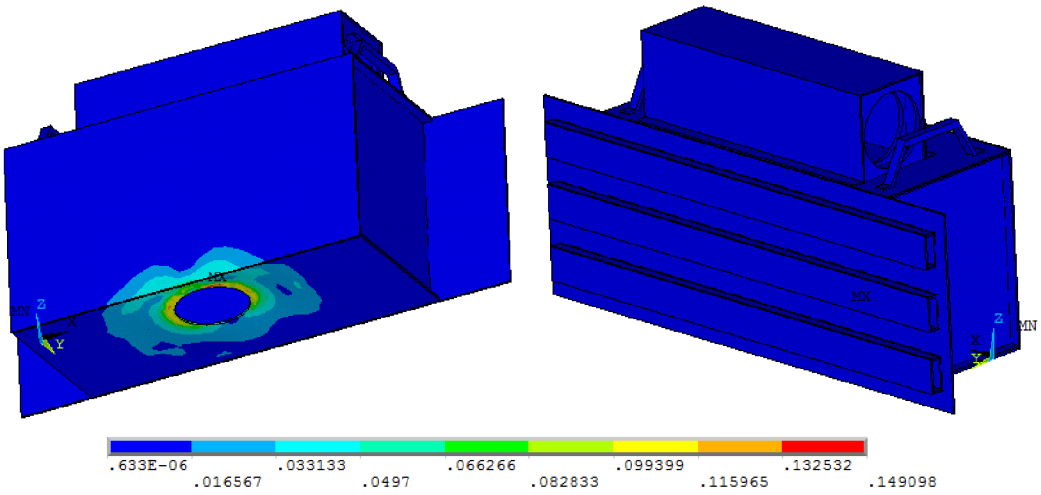

a) von Mises mechanical strain of 1st mode shape.

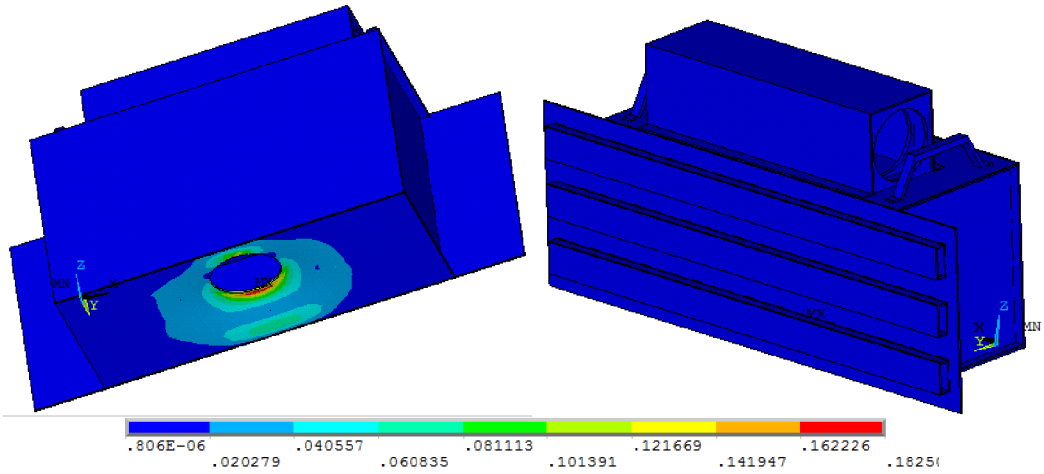

b) von Mises mechanical strain of 2nd mode shape.

Figure 4.1 von Mises mechanical strain (a-b) of the critical modes (1st and 2nd modes) (dimension in m).

4.2 CASE 1: TOPOLOGY OPTIMIZATION

The purpose of topology optimization is to find the best material distribution of the system. The main purpose is maximizing or minimizing the objective function (stiffness of the system, natural frequency etc.) under certain constraints such as total volume reduction. For this part of the optimization study performed in this thesis (CASE-1) topology optimization module of the ANSYS software is used.

4.2.1 Topology Optimization Parameters

Topology optimization parameters consist of design space, design constraint and an objective function as it is mentioned in Chapter 2. In this work the aluminum plates, which are shown in blue colors in Figure 4.2 and Figure 4.3, are added to the original radar antenna structure. In ANSYS, these aluminum plates are also modeled as three dimensional SOLID95 elements which have 20 nodes including midside nodes with an element size 0.02 m. All nodes laying on the contact surfaces of aluminum plates are used for attaching the plates to the FEM of the original radar antenna structure resulting in a rigid connection. These added volumes will serve as the design space which is also be made up of the same material as the original radar antenna structure. The first design space is denoted as DS1 and the thicknesses of this plate like added design volumes plates are all 5 mm. Actually this thickness is selected arbitrarily to find the material distribution characteristics of the determined design space with topology optimization in ANSYS. In other words how additional material can be used effectively within a fixed design space (or fixed thickness of the added plates) after optimization for maximizing the identified critical natural frequency. For other design spaces (DS2, DS3 and DS4) the material and thickness of the plates are the same with DS1. The only difference is the orientation and the size of the plates used as a design space. DS2 has two plates, DS3 has one plate and DS4 has two plates shown in Figures 4.2-4.3. Once a satisfactory material distribution is reached through topology optimization, thicknesses of the added plates will also be optimized such that the

maximum added mass due to added reinforcements reaches the limiting value, which is 20% of the mass of the original radar antenna structure.

As it is mentioned in Chapter 3, the most critical natural frequencies are first and second ones. In this study maximization of the first natural frequency of the radar antenna structure is selected as the objective function. After the design space and the objective function are determined, another important parameter which is the design constraint of the topology optimization in ANSYS must be selected. Three topology optimizations are performed for volume reduction constraints of 30%, 50% and 75% for each specified design spaces for maximizing the first natural frequency. Hence, twelve set of results are obtained from topology optimization runs that are performed in ANSYS. The error tolerances used for objective function and volume constraint checking for all topology optimization cases is 10^{-3} and all of the optimizations given in this study are converged with respect to these defined criteria.

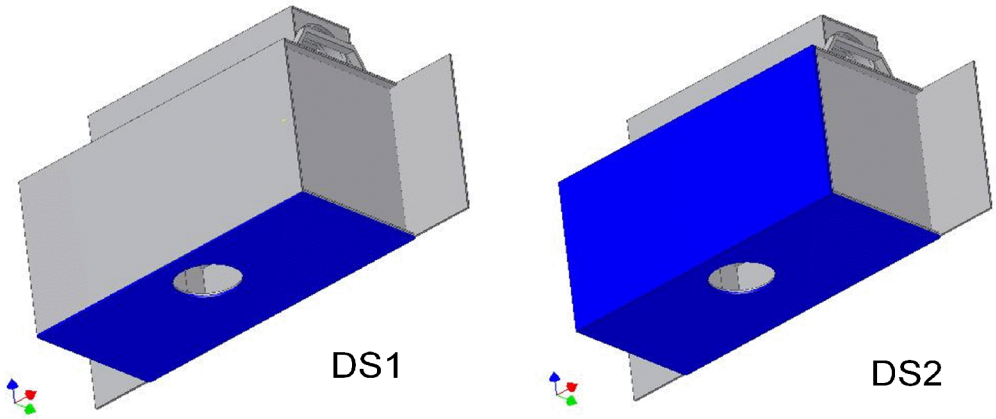

Figure 4.2 Design spaces (DS1 in left and DS2 in right) that will be used for topology optimization (in blue colors).

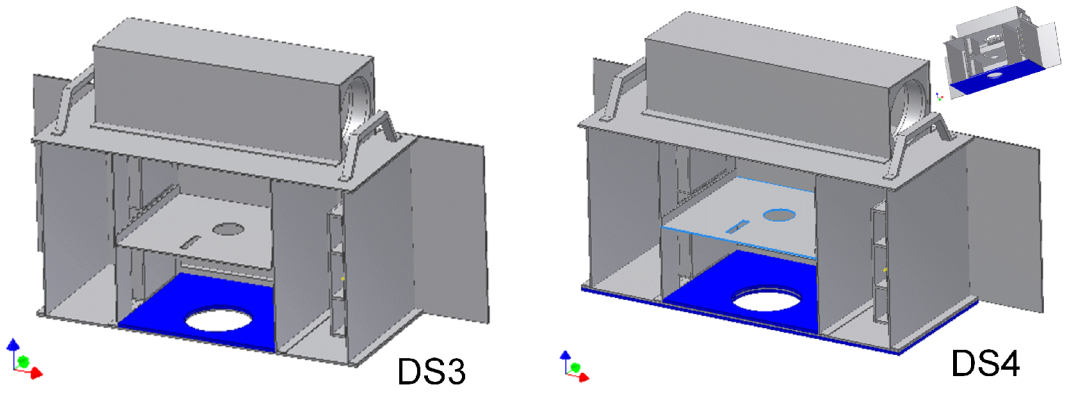

Figure 4.3 Design spaces (DS3 in left and DS4 in right) that will be used for topology optimization (in blue colors).

4.2.2 Topology Optimization Results

The results of topology optimization for the first natural frequency maximization can be seen in Figures 4.4, 4.5, 4.6 and 4.7 for cases DS1, DS2, DS3 and DS4, respectively. For each design space configuration, optimization is performed for design constraints of 30%, 50% and 75% of volume reduction in the optimized topologies.

As it is seen from the topology optimization results that elements having a pseudo density value around 1.0 ($\rho_e \approx 1.0$) are in red colors and elements having a pseudo density value around 0 ($\rho_e \approx 0$) are in blue colors. Therefore, it can be understand from Figures 4.4, 4.5, 4.6 and 4.7, that elements which must be kept (red colors) in design space and which must be removed (blue colors) from design spaces (denoted as DS1, DS2, DS3 and DS4 respectively) to maximize the objective function.

According to the topology optimization results based on 30%, 50%, and 75% volume reduction in design space configurations of DS1, DS2, DS3 and DS4, the

structure of the reinforced material that can be added to the original radar antenna are given in Figure 4.8, 4.9, 4.10 and 4.11 (proposed reinforcement plates are shown in blue color in these figures). In these figures, topology optimization results are designated as a name which indicates the specifications of the optimization. For instance, "Topo_DS1 %30" means that this is the reinforcement plate(s) designed based on the topology optimization ("Topo") using design space ("DS1") with a design space volume reduction constraint of 30%.

While deciding the shape of the reinforcement material according to the corresponding topology optimization results, manufacturing convenience of the reinforcement is also taken into account. It should be noted that these reinforcement plates are rigidly connected to the original FEM; hence, they should be milled out from a thicker plate which will reflect the analysis exactly or they should be attached by spot welding or the use of rivets which may result in discrepancy between the simulations and the actual case. Moreover, the use of arc or gas welding techniques is not appropriate for the reinforced radar antenna structure, since they do not reflect the simulations presented in this study.

The natural frequencies of the reinforced antenna structures are given in Table 4.1, and Figure 4.12. Furthermore corresponding $\boldsymbol{k}$ values are given in Table 4.2, and Figure 4.13. It should be noted that between 0-500 Hz total mode shape number for each reinforced radar antenna configuration may vary.

According to the Table 4.1, and Figure 4.12 the usage of material distribution of the design space after topology optimization performed in ANSYS increases the first and the second natural frequencies of the original system to higher values. The percentage of increase in first and the second natural frequencies is the highest one compared with other modes. For example from Table 4.1 it is seen that in general the first two natural frequencies are increased more than 300%, the 3rd and the 4th ones are increased more than 50%, the 6th, the 8th, the 9th and the 10th ones are increased by approximately 10%, the 5th and the 7th ones remained the same as the natural frequencies of the original radar antenna.

From Figure 4.12 the reinforcement plate is designed based on topology optimization results of DS4 with 30% percent volume reduction (i.e. configuration "Topo_DS4 %30") is the most effective reinforcement solution for low frequency mode shapes such that the first and the second natural frequency values get their maximum values for this configuration as compared to other reinforcement plate configurations (see Table 4.1 and Figure 4.12). It should be noted that the same configuration is not as effective for high frequency mode shapes as it is for the lowest two frequencies while all frequencies are still increases.

In Table 4.1, for each reinforcement plate configuration total final weight of the modified radar antenna structure and added weight of the reinforcement plates are also given (in addition to the modal frequencies of the modified structures that fall in the frequency range of 0-500 Hz). Investigating the modal frequency increases and corresponding weight increases for all reinforcement configurations, it is concluded that the "Topo_DS4 %30" configuration is the optimum solution. It is obvious that from topology optimization results for design spaces DS1 and DS2, the use of bottom plate is much more efficient than back plate for maximizing the fundamental natural frequency of the system. Therefore the best material distribution is obtained from DS4 which is in fact the combination of design spaces DS1 and DS3. In addition to that reinforced radar antenna configuration ("Topo_DS1 %75") which has same weight as the intuitively reinforced antenna gives better results compared with the intuitive design such that the first natural frequency is 40.1 Hz for "Topo_DS1 %75" configuration however it is 33.5 Hz for intuitive design. Calculated k values for all reinforcement configurations at the natural frequencies are shown in Table 4.2, and Figure 4.13. Reinforcements designed based on topology optimization, causes k values of some of mode shapes to decrease but for some of the modes k values increase. For the sixth mode shape, k value decreases for the reinforced radar structures while original radar antenna design has the highest $\boldsymbol{k}$ value for its sixth mode compared to its other modes. In contrast for the reinforced designs, $\boldsymbol{k}$ values of the last two mode shapes (the 9^{th} or the 10^{th} mode shape) are increased considerably compared to the original radar antenna design. For the reinforcement configuration of "Topo_DS4 %30" there is an increase in $\boldsymbol{k}$ value for the first mode shape and $\boldsymbol{k}$ value for the second mode

shape remains the same compared with ***k*** value of the original radar antenna for its second mode. On the other hand if the frequency range out of dominant peak sinusoids is considered (60-500 Hz), the ***k*** values of "Topo_DS4 %30" configuration are much lower than the ***k*** values of other configurations, since the natural frequencies of "Topo_DS4 %30" configuration are shifted out of the frequency range of 0-60 Hz.

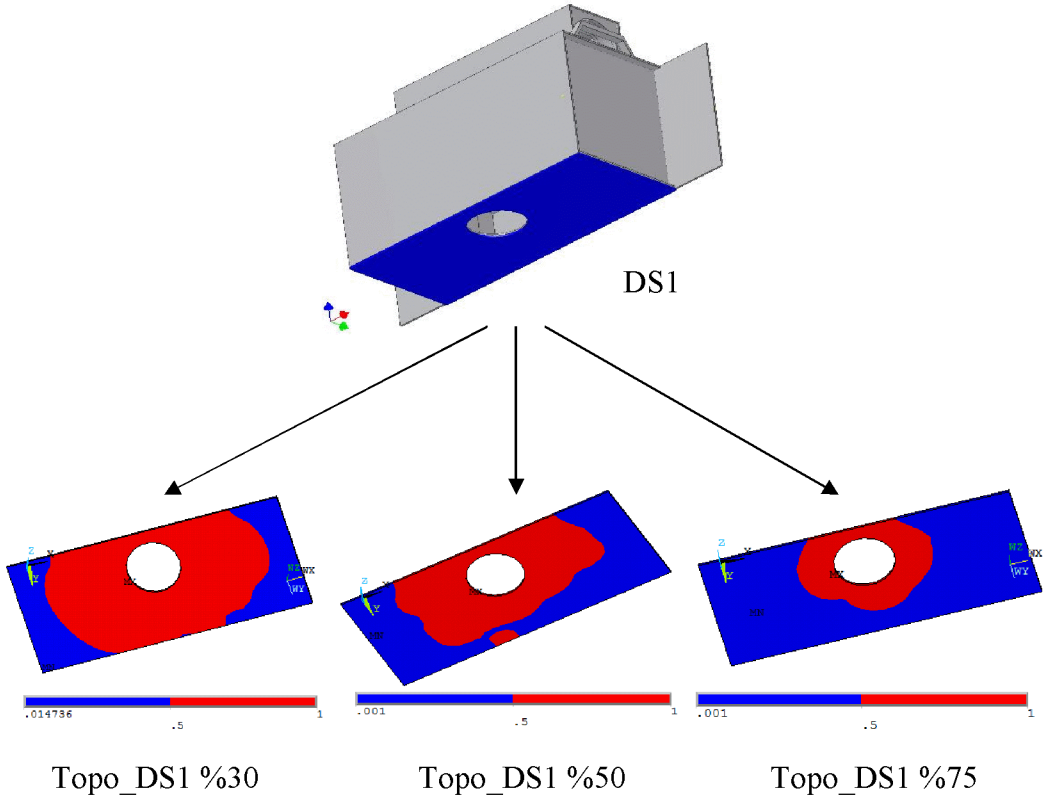

Figure 4.4 Topology optimization results for volume reduction (30%, 50% and 75% respectively) in design space (DS1) to maximize the first natural frequency.

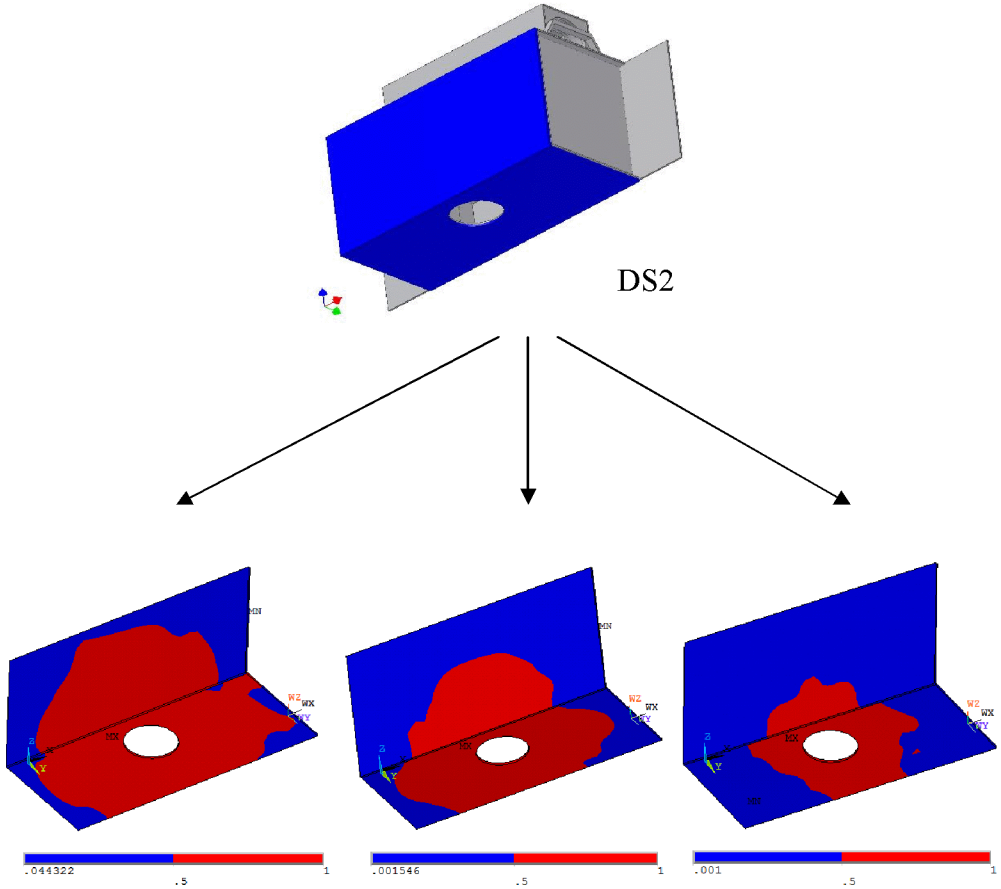

Figure 4.5 Topology optimization results for volume reduction (30%, 50% and 75% respectively) in design space (DS2) to maximize the first natural frequency.

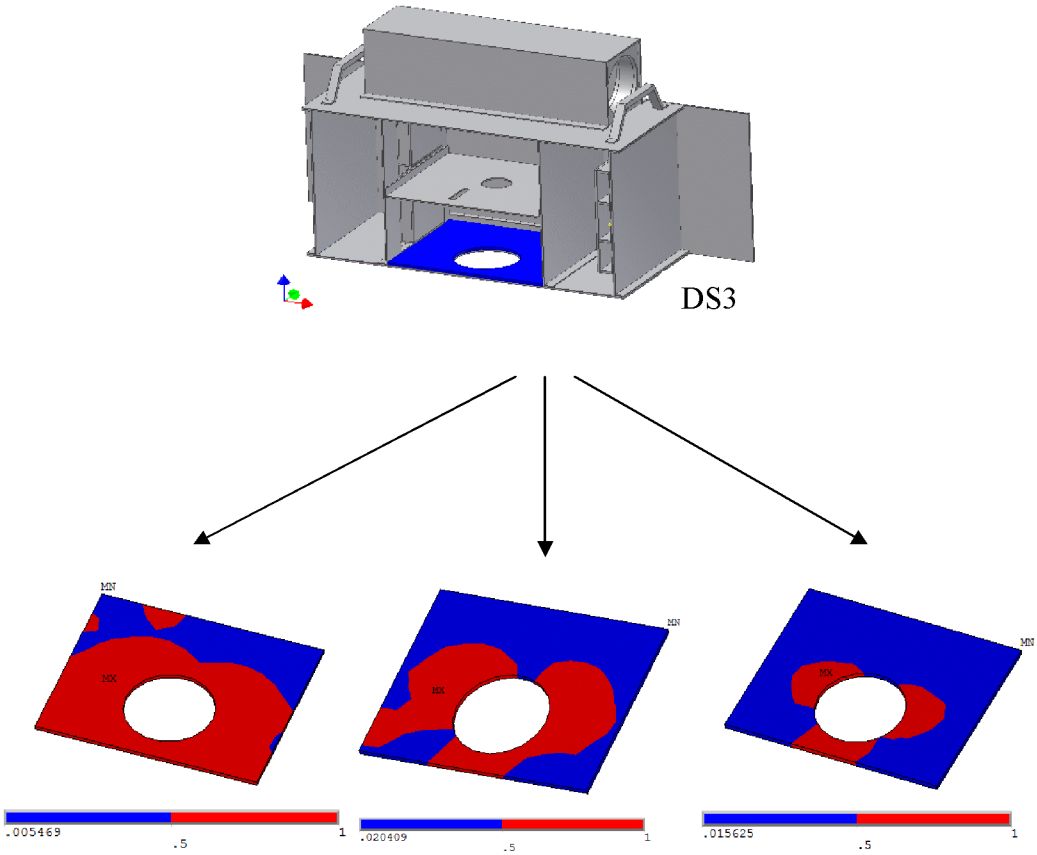

Topo_DS3 %30 Topo_DS3 %50 Topo_DS3 %75

Figure 4.6 Topology optimization results for volume reduction (30%, 50% and 75% respectively) in design space (DS3) to maximize the first natural frequency.

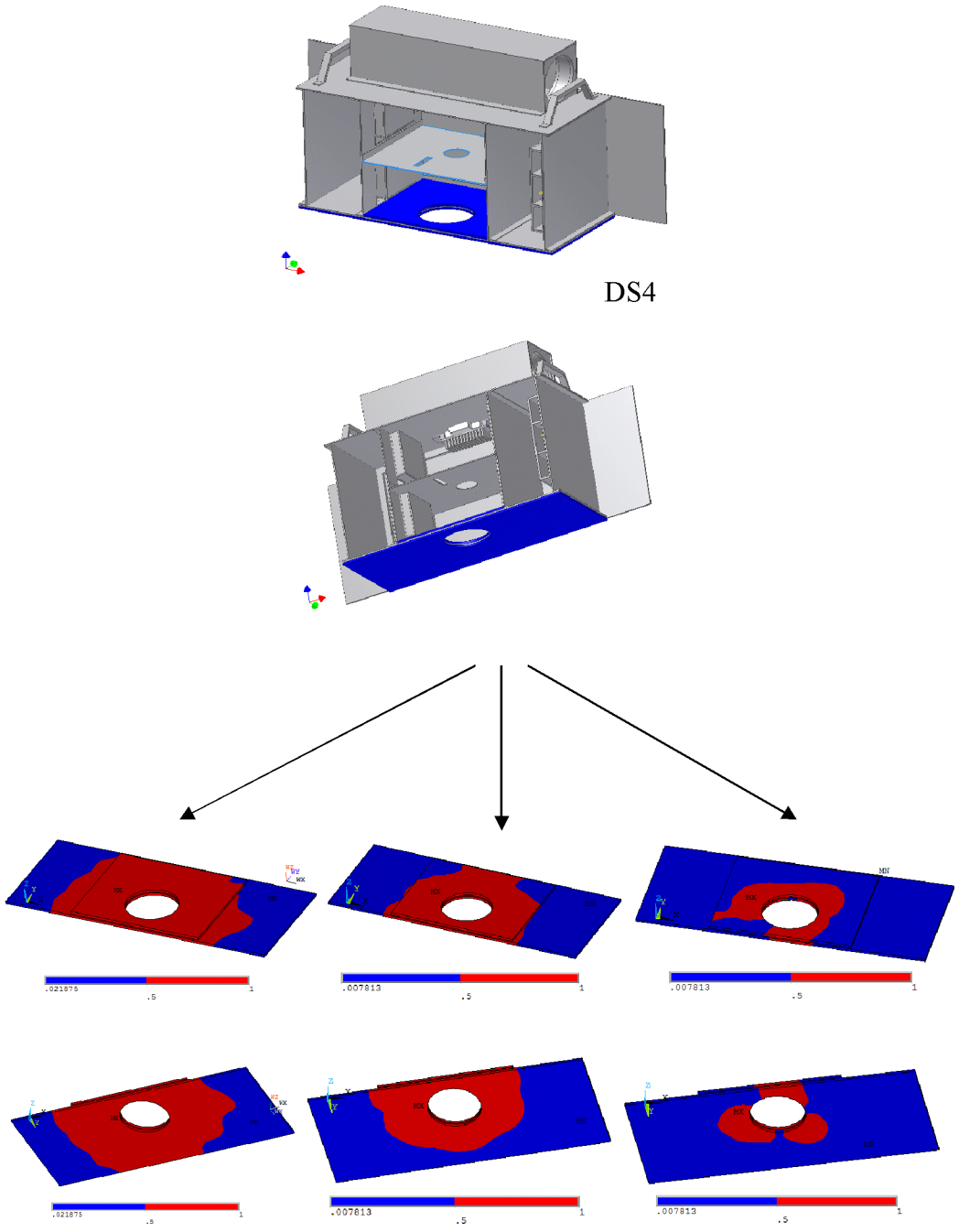

Figure 4.7 Topology optimization results based on volume reduction (30%, 50% and 75% respectively) in design space (DS4) to maximize the first natural frequency.

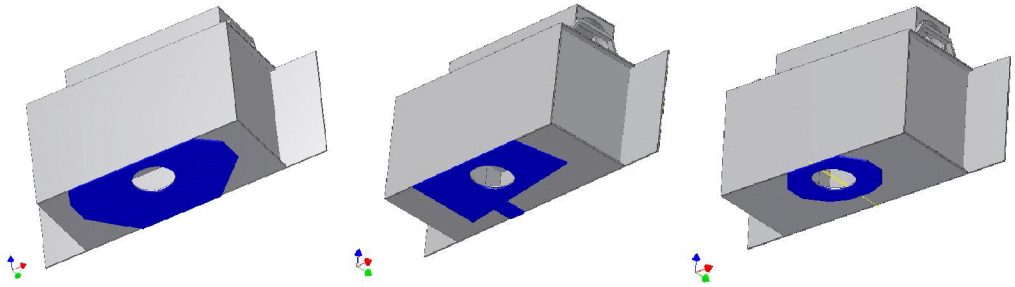

Figure 4.8 Reinforcement (blue color) according to the topology optimization results for volume reduction (30%, 50% and 75% respectively) in design space (DS1) to maximize the first natural frequency.

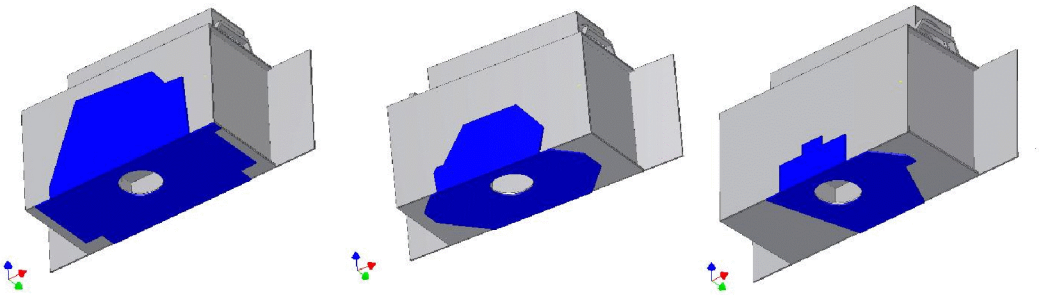

Figure 4.9 Reinforcement (blue color) according to the topology optimization results for volume reduction (30%, 50% and 75% respectively) in design space (DS2) to maximize the first natural frequency.

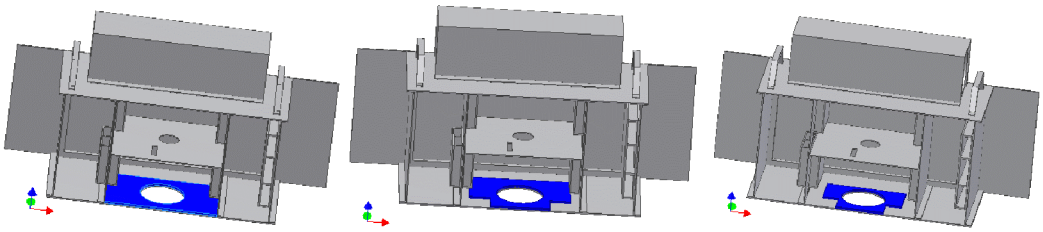

Figure 4.10 Reinforcement (blue color) according to the topology optimization results for volume reduction (30%, 50% and 75% respectively) in design space (DS3) to maximize the first natural frequency.

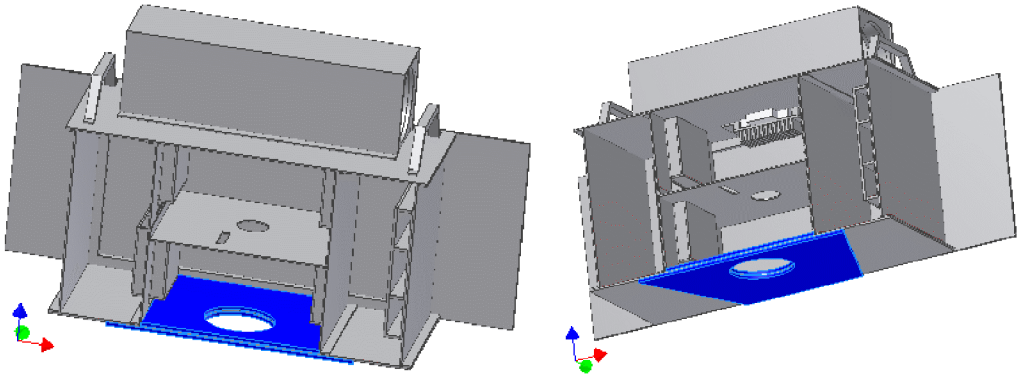

a)

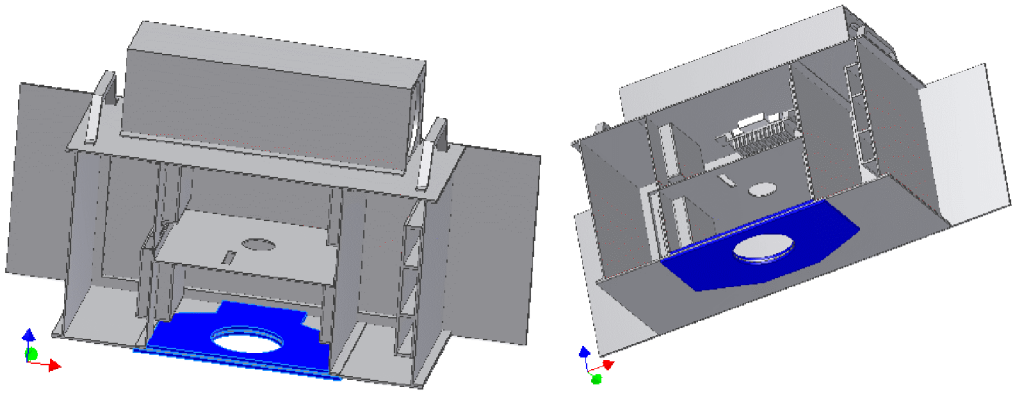

b)

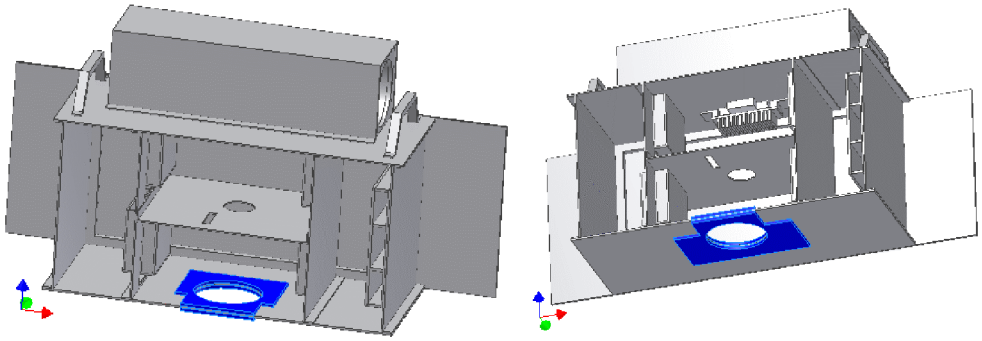

c)

Figure 4.11 Reinforcement (blue color) according to the topology optimization results based on volume reduction (30% (a), 50% (b) and 75% (c)) in design space (DS4) to maximize the first natural frequency.

Table 4.1 Natural frequencies of radar antenna structure for different reinforced configurations and the corresponding weight of the radar antenna structures (CASE-1). (Hz)

	Mode Shape 1	Mode Shape 2	Mode Shape 3	Mode Shape 4	Mode Shape 5	Mode Shape 6	Mode Shape 7	Mode Shape 8	Mode Shape 9	Mode Shape 10	Total Weight (kg)	Total Weight Increase %
Original Radar Antenna	14.7	16.2	96.5	148.1	296.6	300.4	320.0	322.5	372.8	409.0	16.6	-
Topo_DS1 %30	53	58.6	147.2	282	300.9	323.1	324.8	373.3	408.8	438.4	17.7	6.6
Topo_DS1 %50	46.7	51.7	147.2	278.8	300	322.8	324.6	373.2	408.9	418.8	17.4	4.8
Topo_DS1 %75	40.1	46.8	147.2	274.3	299.2	320.4	322.7	372.6	400	409.1	17	2.4
Topo_DS2 %30	55.4	59.6	147.8	296.4	310.8	326	327.2	373.7	410.4	447.5	19.3	16.3
Topo_DS2 %50	55	59.2	147.7	288	307.1	324	325.9	373.7	409	447.9	18.4	10.8
Topo_DS2 %75	53	57.6	147.3	288.9	308.7	320.8	322.8	373	409	436.4	17.6	6.0
Topo_DS3 %30	39.2	50.6	147.3	276.3	300	322.3	341.8	377.4	406.9	409.675	17.8	2.9
Topo_DS3 %50	40	45.8	147.2	267.2	298.7	320.2	322.6	372.4	394.8	409	17	2.4
Topo_DS3 %75	29	38.1	147.3	260.1	298.3	319.8	322.6	364.4	374	409	16.8	1.2
Topo_DS4 %30	94	99.5	147.6	296.6	322.5	345.6	379.4	404.7	416	>500	18.2	9.6
Topo_DS4 %50	88.5	92.2	147.5	296.6	322.5	342	377.8	401	413	489.4	17.8	7.2
Topo_DS4 %75	46	59.4	147.4	147.4	362.7	296	320.2	372.8	409.3	417.6	17.1	3.0

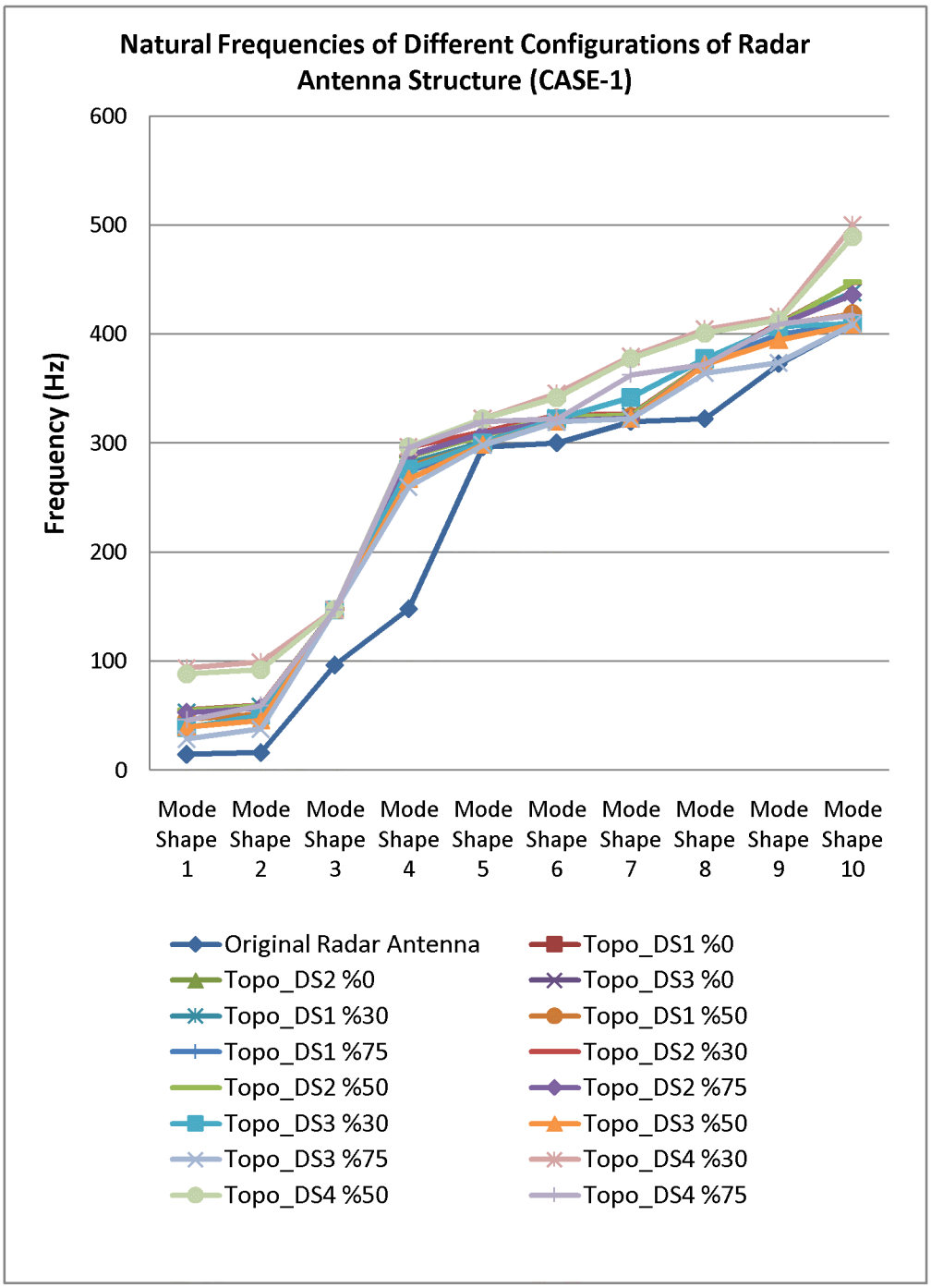

Figure 4.12 Natural frequencies of different reinforced radar antenna structures (CASE-1).

Table 4.2 Calculated k Values of Different Configuration of the Radar Antenna Structures (CASE-1).

	Mode Shape 1	**Mode Shape 2**	**Mode Shape 3**	**Mode Shape 4**	**Mode Shape 5**	**Mode Shape 6**	**Mode Shape 7**	**Mode Shape 8**	**Mode Shape 9**	**Mode Shape 10**
Original Radar Antenna	0.014	0.500	0.266	0.002	0.022	1.540	0.065	0.015	0.011	0.002
Topo_DS1 %30	0.030	0.509	0.003	0.053	0.018	0.014	0.008	0.008	0.012	1.747
Topo_DS1 %50	0.460	0.156	0.003	0.009	0.013	0.014	0.008	0.013	0.024	1.719
Topo_DS1 %75	0.469	0.069	0.003	0.088	0.011	0.017	0.015	0.022	1.754	0.025
Topo_DS2 %30	0.083	0.481	0.003	0.024	0.032	0.011	0.011	0.008	0.003	1.719
Topo_DS2 %50	0.042	0.507	0.003	0.047	0.018	0.013	0.007	0.008	0.003	1.723
Topo_DS2 %75	0.191	0.440	0.003	0.027	0.036	0.017	0.012	0.010	0.010	1.729
Topo_DS3 %30	0.488	0.035	0.003	0.067	0.011	0.015	0.011	0.032	1.731	0.020
Topo_DS3 %50	0.495	0.039	0.003	0.092	0.008	0.019	0.015	0.028	1.721	0.007
Topo_DS3 %75	0.481	0.036	0.004	0.108	0.006	0.030	0.014	0.617	0.092	0.003
Topo_DS4 %30	0.118	0.503	0.004	0.002	0.013	0.003	0.005	0.057	0.079	-
Topo_DS4 %50	0.413	0.279	0.004	0.002	0.014	0.005	0.007	0.095	0.042	1.729
Topo_DS4 %75	0.482	0.038	0.003	0.003	0.014	0.015	0.209	0.013	0.033	1.730

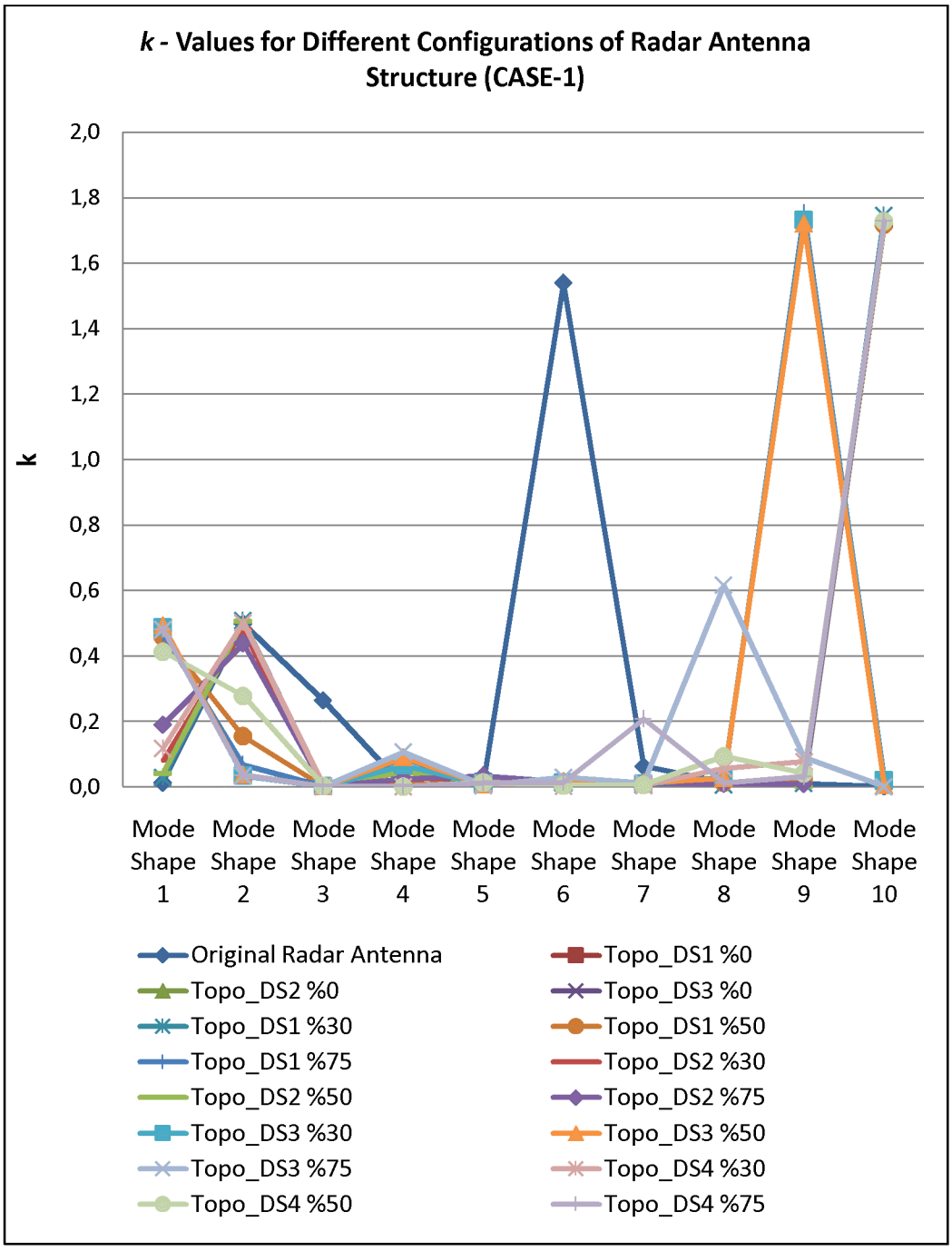

Figure 4.13 ***k*** values of mode shapes for different reinforced radar antenna structures (CASE-1).

4.2.3 Parameter Optimization on the Reinforcement Plates Designed Using Topology Optimization Results

Following the design of reinforcement plates based on topology optimization runs, the thicknesses of the reinforcement plates are optimized using the design parameter optimization module of ANSYS for the objective of maximizing the critical natural frequency. The maximum total weight of the system cannot exceed 20 kg i.e. maximum weight of the additional material integrated to the radar antenna system after the topology optimization must be around 3.4 kg. This weight limit is defined as a design constraint in the thickness optimization runs in ANSYS.

It should be kept in mind that the material distribution (reinforcement plate geometries) of the design space is identified from topology optimization to maximize the critical natural frequencies of the original radar antenna system. The reinforcement plate designed base on the topology optimization results for 30% volume reduction in design space DS4 with the objective of maximizing the first natural frequency (Reinforced Antenna "Topo_DS4 %30") give us the highest frequencies for the first two mode shapes of the radar antenna. Therefore, this reinforcement plate is chosen for the thickness optimization such that we reach the limit of added mass thus we can reach to the highest potential for the designed reinforcement (highest possible increase in critical natural frequencies).

Design variables of parameter optimization process shown in Figure 4.14 are the thickness values of the reinforcement plates from topology optimization results Topo_DS4 %30. The initial value of $\boldsymbol{t_1}$ and $\boldsymbol{t_2}$ are 5 mm which is used in the previous topology optimizations performed in ANSYS.

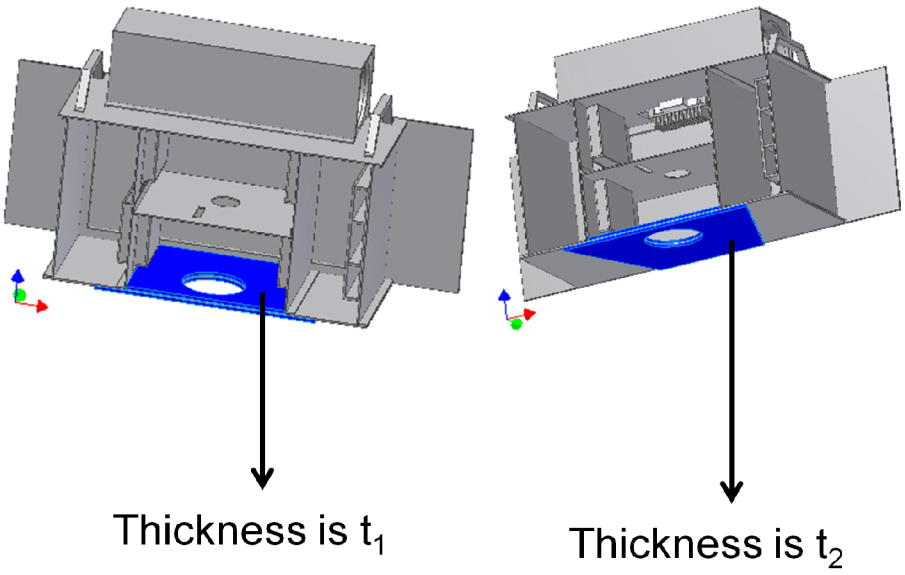

Figure 4.14 Design variables of parameter optimization in ANSYS.

Design constraint of the system is that the maximum weight must not be exceeded. The available maximum total weight is given as approximately 20 kg. Therefore the range of the design constraint variable (Total weight of the radar antenna structure) is specified between 0 and 20 kg in design optimization module of ANSYS i.e. 0 < total weight < 20 kg.

For the thickness optimization, the objective function is the same as the one in topology optimization runs that is maximizing the first natural frequency of the original radar antenna system. Hence for the design optimization problem defined in ANSYS the objective function is defined as the reverse of the first natural frequency of the reinforced system (Reinforced Antenna "Topo_DS4 %30") i.e. 1/ (First natural frequency). By doing this, the first natural frequency can be maximized as a result of the ANSYS design optimization run.

As the design optimization method, both first order method and sub-problem approximation methods are used in ANSYS for optimizing the thickness of the reinforcement plates used in configuration Topo_DS4 %30. It turns out that both methods are converged and give the same thickness results as shown in Table 4.3.

The tolerance value used in design optimization is "10^{-3}·(Current value)" for the objective function, design variables and constraints. Natural frequencies and corresponding $\boldsymbol{k}$ values obtained for the final design reached at the end of the optimization run are given in Table 4.3. Computer Aided Design (CAD) model images of the final configuration of the modified radar antenna structure are given in Figure 4.15 and Figure 4.16.

The mode shapes that fall between 0-500 Hz for the final configuration of the modified radar antenna structure are given in Figures 4.17 through 4.24. It is seen that the first and the second natural frequencies of the original radar antenna system are shifted out of the dominant sinusoid range (approximately 0-60 Hz) of the helicopter platform. Furthermore between 0-500 Hz there is no mode shape having high $\boldsymbol{k}$ values (when compared with $\boldsymbol{k}$ values of the original radar antenna configuration).

Table 4.3 Parameter (design) optimization results.

	Initial	**Final**
$\boldsymbol{t_1}$ **(mm)**	5	2.2
$\boldsymbol{t_2}$ **(mm)**	5	15.9
Total Weight (kg)	18.2	19.7

Table 4.4 Natural frequencies and $\boldsymbol{k}$ values of reinforced radar antenna structure after parameter (design) optimization is performed.

Mode Shape	**1**	**2**	**3**	**4**	**5**	**6**	**7**	**8**
Frequency (Hz)	146.7	161.5	172	296.4	322.7	328.1	374	408.3
$\boldsymbol{k}$	0.006	0.169	0.351	0.001	0.013	0.002	0.002	0.007

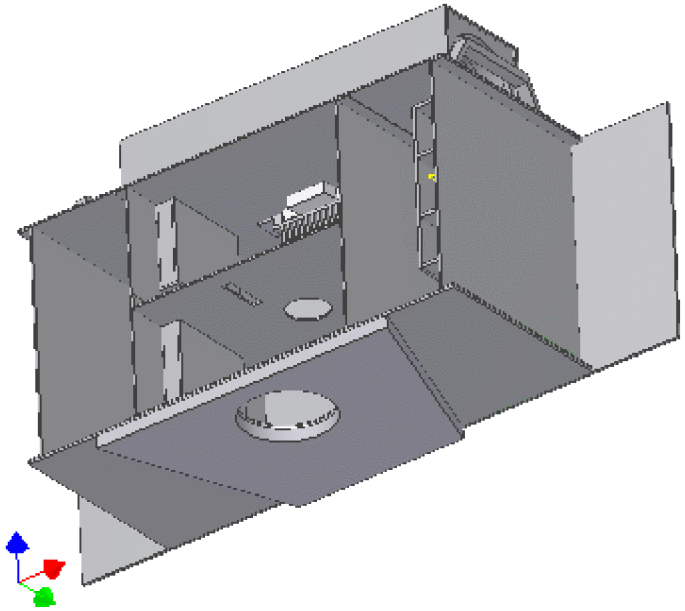

Figure 4.15 Final configuration of the radar antenna after design optimization (right/back/bottom isometric view, back plate is invisible).

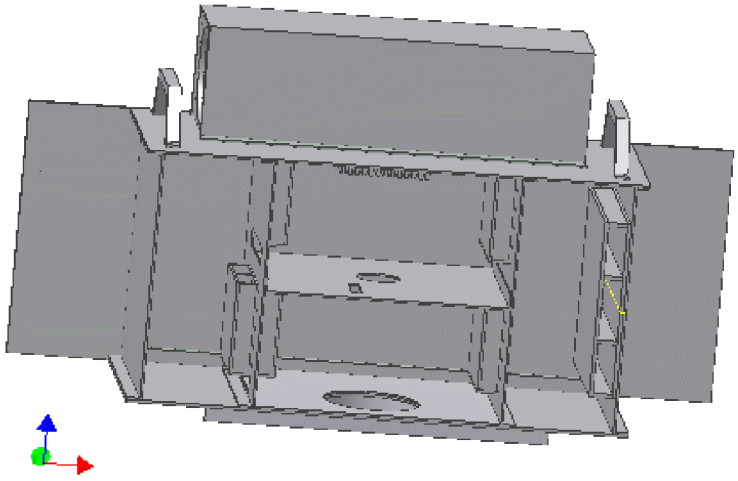

Figure 4.16 Final configuration of the radar antenna after design optimization (left/back/top isometric view, back plate is invisible).

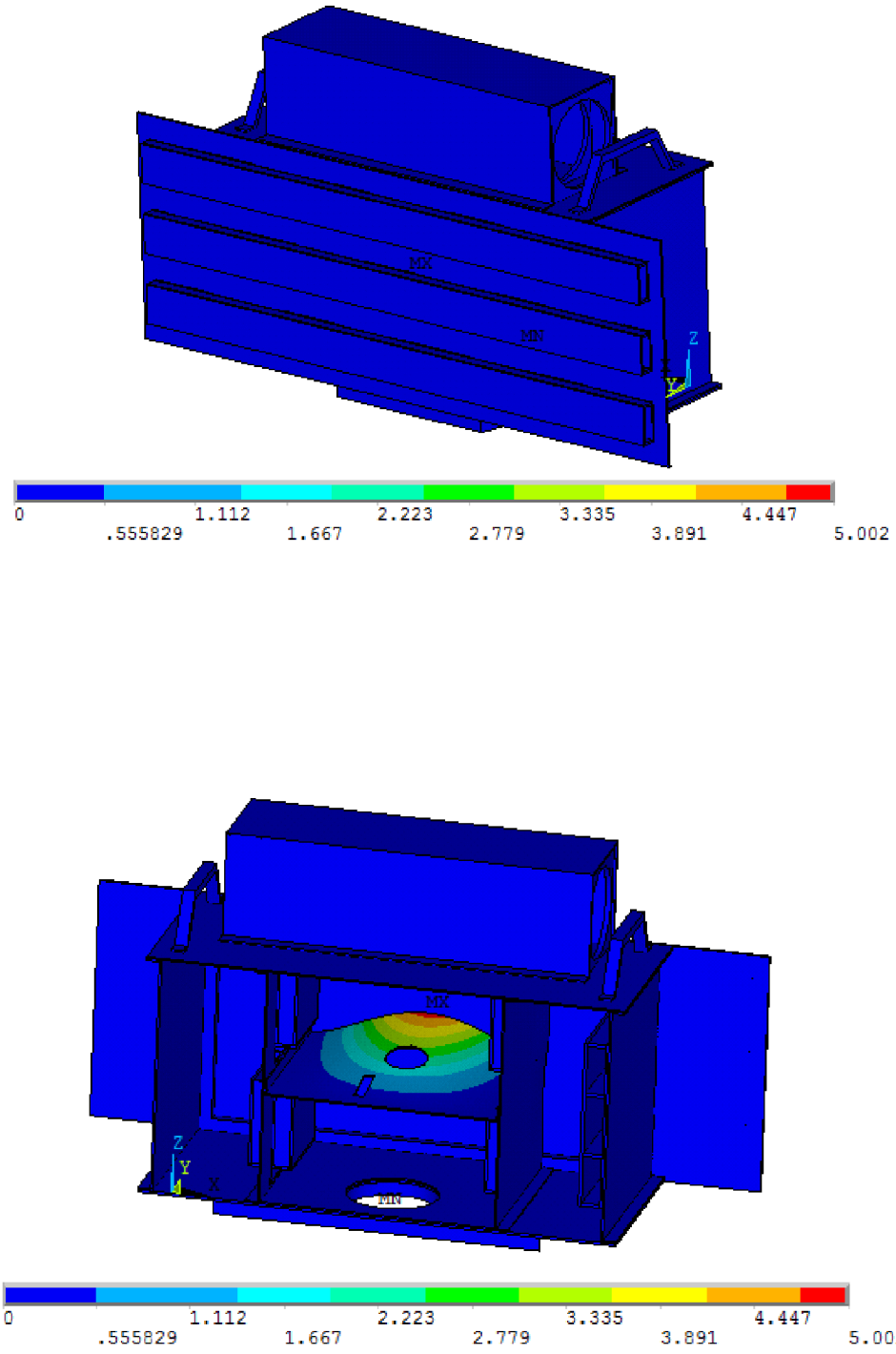

Figure 4.17 Total displacement of 1st mode shape at 146.7 Hz.

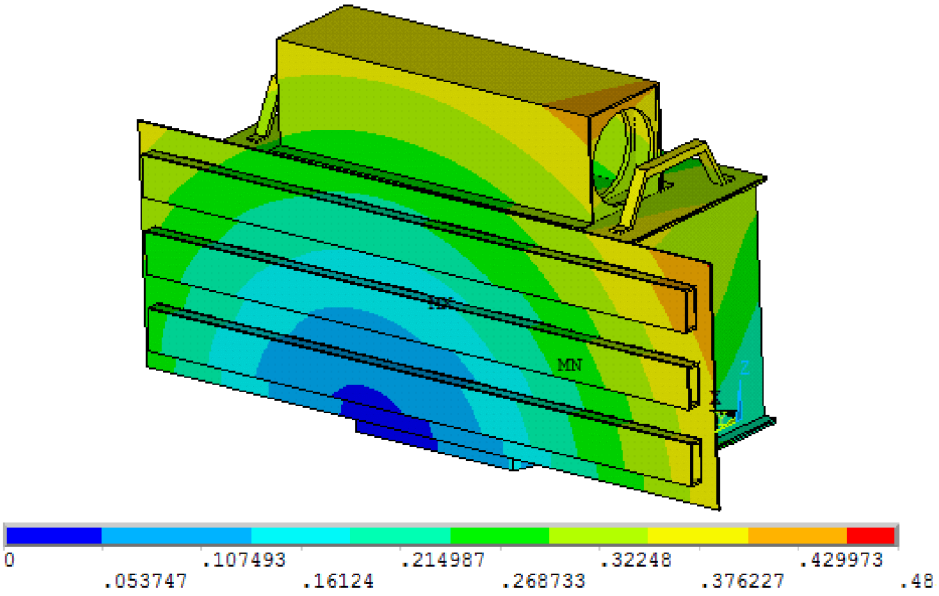

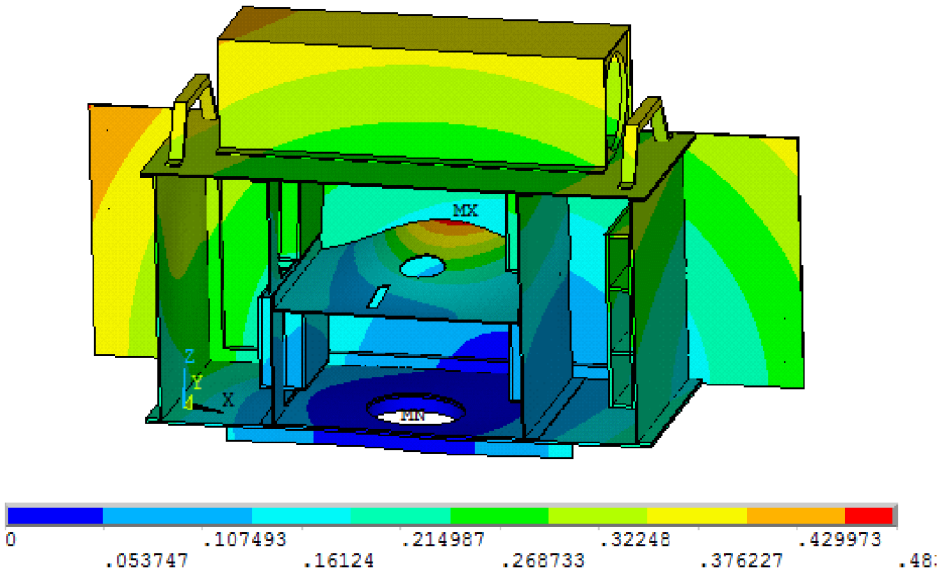

Figure 4.18 Total displacement of 2nd mode shape at 161.5 Hz.

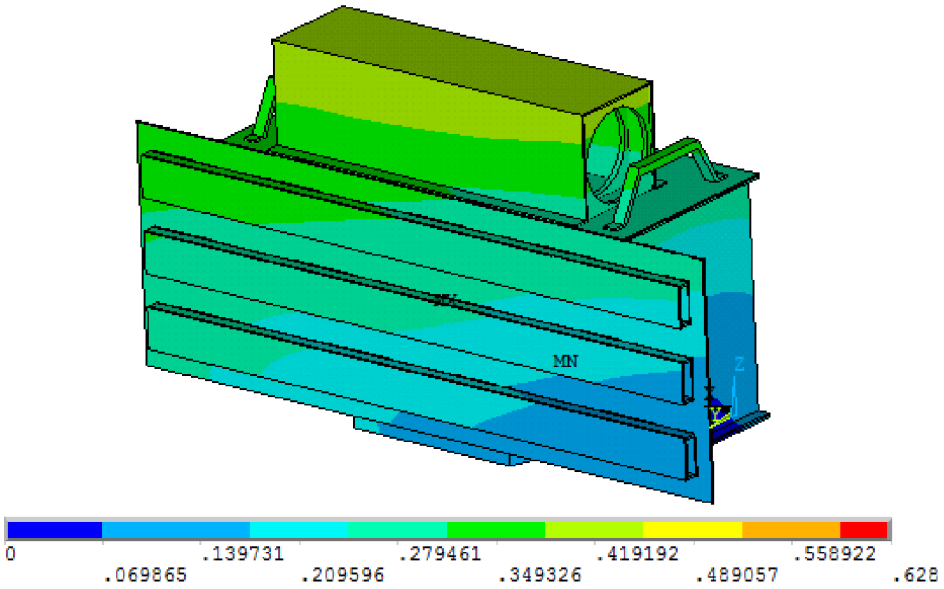

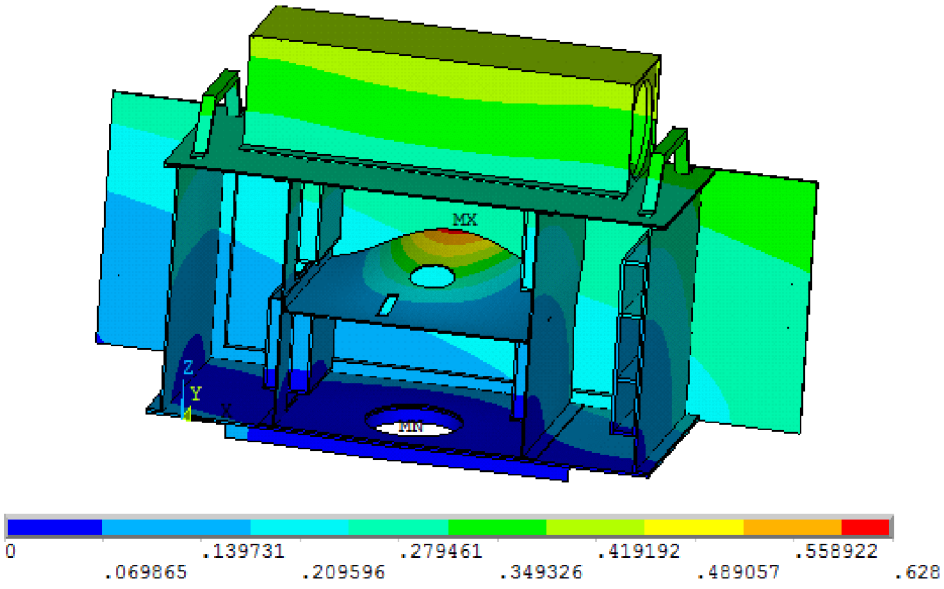

Figure 4.19 Total displacement of 3rd mode shape at 172 Hz.

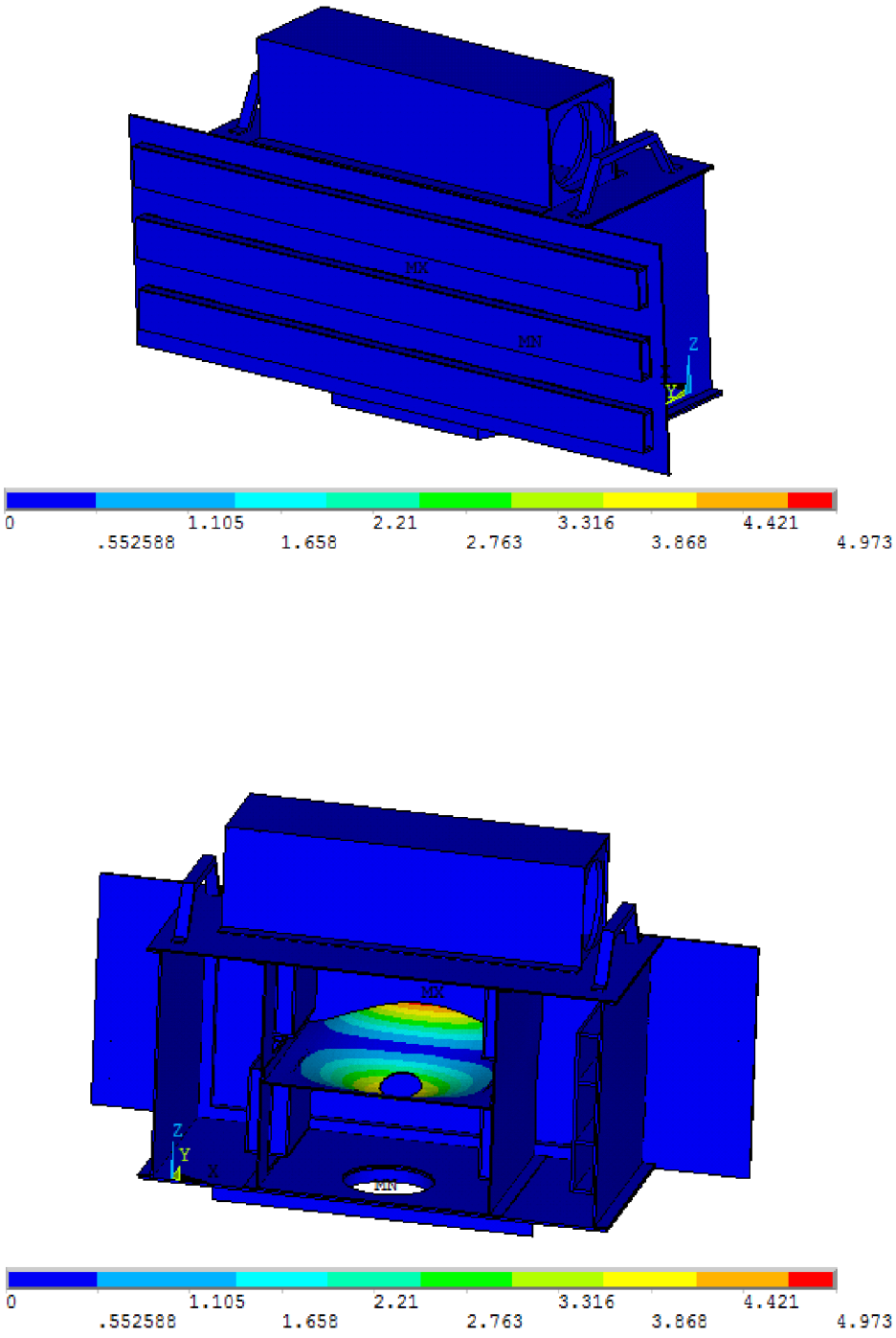

Figure 4.20 Total displacement of 4th mode shape at 296.4 Hz.

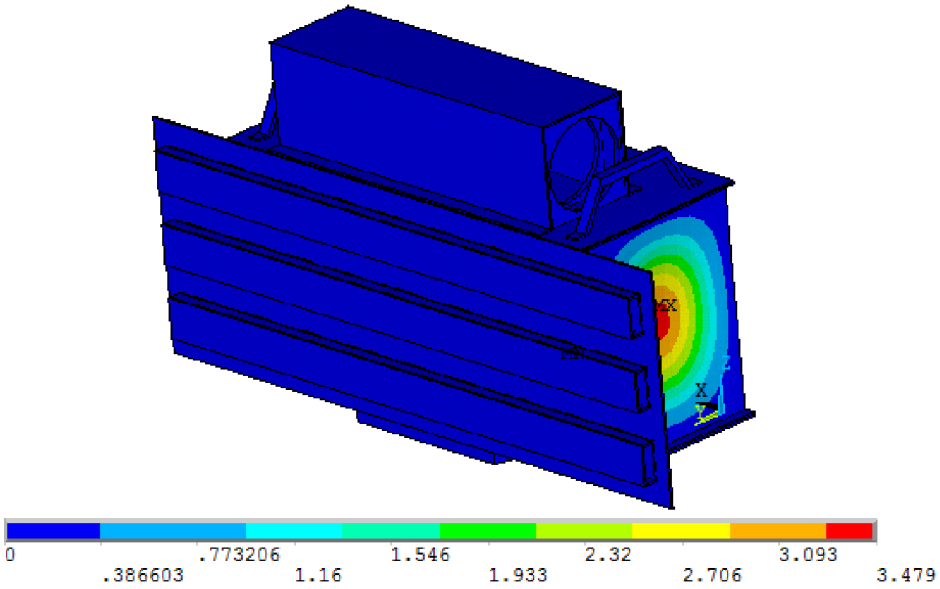

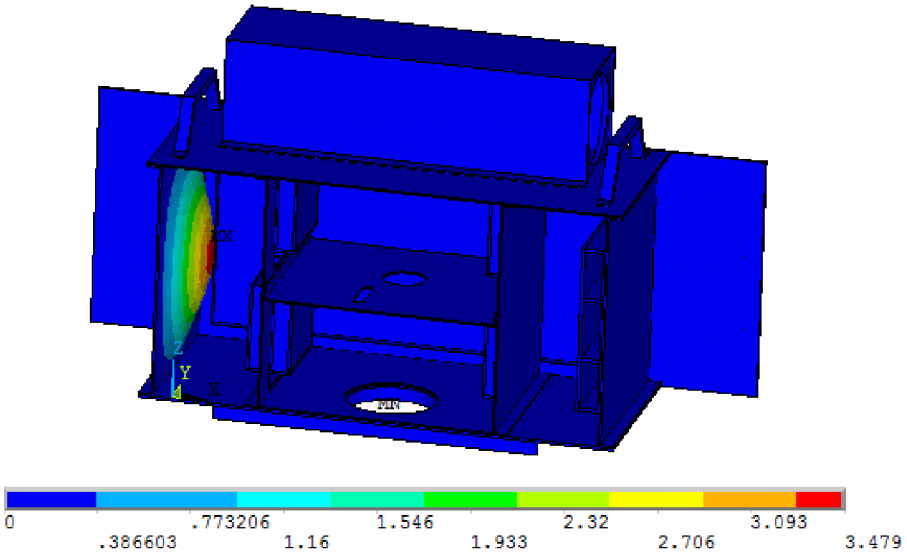

Figure 4.21 Total displacement of 5th mode shape at 322.5 Hz.

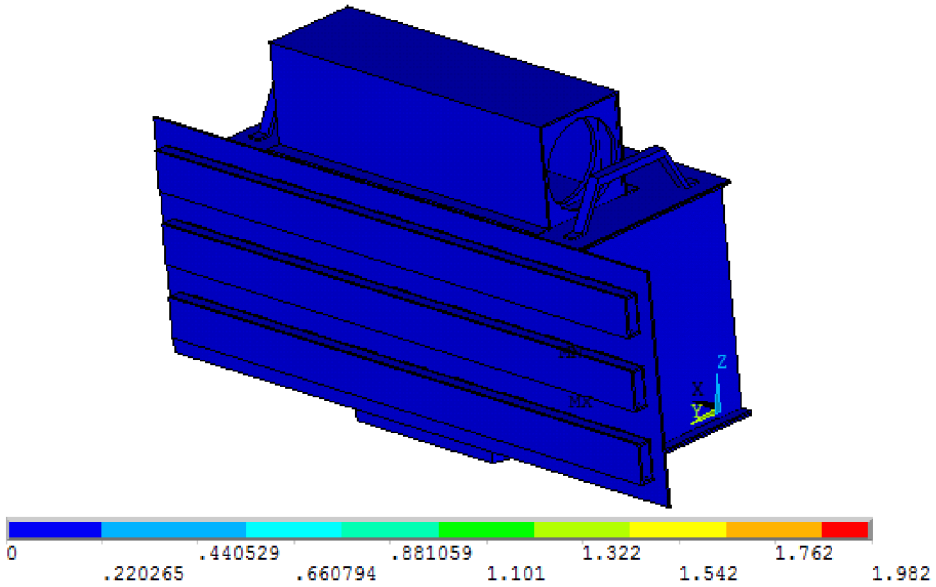

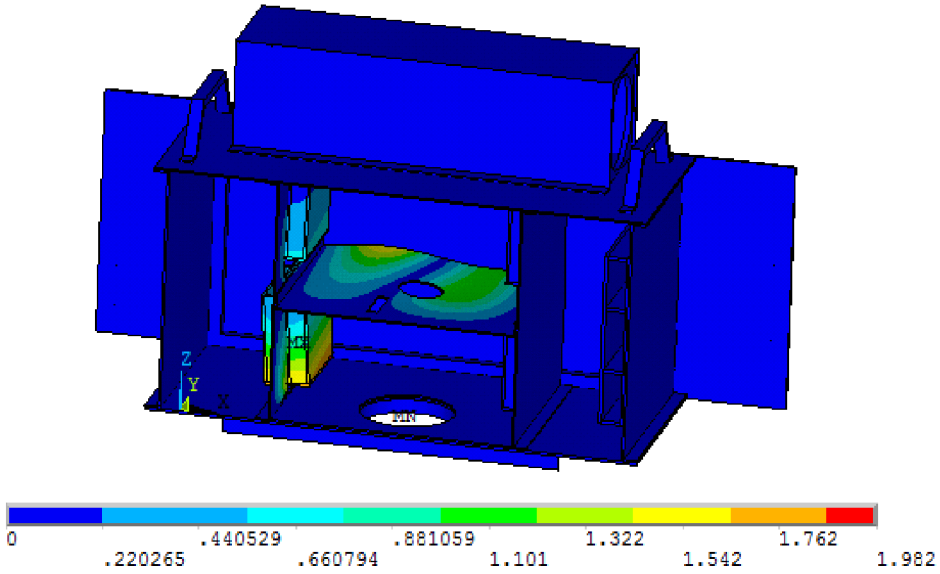

Figure 4.22 Total displacement of 6th mode shape at 328.1 Hz.

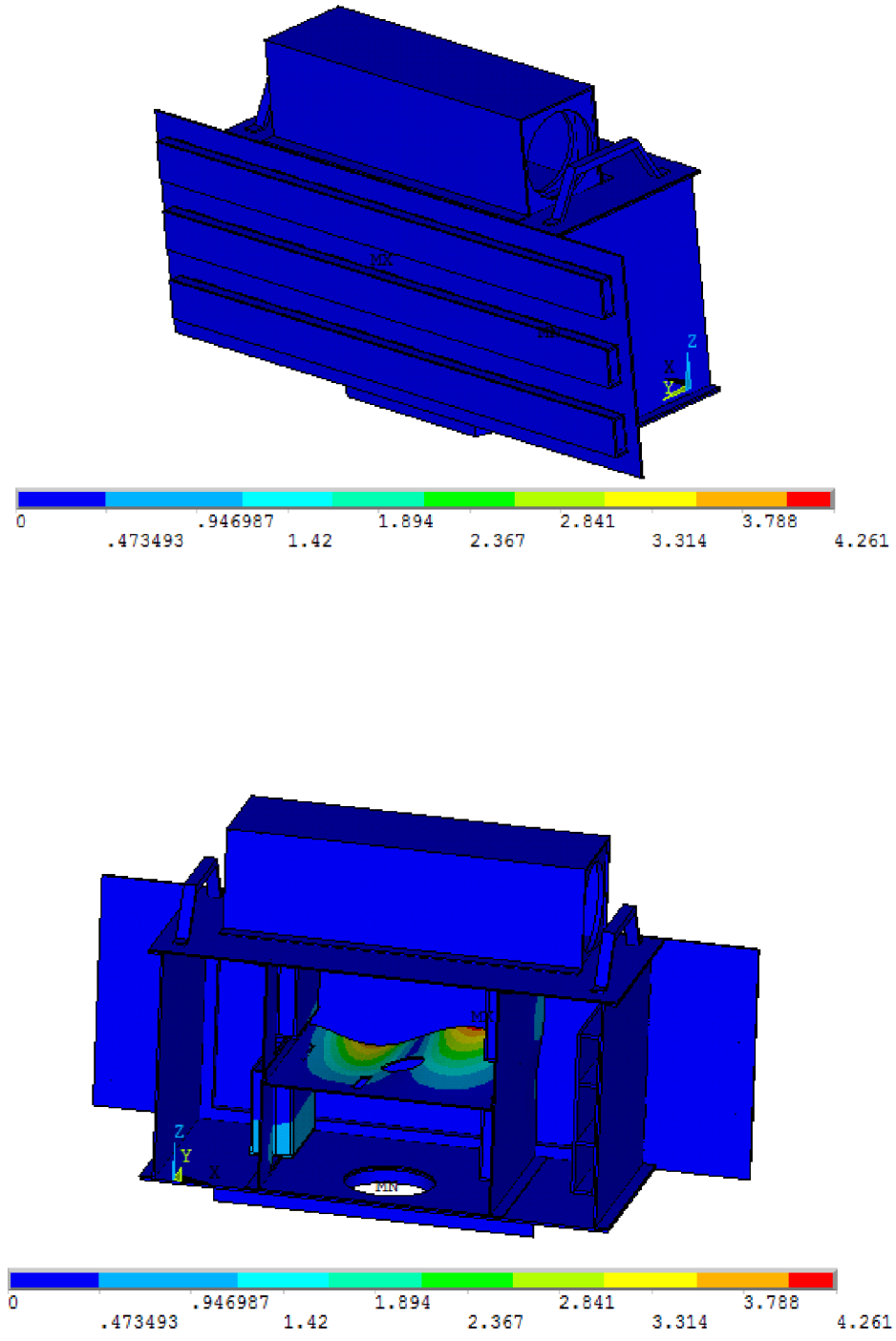

Figure 4.23 Total displacement of 7th mode shape at 374 Hz.

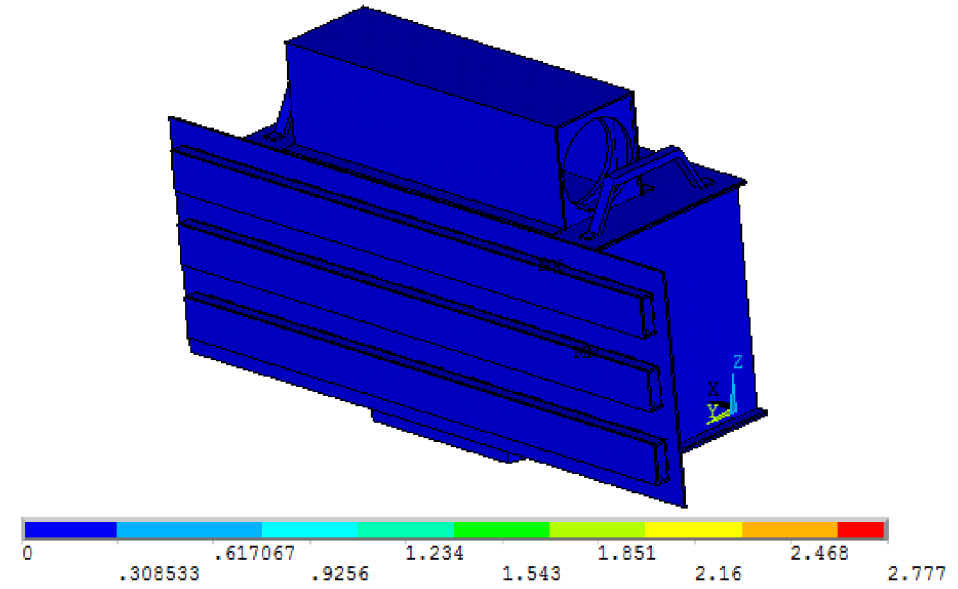

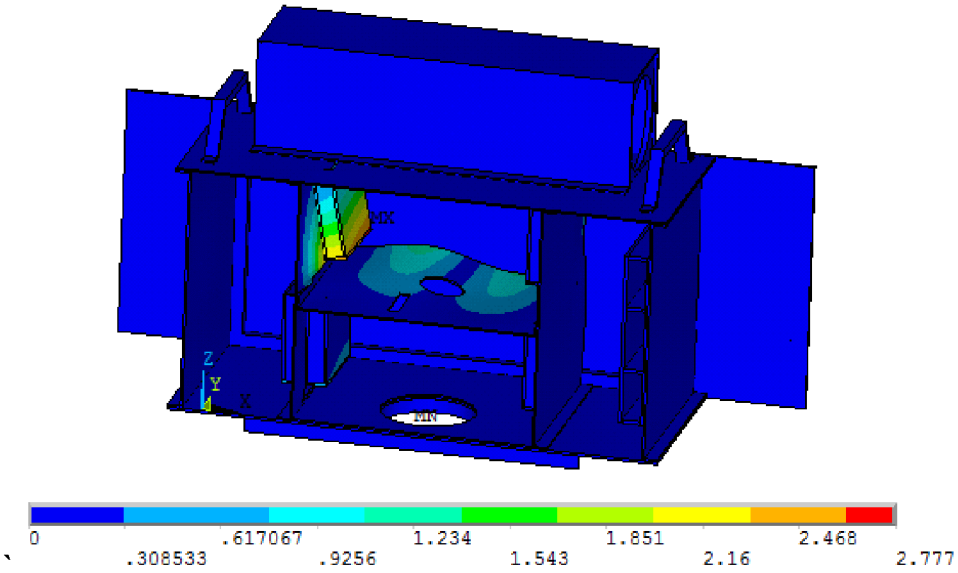

Figure 4.24 Total displacement of 8th mode shape at 408.3 Hz.

4.2.4 Random Vibration Analysis of the Optimum Antenna Design

As a final performance evaluation of the final optimized radar antenna structure, random vibration base excitation which is defined previously (Figure 3.28) is applied to the optimized (reinforced) radar antenna configuration in each axis (*x*-*y*-*z*), than the output displacements (directional deformation normal to the green surface in Figure 3.27) are obtained for *y*-axis. For surfaces where phased array antenna elements are attached, ANSYS results for PSD base excitation analysis in each direction are given in Table 4.5 and Figure 4.25 through Figure 4.27. In addition to this, the improvements in random vibration results compared with the original radar antenna structure are also given in Table 4.5.

It is seen from Table 4.5 that ($\boldsymbol{Y_{max} - Y_{min}}$) gets its maximum value which is $8.25 \cdot 10^{-5}$ m when the random vibration input is in *y*-direction. This response level is decreased approximately 92% compared to its maximum value for the original radar antenna (Table 3.5) and decreases approximately 78% compared to the intuitive design. Moreover according to the results given in Table 4.5, ($\boldsymbol{Y_{max} - Y_{min}}$) term gets much smaller values for random input in *x* and *z*-direction than original radar antenna and the percentages of improvement are 51% and 94%, respectively. It can be understood that after parameter optimization the random vibration results in critical directions are improved according to the original design of the radar antenna system.

Table 4.5 Random vibration analysis results for reinforced radar antenna structure (deformation in *y*-direction)

	Random Vibration Input in *x*-Direction	**Random Vibration Input in *y*-Direction**	**Random Vibration Input in *z*-Direction**
$\boldsymbol{Y_{max}}$ **(m)**	$3.77 \cdot 10^{-5}$	$9.34 \cdot 10^{-5}$	$5.60 \cdot 10^{-5}$
$\boldsymbol{Y_{min}}$ **(m)**	$3.83 \cdot 10^{-6}$	$1.09 \cdot 10^{-5}$	$6.45 \cdot 10^{-6}$
$\boldsymbol{Y_{max} - Y_{min}}$ **(m)**	$3.39 \cdot 10^{-5}$	$8.25 \cdot 10^{-5}$	$4.96 \cdot 10^{-5}$
Improvement (%)	51	92	94

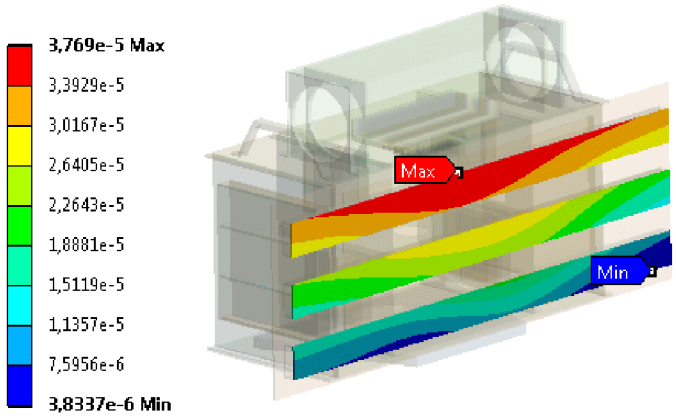

Figure 4.25 Directional deformation in *y*- direction for random input in *x* direction (reinforced radar antenna after design optimization).

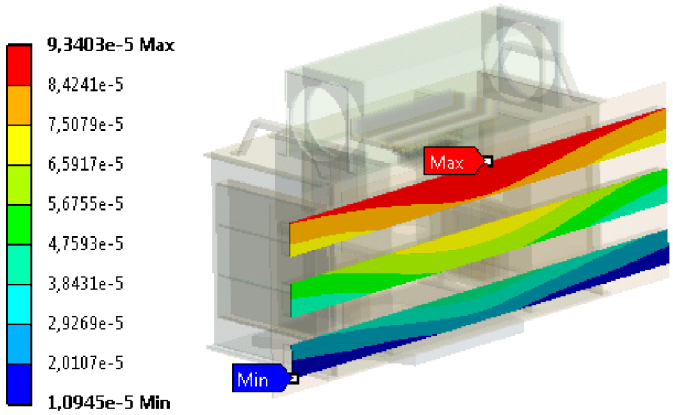

Figure 4.26 Directional deformation in *y*- direction for random input in *y*- direction (reinforced radar antenna after design optimization).

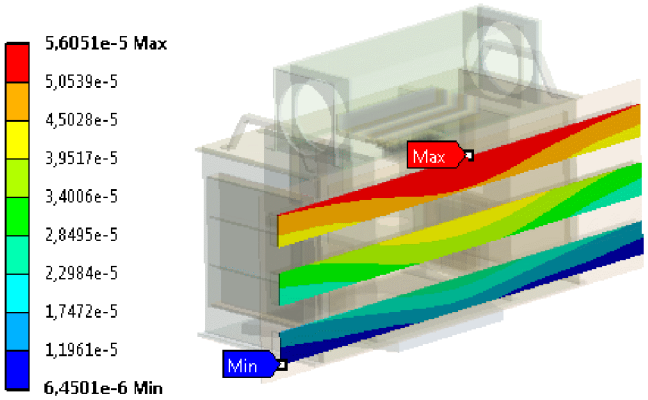

Figure 4.27 Directional deformation in *y*- direction for random input in *z* direction (reinforced radar antenna after design optimization).

4.3 CASE 2: STIFFENER OPTIMIZATION

In this thesis, "C", "T", box and rectangular types of stiffeners are used according to the point of view of easy production and one axis of symmetry of stiffener section mentioned in Chapter 2. In general, the cross-sectional dimensions of stiffeners, i.e. size variables and their positions are considered as main design variables while their lengths are predetermined in the optimization process as it is in this thesis work. The feasible stiffener locations on the original radar antenna structure is selected from the modal mechanical strain information as was the case for design space selection process for topology optimization study performed previously. Design optimization tool of ANSYS software is used for this type of optimization method.

4.3.1 Stiffener Optimization Parameters

Modal mechanical strain distributions of the original radar antenna structure (Figure 4.1) indicate that outer region of the bottom plate is much more appropriate for attaching the stiffeners since stiffeners may cause large protrusions at the inner part of the radar antenna structure which may not appropriate for the

configuration of electronic devices. Therefore stiffener locations are selected as shown in Figure 4.28. These design regions are denoted as “DR”. For the first design region it is defined as “DR1” and for the second one it is defined as “DR2”. The area of these design regions is constant and the dimensions of them are shown in Figures 4.29 and 4.30.

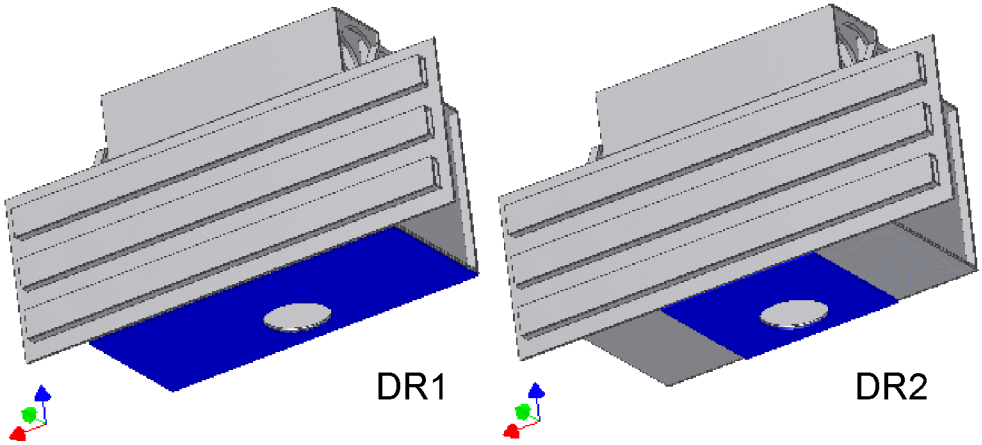

Figure 4.28 Feasible stiffener positioning regions (DS1 in left and DS2 in right) that will be used for stiffener optimization (in blue colors).

In this study, stiffeners are modeled by BEAM189 beam elements in ANSYS FE software which is a. 3D quadratic (3 node) element type having “C”, “T”, “Box” and “Rectangular” type of cross sections. In order to attach the beam elements to the solid elements properly, contact elements (CONTA177) are used as an interface between the beam and the solid elements in ANSYS.

Stiffeners are attached to specified feasible design regions along longitudinal (along x-axis) and transverse (along y-axis) directions in equally spaced configuration (i.e. all stiffeners have an equal spacing along x-axis and y-axis). Types of stiffeners are the same in both directions and the orientation of these

stiffeners are shown in Figures 4.29 and 4.30. The spacing between stiffeners parallel to the *y*-axis and *x*-axis are defined as independent variables $\boldsymbol{s}$ and $\boldsymbol{s_1}$ respectively.

The configuration of each bidirectional stiffened structures and design variables of each stiffener's cross section are shown in Figure 4.31 through Figure 4.38. In Figures 4.31 and 4.32, the orientation and design variables of closed form "C" stiffeners are presented, respectively. Similarly, the orientation and design variables of "T", "Box" and "Rectangular" type stiffeners are shown in Figures 4.33-4.34, 4.35-4.36 and 4.37-4.38, respectively. Here, configuration of stiffeners is identified using a name which indicates the orientation and types of stiffeners on specified design region. For example, "DR1_C" (see Figure 4.31(a)) means that this is the stiffener configuration in which "C" type stiffeners are used in closed form on design region DR1. Width $\boldsymbol{w1}$, height $\boldsymbol{w2}$ and thickness $\boldsymbol{t}$ of stiffener cross sections are identified as independent design variables while spacing of stiffeners were previously defined as $\boldsymbol{s}$ and $\boldsymbol{s_1}$. Defining the design parameters for stiffener optimization, design optimization module of ANSYS is used to find the optimum layout and configuration of the stiffeners for each stiffener configuration. While performing the optimizations, the number of stiffeners is defined according to the width and spacing of the stiffeners. For example for a particular optimization iteration, the number of stiffeners which are parallel to *y*-axis can be calculated from the formula $\boldsymbol{570/(s_1 + w1)}$. It should be kept in mind that the length of stiffeners remains the same during optimization process.

Design constraint is specified similar to the topology optimization study, which is the maximum value of the added mass (or the net volume of the stiffeners added). For this purpose the range of the total weight of the radar antenna structure, which is defined as a design constraint variable is specified to be between 0 and 20 kg in the optimization problem defined in ANSYS.

The objective of the optimization is the maximization of the first natural frequency of the radar antenna structure which is the same as in topology optimization study.

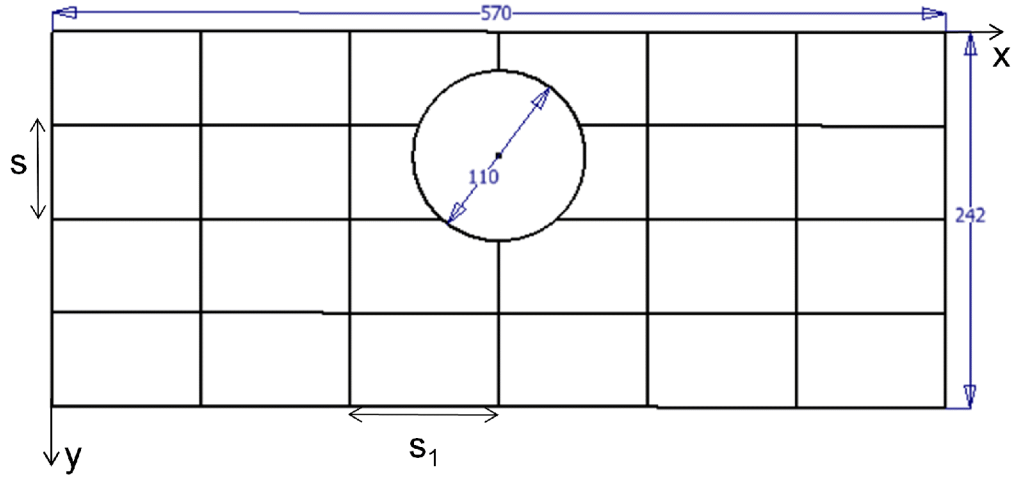

Figure 4.29 Orientation of stiffeners for DR1.

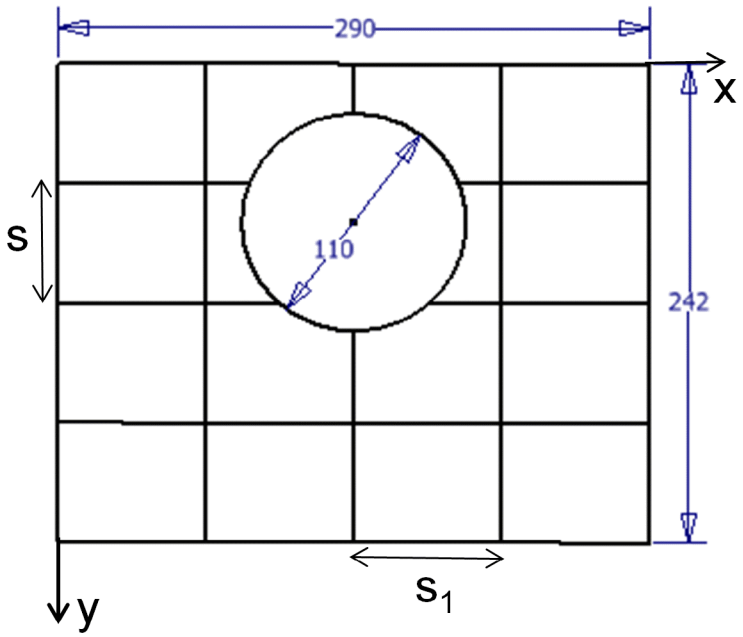

Figure 4.30 Orientation of stiffeners for DR2.

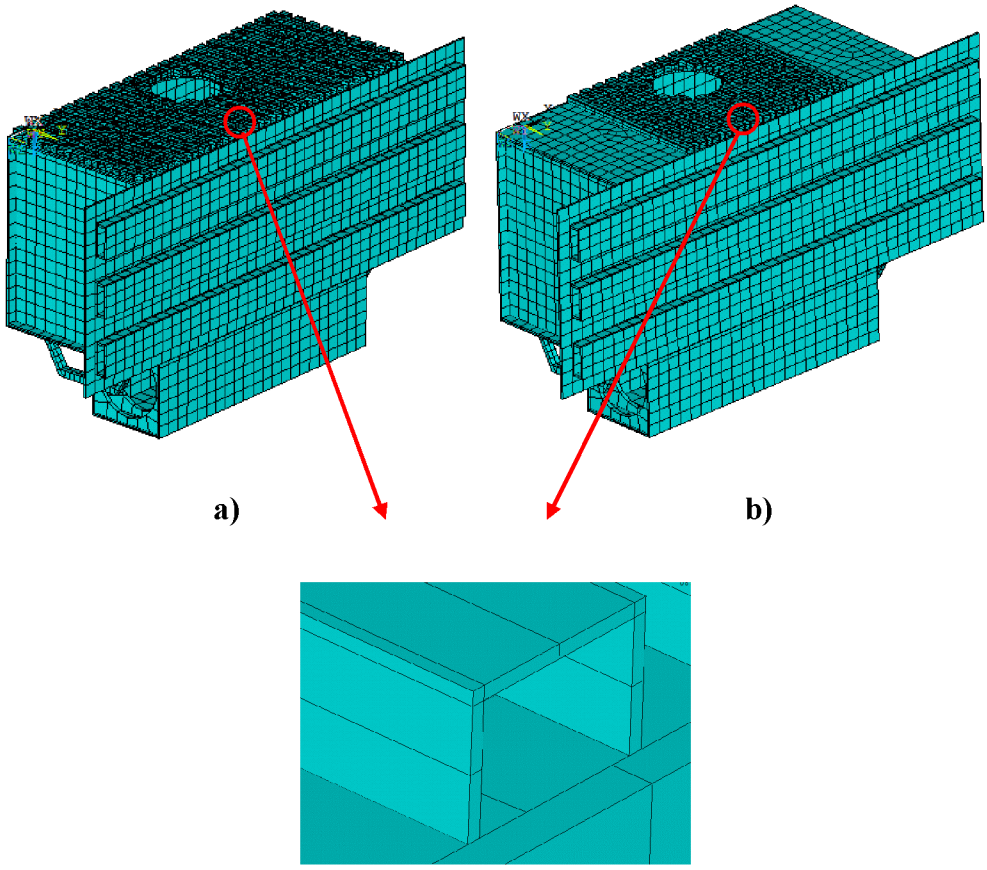

Figure 4.31 Configuration of bidirectional stiffened radar antenna structure ("DR1_C" (a) and "DR2_C" (b)) and orientation of closed form "C" Stiffener (c).

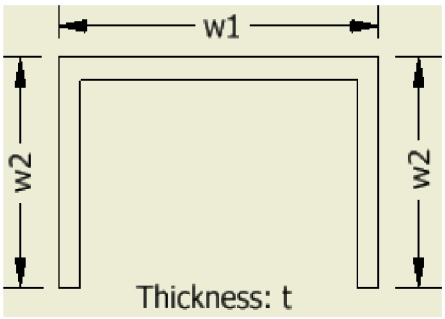

Figure 4.32 Design variables of closed form "C" type stiffener cross section.

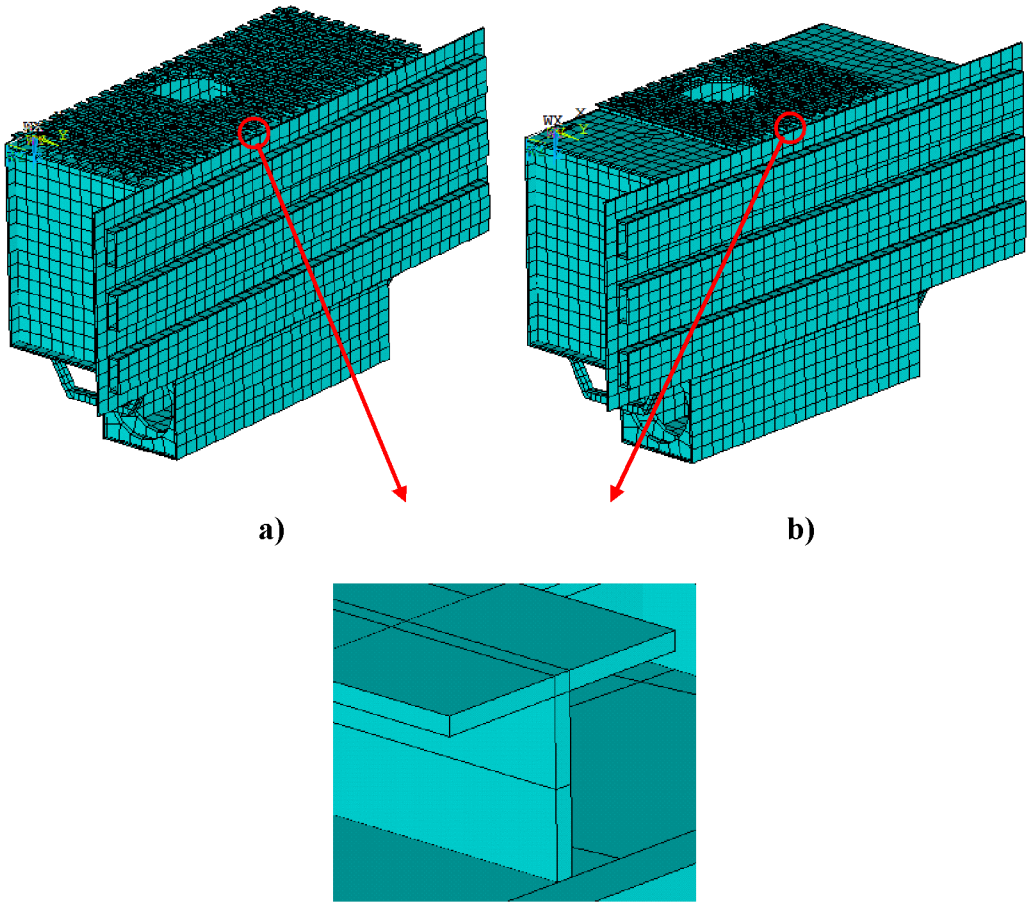

Figure 4.33 Configuration of bidirectional stiffened radar antenna structure ("DR1_T" (a) and "DR2_T" (b)) and orientation of "T" type stiffener (c).

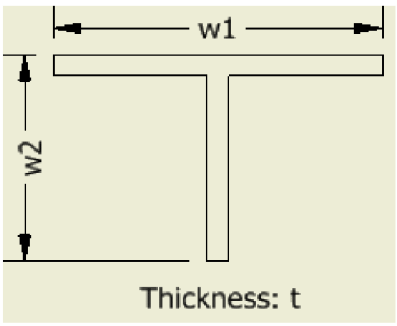

Figure 4.34 Design variables of "T" type stiffener cross section.

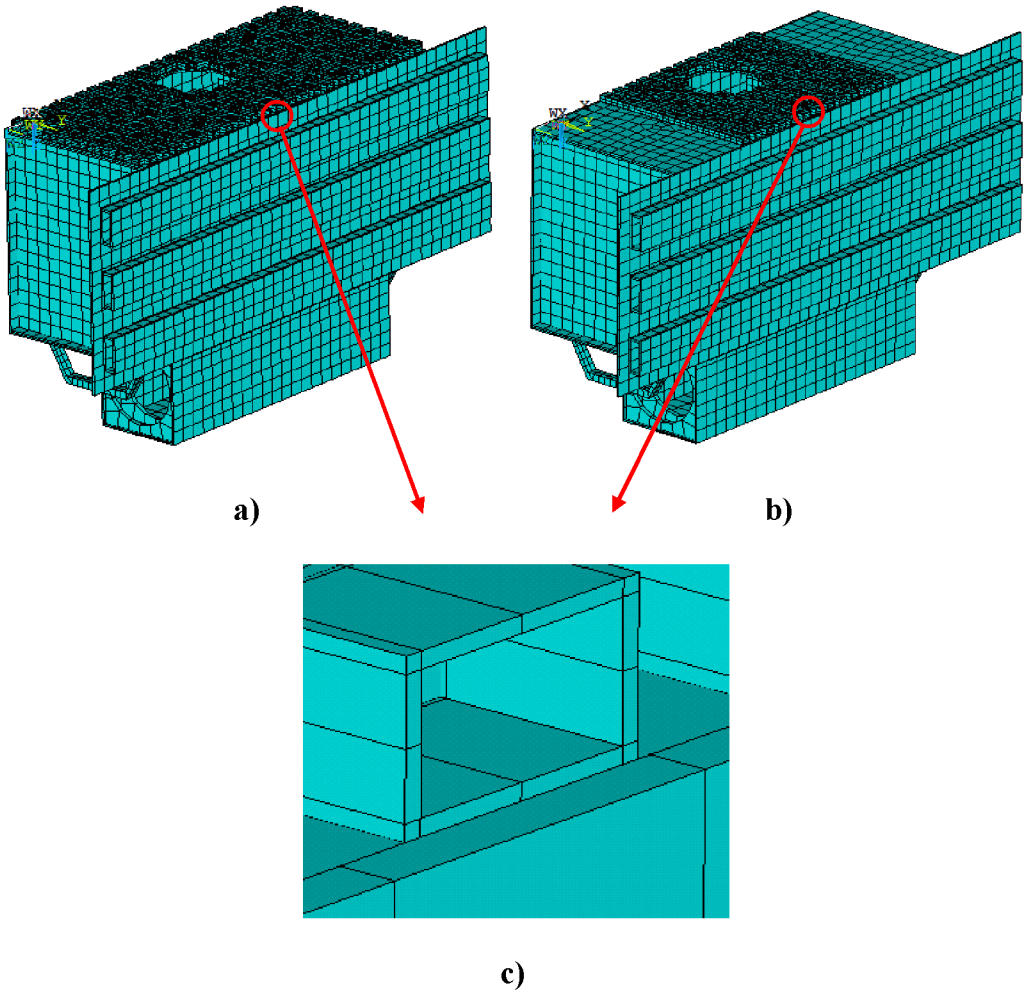

Figure 4.35 Configuration of bidirectional stiffened radar antenna structure ("DR1_Box" (a) and "DR2_Box" (b)) and orientation of "Box" type stiffener (c).

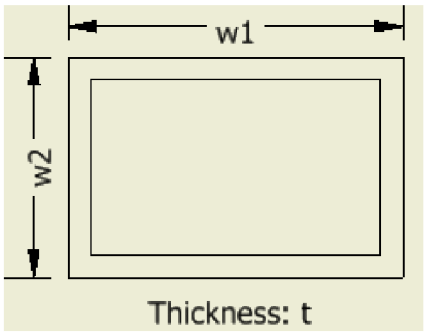

Figure 4.36 Design variables of "Box" type stiffener cross section.

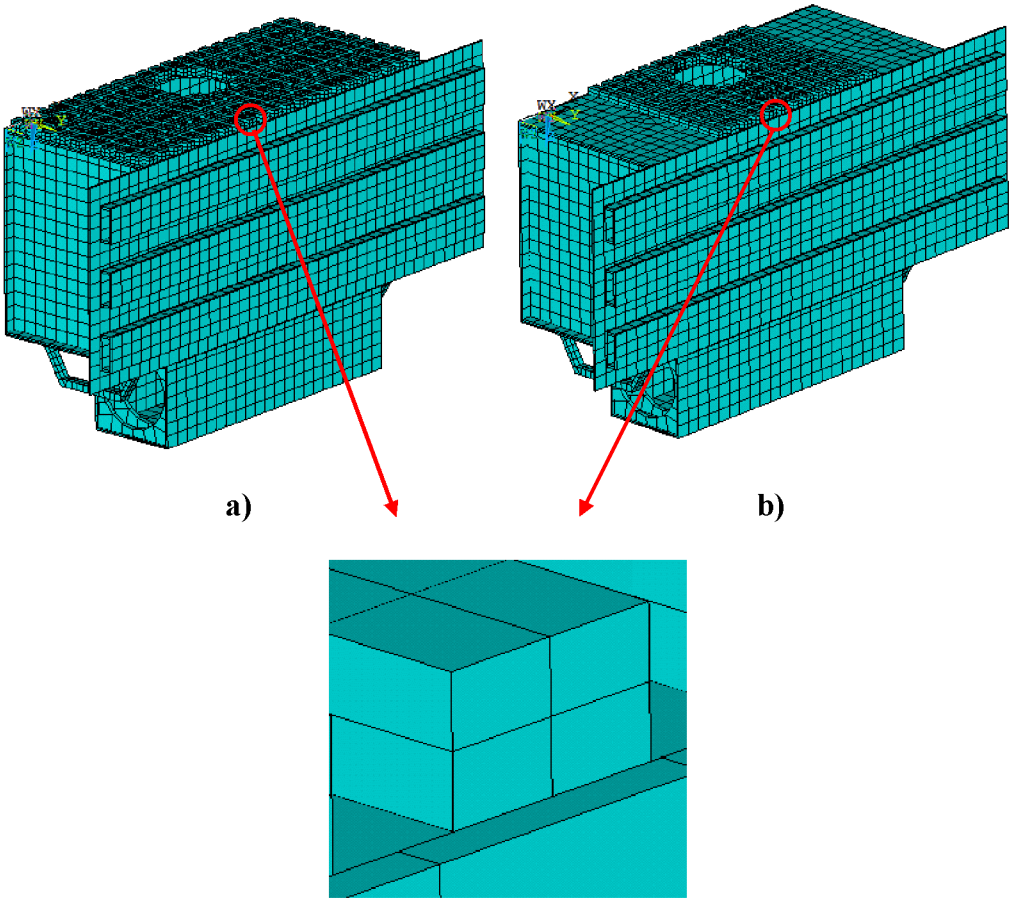

Figure 4.37 Configuration of bidirectional stiffened radar antenna structure ("DR1_Rect" (a) and "DR2_Rect" (b)) and orientation of "Rectangular" type stiffener (c).

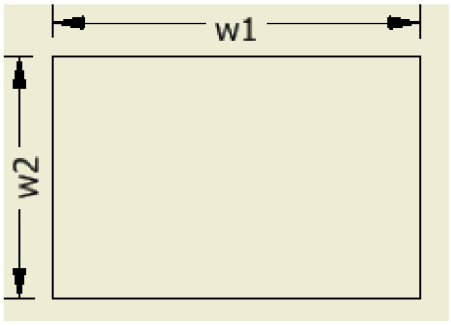

Figure 4.38 Design variables of "Rectangular" type stiffener cross section.

4.3.2 Stiffener Optimization Results

The initial values of the design variables and the optimum values obtained from design optimization in ANSYS are given in Table 4.6 and it should be noted that all design optimization cases are converged. The tolerance value used in stiffener design optimization is "10^{-3}·(Current value)" for the objective function, design variables and constraints. Natural frequencies of the radar antenna structure with the optimized stiffener configurations are given in Table 4.7 and Figure 4.39. For the same optimized radar configurations, $\boldsymbol{k}$ values are given in Table 4.8 and Figure 4.40.

From Table 4.7 and Figure 4.39 it is observed that use of design region DR2 for maximizing the first natural frequency gives much better results than the use of DR1. Moreover other natural frequencies are also increased after design optimization of stiffeners is done. The first two natural frequencies of stiffened radar antenna structure based on DR2 are increased approximately to 8 times of the original radar antenna natural frequencies. From Figure 4.39 it can be concluded that the stiffener configuration "DR2_C" obtained from design optimization is the most effective one such that the first and the second natural frequency values get their maximum values for this configuration compared to others. For this best case all natural frequencies are shifted out of the dominant sinusoid frequency range of 0-60 Hz for the AH-64 helicopter platform.

It is seen from Table 4.8 and Figure 4.40 that for all optimized stiffener configurations, $\boldsymbol{k}$ values of the sixth mode shape of the original radar antenna decreases. However $\boldsymbol{k}$ values for the 7^{th}, the 8^{th} and the 9^{th} mode shapes increased evidently. For the optimum configuration ("DR2_C"), $\boldsymbol{k}$ value for the 1^{st} mode shape remains almost the same as the original radar antenna and $\boldsymbol{k}$ value for the 2^{nd} mode shape has decreased compared with the original radar antenna.

Table 4.6 Design variables for different radar antenna configuration and the corresponding weight of the antenna.

	$w1$ (mm)	$w2$ (mm)	t (mm)	s (mm)	s_1 (mm)	Total Weight (kg)	Total Weight Increase (%)
Initial Value	15	10	1	10	10	16.6	-
DR1-C	17.3	33.6	1.7	10.8	11	19.9	19.9
DR2-C	27.7	59	2.5	11	17	19.9	19.9
DR1-T	19	44.7	2.3	12	10	19.9	19.9
DR2-T	27.5	59	4.3	10	10.5	20.0	20.5
DR1-Box	16.6	25.6	1.5	11	12	19.6	18.1
DR2-Box	24.8	52.7	2.4	10.4	14	19.9	19.9
DR1-Rect	5.42	20.1	-	22.6	37.8	19.3	16.4
DR2-Rect	10.7	26.6	-	11.7	32.5	19.8	19.5

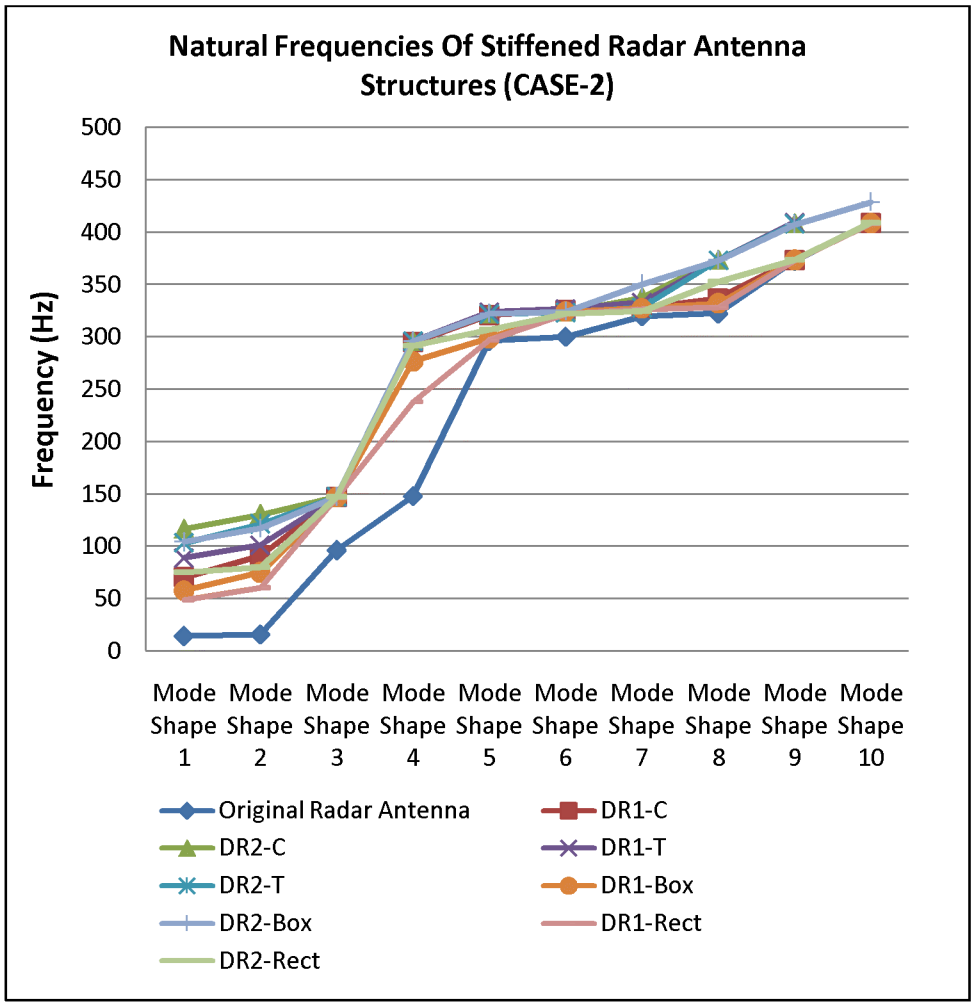

Figure 4.39 Natural frequencies of different stiffened radar antenna structures (CASE-2).

Table 4.7 Natural frequencies of stiffened radar antenna structure for different stiffener configurations (CASE-2). (Hz)

	Mode Shape 1	**Mode Shape 2**	**Mode Shape 3**	**Mode Shape 4**	**Mode Shape 5**	**Mode Shape 6**	**Mode Shape 7**	**Mode Shape 8**	**Mode Shape 9**	**Mode Shape 10**
Original Radar Antenna	14.7	16.2	96.5	148.1	296.6	300.4	320.0	322.5	372.8	409.0
DR1-C	70.6	91.5	147.3	295	321	325.6	328	336.8	373.7	409
DR2-C	117	130.7	147.6	296.2	322.5	324.1	338	373.7	408.7	>500
DR1-T	89.2	101.3	147.3	296	324.3	327	333	373.7	409.7	>500
DR2-T	103.6	121.6	147.5	296.2	322	323.6	328.4	373.7	408.3	>500
DR1-Box	58.2	75.5	147.2	277	299	324.3	327.8	332.6	373.7	408.8
DR2-Box	104.5	117.2	147.5	296.1	322.5	324.6	350.6	373.5	407.7	429
DR1-Rect	48.9	60.4	147.1	238.3	297.3	322.3	326.9	328.8	373.6	408.8
DR2-Rect	75.3	80.3	147.3	291.7	307.4	322.5	324.9	353.2	373.9	409.3

Table 4.8 Calculated ***k*** values of different stiffener configuration of the stiffened radar antenna structures. (CASE-2)

	Mode Shape 1	**Mode Shape 2**	**Mode Shape 3**	**Mode Shape 4**	**Mode Shape 5**	**Mode Shape 6**	**Mode Shape 7**	**Mode Shape 8**	**Mode Shape 9**	**Mode Shape 10**
Original Radar Antenna	0.014	0.500	0.266	0.002	0.022	1.540	0.065	0.015	0.011	0.002
DR1-C	0.075	0.516	0.004	0.008	0.169	0.079	0.040	1.372	0.016	0.005
DR2-C	0.044	0.273	0.008	0.002	0.041	0.074	1.702	0.018	0.005	-
DR1-T	0.087	0.516	0.003	0.002	0.126	0.057	0.872	0.015	0.011	-
DR2-T	0.049	0.403	0.006	0.002	0.124	0.151	0.817	0.019	0.008	-
DR1-Box	0.051	0.517	0.003	0.086	0.013	0.162	0.060	0.890	0.016	0.004
DR2-Box	0.029	0.440	0.005	0.001	0.021	0.038	1.657	0.018	0.014	0.185
DR1-Rect	0.051	0.515	0.004	0.175	0.006	0.505	0.276	0.133	0.015	0.003
DR2-Rect	0.040	0.520	0.003	0.021	0.055	0.022	0.037	1.610	0.030	0.004

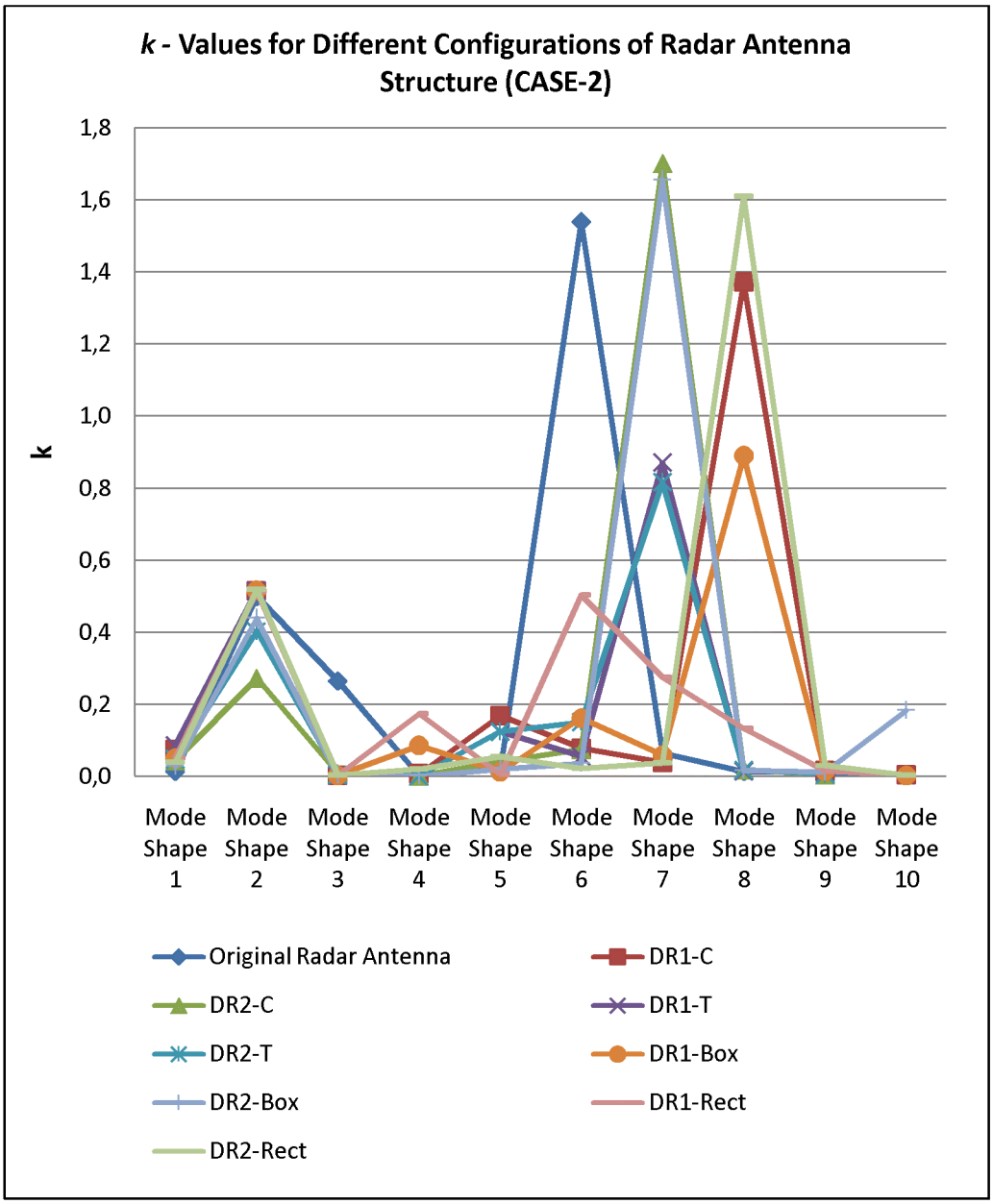

Figure 4.40 ***k*** values of mode shapes for different stiffened radar antenna structures (CASE-2).

4.3.3 Random Vibration Analysis of the Optimum Antenna Design

Previously defined broadband random vibration input in each axis (*x*-*y*-*z*) is also applied separately to the optimum configuration obtained from stiffener configuration "DR2_C". ANSYS results for PSD platform base excitation in each direction and the improvements compared with the original radar antenna structure are given in Table 4.9 for the surfaces where phased array antenna elements are attached. It is seen from Table 4.9 that ($\boldsymbol{Y_{max} - Y_{min}}$) gets its maximum value of $1.32 \cdot 10^{-4}$ m for random vibration input in *y*-direction. It is decreased by 87%compared to the original radar antenna but higher than the maximum value of ($\boldsymbol{Y_{max} - Y_{min}}$) obtained for the case of optimum configuration of the modified radar antenna structure constructed by the use of reinforcement plates obtained through topology optimization (see Section 4.2) which has same weight increase with "DR2_C" stiffener configuration. In addition to that the values of ($\boldsymbol{Y_{max} - Y_{min}}$) for random vibration inputs in *x* and *z*-direction are also decreased by 74% and 92%, respectively compared with the values obtained for the original radar antenna.

Table 4.9 Random vibration analysis results for stiffened radar antenna Structure ("DR2_C") (deformation in *y*-direction).

	Random Vibration Input in *x*-Direction	**Random Vibration Input in *y*-Direction**	**Random Vibration Input in *z*-Direction**
$\boldsymbol{Y_{max}}$ **(m)**	$1.83 \cdot 10^{-5}$	$1.49 \cdot 10^{-4}$	$7.53 \cdot 10^{-5}$
$\boldsymbol{Y_{min}}$ **(m)**	$5.08 \cdot 10^{-7}$	$1.69 \cdot 10^{-5}$	$8.58 \cdot 10^{-6}$
$\boldsymbol{Y_{max} - Y_{min}}$ **(m)**	$1.78 \cdot 10^{-5}$	$1.32 \cdot 10^{-4}$	$6.67 \cdot 10^{-5}$
Improvement (%)	74	87	92

4.4 CASE 3: TOPOLOGY AND STIFFENER OPTIMIZATION

In this part combination of topology and design optimization techniques are studied. Stiffener design optimization is performed on top of reinforced radar antenna structure with configuration Topo_DS3 %50 (see Figure 4.41) since this is the only suitable configuration constructed in Section 4.2 to easily attach stiffeners to the bottom plate of the radar antenna. According to the results of stiffener design optimization in section 4.3, the use of design region "DR2" gives much better results than the use of "DR1". Therefore stiffener design is performed for design configuration "DR2".

4.4.1 Optimization Parameters

The orientation and types of stiffeners and design optimization parameters are the same as the ones used in Section 4.3 but initial total weight of the system is not the same since in this case design optimization is applied on reinforced antenna structure "Topo_DS3 %50". Stiffeners to be optimized are attached to the outer side of the bottom plate of radar antenna (opposite side of the reinforcement plates of configuration "Topo_DS3 %50"). The modified radar antenna structure with reinforcement plate configuration "Topo_DS3 %50" used is shown in Figure 4.34. From previous stiffener design optimization results, it has been the case that design region DR2 gives better results, so that here the same design region is selected for optimizing stiffeners.

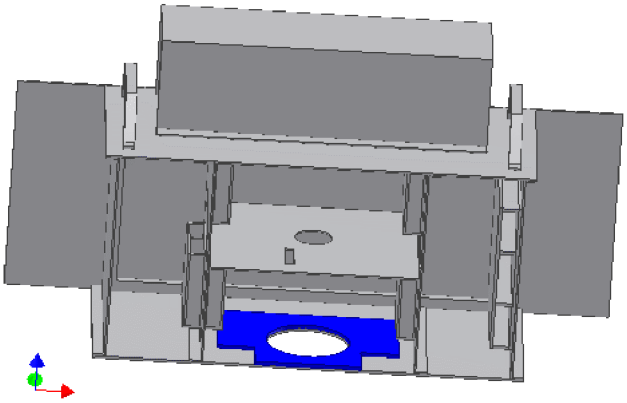

Figure 4.41 Reinforced radar antenna structure according to the topology optimization ("Topo_DS3 %50").

4.4.2 Optimization Results

The initial design variables and the optimum values for the stiffeners obtained from design optimization results are given in Table 4.10 and it is noted that all design optimization cases are converged. The tolerance value used in design optimization is the same as used in Section 4.3. Natural frequencies of modified radar antenna structure configurations which are combinations of "Topo_DS3 %50" configurations and optimized stiffeners at design region DR2 are given in Table 4.11 and Figure 4.42. Corresponding $\boldsymbol{k}$ values are given in Table 4.12, and Figure 4.43. Here configuration of stiffeners is designated a name which indicates the orientation and types of stiffeners. For example, "Topo_Stiff_C" means that this is the stiffener design optimization with "C" type stiffeners combined with "Topo_DS3 %50" reinforcement plate configuration. Other designation of stiffener configurations can be deduced from Table 4.10 for each type of stiffeners.

Stiffener design optimization on modified radar antenna structure with reinforcement plate configuration"Topo_DS3 %50" gives better results compared with the results presented in Section 4.3. From Table 4.11 and Figure 4.42 it is seen that critical natural frequencies are shifted out of the frequency range 0-60 Hz and it can also be concluded that the first two natural frequencies of stiffened radar

antenna structure are increased approximately to 10 times of the original radar antenna structure. In addition to that according to Table 4.12 and Figure 4.43, critical $\boldsymbol{k}$ value of original radar antenna structure is decreased evidently but for 9^{th} and 10^{th} mode shapes of reinforced antenna $\boldsymbol{k}$ values are considerably high.

According to these results the optimum solution is obtained for "Topo_Stiff_T" configuration after stiffener design optimization performed along with the reinforcement plate configuration "Topo_DS3 %50".

Table 4.10 Design variables for reinforced radar antenna configurations and the corresponding weight of the antennas.

	$w1$ (mm)	$w2$ (mm)	t (mm)	s (mm)	s_1 (mm)	Total Weight (kg)	Total Weight Increase (%)
Initial Value	15	10	1	10	10	17	-
Topo_Stiff_C	15.2	42.8	2.2	11.2	10.6	19.8	16.5
Topo_Stiff_T	17.3	60	3.2	10.2	10	19.9	17.1
Topo_Stiff_Box	15.8	40.2	2.1	11	10.5	19.9	17.1
Topo_Stiff_Rect	15.9	14	-	10.8	12	19.8	16.5

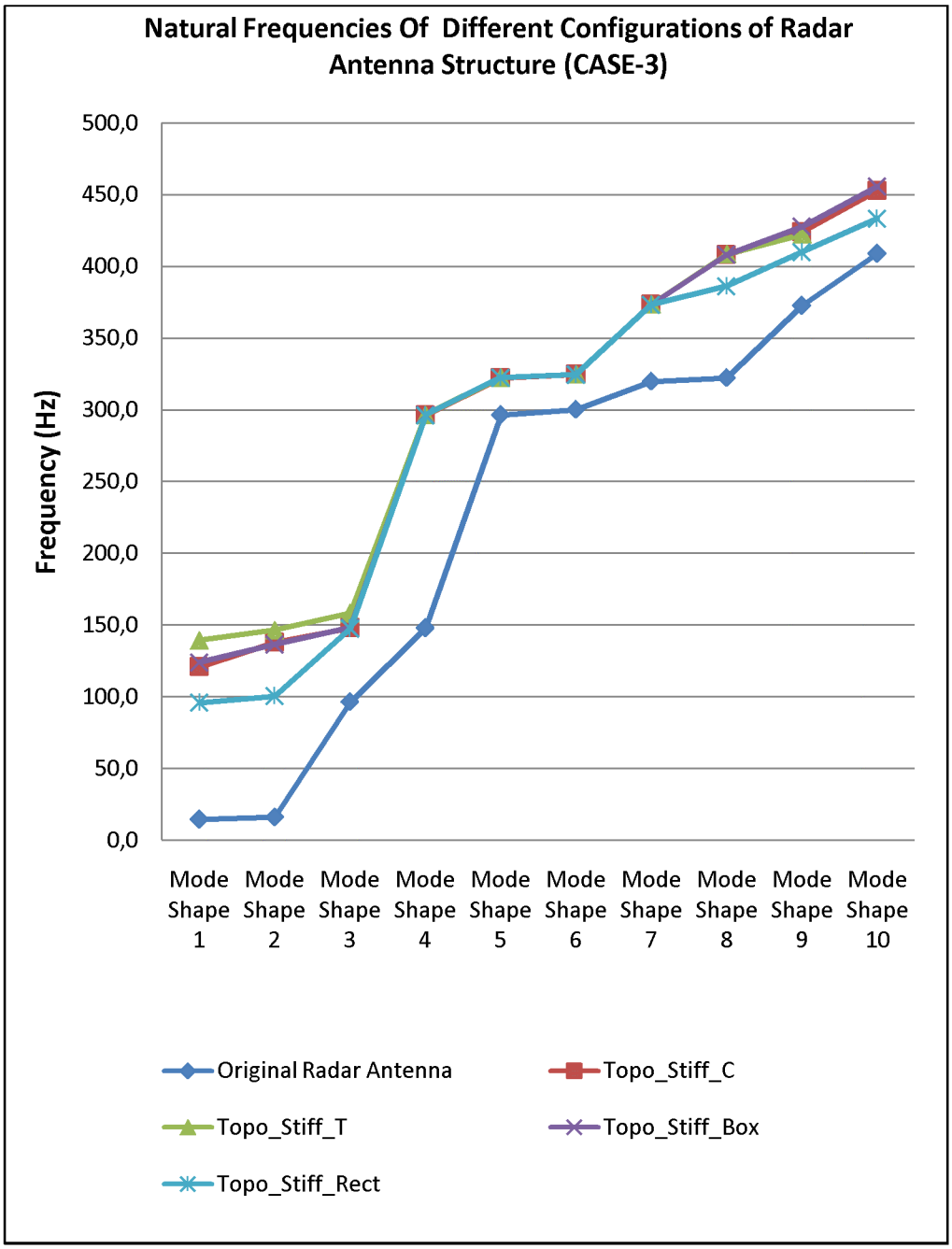

Figure 4.42 Natural frequencies of reinforced radar antenna structures (CASE-3).

Table 4.11 Natural frequencies of reinforced radar antenna structure for different stiffener configurations (CASE-3). (Hz)

	Mode Shape 1	**Mode Shape 2**	**Mode Shape 3**	**Mode Shape 4**	**Mode Shape 5**	**Mode Shape 6**	**Mode Shape 7**	**Mode Shape 8**	**Mode Shape 9**	**Mode Shape 10**
Original Radar Antenna	14.7	16.2	96.5	148.1	296.6	300.4	320.0	322.5	372.8	409.0
Topo_Stiff_C	121	138.1	148.3	296.5	322.5	325	373.5	408.2	424.1	452.8
Topo_Stiff_T	139.6	146.5	158.5	296.6	322.6	324.9	373.5	408.6	422.3	>500
Topo_Stiff_Box	124	136.6	148.2	296.5	322.5	324.9	373.4	408.3	427.8	455.8
Topo_Stiff_Rect	96	100.6	147.5	296.3	322.5	324.8	373.4	386.4	410	433.5

Table 4.12 Calculated k values of different stiffener configuration of the reinforced radar antenna structures. (CASE-3)

	Mode Shape 1	**Mode Shape 2**	**Mode Shape 3**	**Mode Shape 4**	**Mode Shape 5**	**Mode Shape 6**	**Mode Shape 7**	**Mode Shape 8**	**Mode Shape 9**	**Mode Shape 10**
Topo_Stiff_C	0.057	0.128	0.017	0.001	0.011	0.020	0.010	0.027	1.750	0.397
Topo_Stiff_T	0.079	0.010	0.185	0.001	0.014	0.009	0.010	0.036	1.763	-
Topo_Stiff_Box	0.053	0.188	0.014	0.001	0.014	0.007	0.009	0.022	1.746	0.422
Topo_Stiff_Rect	0.037	0.507	0.004	0.002	0.014	0.007	0.009	0.241	0.019	1.734

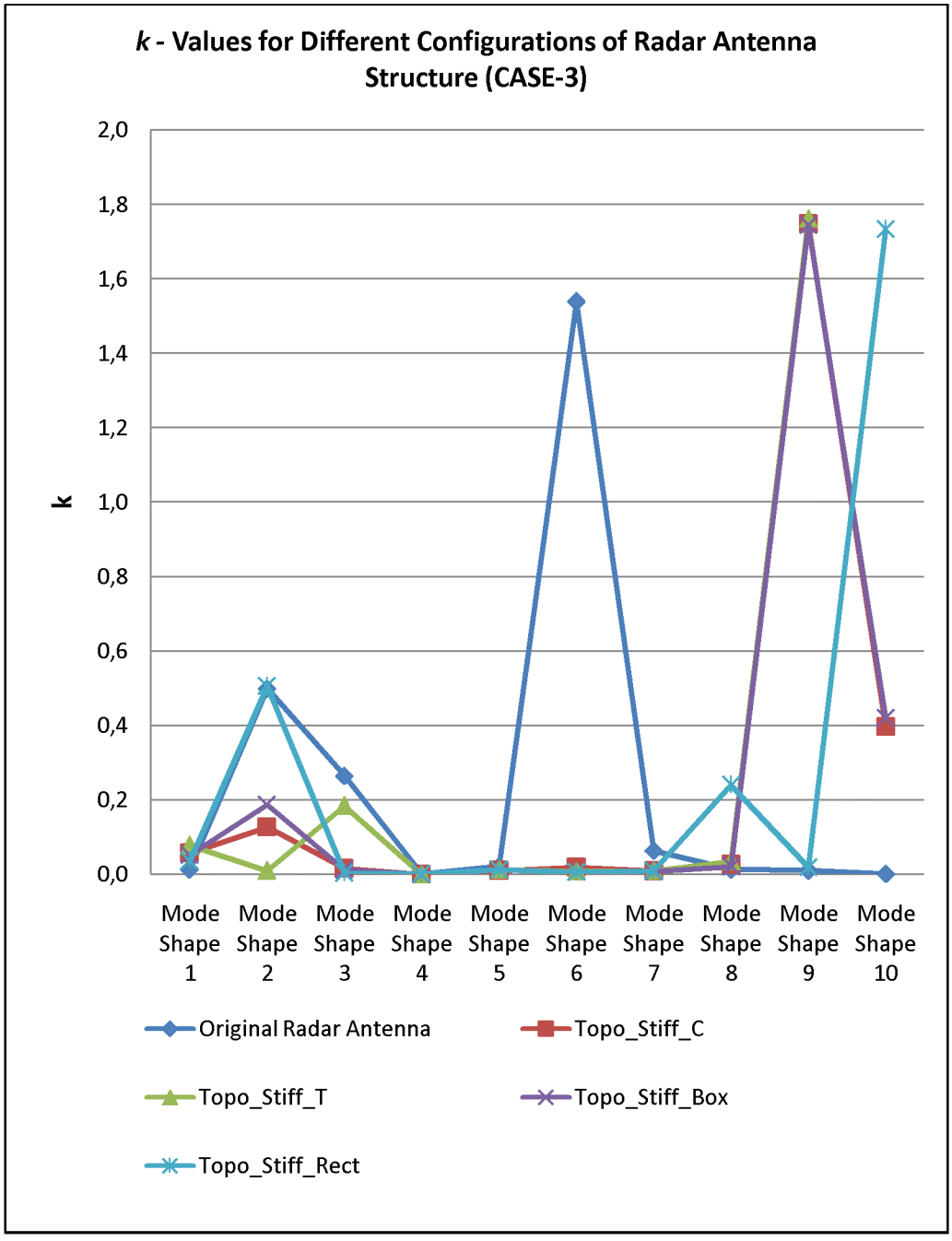

Figure 4.43 ***k*** values of mode shapes for stiffened radar antenna structures (CASE-3).

4.4.3 Random Vibration Analysis of the Optimum Antenna Design

The random vibration results of "Topo_Stiff_T" configuration and the improvements compared with the original radar antenna structure are given in Table 4.13. It is seen from Table 4.13 that $(\boldsymbol{Y_{max} - Y_{min}})$ gets its maximum value $9.23 \cdot 10^{-5}$ m for random vibration input in *y*-direction and for that value $(\boldsymbol{Y_{max} - Y_{min}})$ is decreased by 91% compared with the original radar antenna. Among other optimization studies in Chapter 4, $(\boldsymbol{Y_{max} - Y_{min}})$ value for this type of configuration is worse than the optimum case where topology optimization is applied separately and better than the optimum case obtained from stiffener design optimization in Section 4.3. Combining results from topology optimization study with stiffener optimization seems to present advantage compared to individual application of stiffener design optimization approach In addition to that the values of $(\boldsymbol{Y_{max} - Y_{min}})$ for random vibration inputs in *x* and *z*-direction are also decreased by 83% and 95%, respectively compared with the values obtained for the original radar antenna.

Table 4.13 Random vibration analysis results for stiffened radar antenna structure ("Topo_Stiff_T") (deformation in *y*-direction).

	Random Vibration Input in *x*-Direction	**Random Vibration Input in *y*-Direction**	**Random Vibration Input in *z*-Direction**
$\boldsymbol{Y_{max}}$ **(m)**	$1.22 \cdot 10^{-5}$	$1.06 \cdot 10^{-4}$	$4.78 \cdot 10^{-5}$
$\boldsymbol{Y_{min}}$ **(m)**	$6.93 \cdot 10^{-7}$	$1.33 \cdot 10^{-5}$	$6.05 \cdot 10^{-6}$
$\boldsymbol{Y_{max} - Y_{min}}$ **(m)**	$1.15 \cdot 10^{-5}$	$9.23 \cdot 10^{-5}$	$4.18 \cdot 10^{-5}$
Improvement (%)	83	91	95

CHAPTER 5

DISCUSSION AND CONCLUSION

5.1 OVERVIEW OF RESULTS

Dynamic characteristics of a particular radar antenna structure and vibration effects on its performance are investigated in this thesis. In order to understand the dynamic characteristic of the radar antenna system, a finite element model is constructed in ANSYS and analytical solution of natural frequencies of a simply supported plate is used to validate the mesh size and element type used in the model. Modal characteristics of specified radar antenna structure and phased array antenna elements can be found by using this finite element model. Moreover, by using this model, vibration response of the antenna elements can be found for a given power spectral density specified for the input.

In this thesis, the radar antenna structure is assumed to be externally installed onto Apache AH-64 helicopter platform. First of all, modal characteristics of the radar antenna are studied by using the finite element model. For the finite element model of the radar antenna structure which is mainly composed of plate-like structures, SOLID95 elements are used. As a boundary condition, all degrees of freedoms of shaft connection surface are fixed. Natural frequencies and corresponding mode shapes of the original radar antenna are found for the frequency range of 0-500 Hz which is specified in MIL-STD-810G for AH-64 helicopter platform. There exists 10 natural frequencies between 0-500 Hz and the first two natural frequencies (14.7 Hz and 16.2 Hz) of the radar antenna structure are in the dominant sinusoid frequency range of the platform. Therefore they can be considered as critical.

Bending vibrations of phased array antenna elements in direction normal to the green surface in Figure 3.27 cause serious problems for antenna performance. To control the deformation of antenna elements, factor ***k*** is determined which is as a measure of how much deformation of antenna elements in *y*-direction is contributing to the corresponding mode shape. Although the maximum value of ***k,*** which is equal to 1.54**,** is observed for the 6^{th} mode shape of the original radar antenna structure, 6^{th} natural frequency (300.4Hz) is not considered as critical since it is far away from dominant sinusoid excitation range of the helicopter platform (0-60 Hz).

Moreover broadband random vibration response for base excitation coming from the helicopter platform to the radar antenna should also be checked as an ultimate evaluation of the performance of the modified design. For this purpose, random vibration analyses are performed in ANSYS for vibration exposures of AH-64 helicopter vibration given in MIL-STD-810G.

An intuitive reinforcement design is constructed to improve the vibration characteristics of the original radar antenna system and the modal and dynamic behaviors of this configuration are studied and discussed in Chapter 3.

To compensate the adverse effects of mechanical vibrations caused by helicopter platform optimization studies are performed and the results are given in Chapter 4. Topology and design optimization techniques are used to maximize the critical natural frequencies and fine tune the modal deformation of antenna elements. Feasible design regions used in optimization processes is determined according to the locations where maximum total modal mechanical strain of the pre-determined critical mode shapes (1^{st} and 2^{nd}) of the original radar antenna occur.

Topology optimization (Case-1) is used to find the best material distribution for the determined design space. The optimum material distribution of a certain design space is found after topology optimization is carried out systematically. While searching the best use of added material, it is realized that a reinforced radar antenna structure ("Topo_DS1 %75") has the same added weight as the intuitively reinforced antenna while "Topo_DS1 %75" configuration gives better results

compared with the intuitive design. The first natural frequency is 40.1 Hz for "Topo_DS1 %75" configuration however it is 33.5 Hz for intuitive design.

After optimum reinforcement plate configuration"Topo_DS4 %30" is obtained from several topology optimizations, a design optimization is performed on this reinforced structure. Here design parameters are the thickness values of reinforcement plates and the design constraint is the maximum weight of the system. The dynamic characteristics of reinforced radar antenna structure obtained from the second step of design optimization is much more better than the original radar antenna such that the first two natural frequencies are shifted out of the dominant sinusoid frequency range (0-60 Hz) and there is no factor k having high values compared to the original radar antenna design.

In stiffener design optimization studies (Case-2) four different types of stiffeners are used to maximize the first natural frequency of the antenna. The details of configuration and orientation of stiffeners are given in Section 4.3. The design variables of stiffeners are optimized so that the maximum allowable weight of the system is not exceeded (20 kg). The optimum configuration is obtained for "DS2_C".

Topology and stiffener design optimization is also used simultaneously (Case-3) to find a better result than Case-1 and Case-2. Stiffener design optimization is performed along with reinforcement plate configuration "Topo_DS3 %50". Optimum solution is obtained for "Topo_Stiff_T" configuration

An overview of the best results for each optimization case held in Chapter 4 can be seen in Tables 5.1 through Table 5.3 and Figures 5.1 and 5.2. It is seen from Table 5.1 and Figure 5.1 that the maximum of the first natural frequency is obtained from optimum solution for Case-1. Beside that the use of stiffener design optimization along with topology optimization result (Case-3) gives better solution for maximizing the critical natural frequencies than Case-2. According to Table 5.2 and Figure 5.2, calculated $\boldsymbol{k}$ value is considerably high for all radar antenna structures except Case-1. The bending vibration of antenna elements in direction normal to the green surface (Figure 3.27) is fine tuned for reinforced antenna

structure obtained form Case-1.

In Table 5.3 random vibration results of optimum radar antenna design for each case of the optimization studies and improvements compared with the original radar antenna are given. It can be concluded that optimum configuration for Case-1 has the lowest value of $(\boldsymbol{Y_{max} - Y_{min}})$ among other radar antenna configurations and the value of $(\boldsymbol{Y_{max} - Y_{min}})$ of original radar antenna is decreased by 92% for the best design of Case-1. In addition to that the values of $(\boldsymbol{Y_{max} - Y_{min}})$ are also decreased for other configurations compared with the values obtained for the original radar antenna as it is seen from Table 5.3. The maximum percentage of improvement in the value of $(\boldsymbol{Y_{max} - Y_{min}})$ is obtained for the best design of Case-1, but it should be noted that the percentage improvement for Case-3 (91%) is also close to the percentage improvement of Case-1 (92%). However, it should be noted that the objective function does not consider the response due to random excitation, if included into the objective function which might result in a higher improvement. On the other hand it can be concluded that the random vibration results of Case-3 are more fine than Case-2 also Case-3 gives better solution for maximizing the critical natural frequencies than Case-2.

Table 5.1 Natural frequencies of optimum configurations of radar antenna structures. (Hz)

	Original Radar Antenna	**Intuitive Radar Antenna**	**Case-1 (Best Design)**	**Case-2 (Best Design)**	**Case-3 (Best Design)**
1st Nat. Freq	14.7	33.5	146.7	117	139.6
2nd Nat. Freq	16.2	49	161.5	130.7	146.5
3rd Nat. Freq	96.5	147.2	172	147.6	158.5
4th Nat. Freq	148.1	288.2	296.4	296.2	296.6
5th Nat. Freq	296.6	303.3	322.7	322.5	322.6
6th Nat. Freq	300.4	321	328.1	324.1	324.9
7th Nat. Freq	320	322.6	374	338	373.5
8th Nat. Freq	322.5	350	408.3	373.7	408.6
9th Nat. Freq	372.8	373.2	>500	408.7	422.3
10th Nat. Freq	409	409	>500	>500	>500

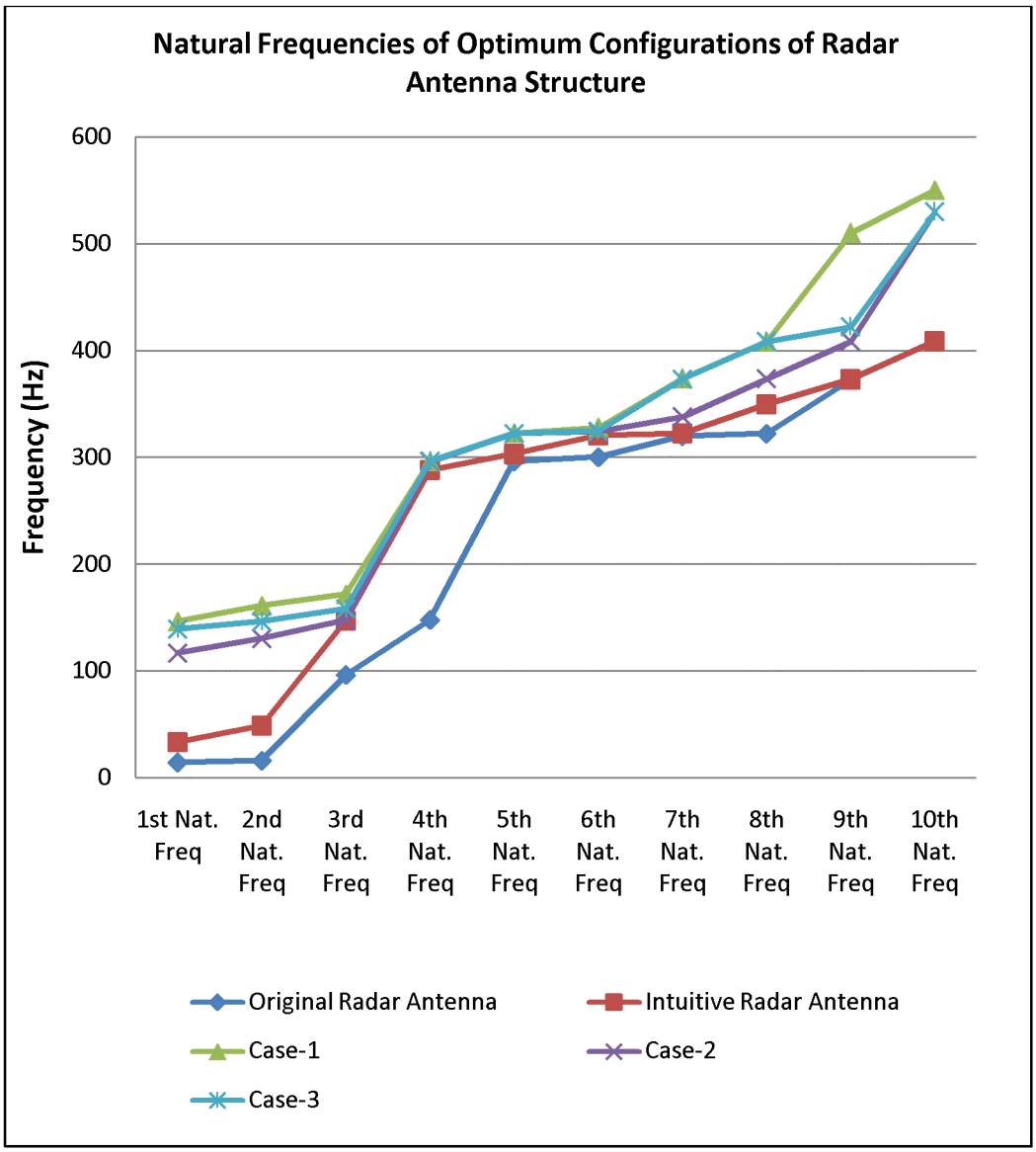

Figure 5.1 Natural frequencies of optimum configurations of radar antenna structure.

Table 5.2 Calculated k values for optimum configurations of radar antenna structure.

	Original Radar Antenna	**Intuitive Radar Antenna**	**Case-1 (Best Design)**	**Case-2 (Best Design)**	**Case-3 (Best Design)**
1st Mode Shape	0.014	0.483	0.006	0.044	0.079
2nd Mode Shape	0.500	0.078	0.169	0.273	0.010
3rd Mode Shape	0.266	0.003	0.351	0.008	0.185
4th Mode Shape	0.002	0.029	0.001	0.002	0.001
5th Mode Shape	0.022	0.027	0.013	0.041	0.014
6th Mode Shape	1.540	0.258	0.002	0.074	0.009
7th Mode Shape	0.065	0.016	0.002	1.702	0.010
8th Mode Shape	0.015	1.752	0.007	0.018	0.036
9th Mode Shape	0.011	0.028	-	0.005	1.763
10th Mode Shape	0.002	0.003	-	-	-

Table 5.3 Random vibration results of optimum configurations in y-direction.

	Original Radar Antenna	**Intuitive Radar Antenna**	**Case-1**	**Case-2**	**Case-3**
$Y_{max} - Y_{min}$ **(m)**	$1.04 \cdot 10^{-3}$	$3.71 \cdot 10^{-4}$	$8.25 \cdot 10^{-5}$	$1.32 \cdot 10^{-4}$	$9.23 \cdot 10^{-5}$
Improvement (%)	-	64	92	87	91

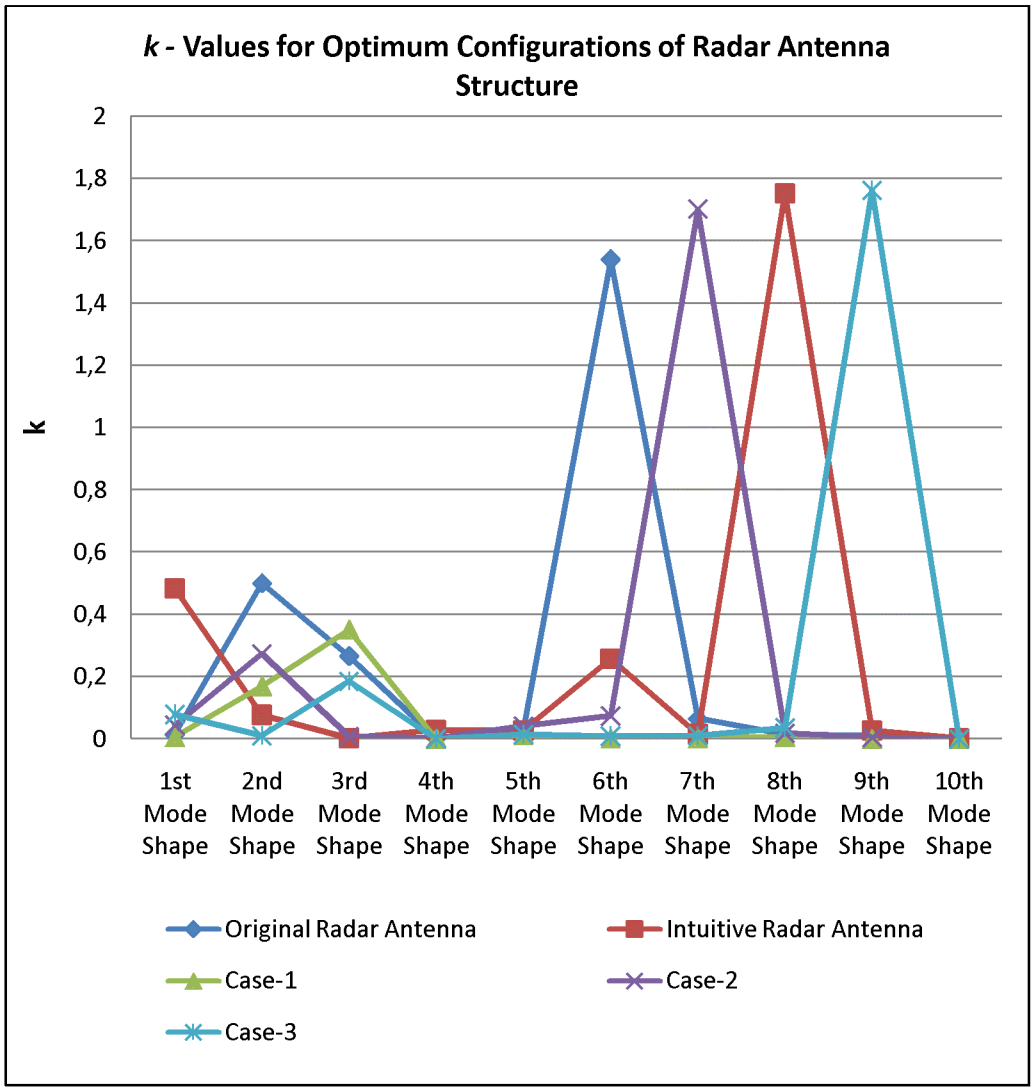

Figure 5.2 Calculated ***k*** values for optimum configurations of radar antenna structures.

5.2 CONCLUSION

The optimization techniques used in this study has been found to improve the vibration characteristics of the radar antenna structure which is externally installed onto the AH-64 (Late) helicopter platform. The critical first two natural frequencies of the original radar antenna structure are shifted out of the dominant sinusoid frequency range (0-60 Hz) of the platform and in this study it is pointed out that topology and stiffener design optimization techniques have great potential to shift out the critical natural frequencies out of frequency range of interest (0-500 Hz). However this cannot be achieved in this study because of the constraint on total added mass. However, if there is flexibility for total weight of the radar antenna or material type used for design space in topology optimization, the critical natural frequencies are likely to be shifted out of the frequency range of 0-500 Hz.

5.3 RECOMMENDATION FOR FUTURE STUDIES

It is good engineering practice for finite element analyses to be verified by experiments, which are performed on prototypes of the analysis model. Although a fine mesh size is used for the finite element model of the radar antenna studied in this thesis, this does not guarantee that the analysis results are accurate enough. Every analysis performed in this study should be verified by performing proper experimental procedures and measurements on a physical model of the specified model. Because of the time limitations, experimental verification of the results obtained in this study are left as a future study.

In addition to topology and stiffener design optimization techniques it is possible to use viscoelastic material based vibration damping systems in order to fine tune the vibration response of the antenna under operation conditions. Also honeycomb panels can be used instead of sheet metal panels to increase the structural stiffness of the radar with lesser mass addition.

REFERENCES

[1] Radar Basics, http://radartutorial.eu/, last visited on 20th of July 2010.

[2] Adamy, D., *EW101 - A First Course in Electronic Warfare*, Artech House, 2000.

[3] Detlef Brumbi, *Fundamentals of Radar Technology for Level Gauging, 4th Ed.,* Krohne Messtechnik GmbH & Co. KG, 2003

[4] Bhavsar, V., Blas, N., Nguyen, H., and Balandin, A., *EE117 Laboratory Manual*, UC-Riverside, 2000

[5] Mailloux, R.J., *Phased Array Antenna* Handbook,2nd Ed., Artech House, Norwood (MA), 2005

[6] Knott, P., *Deformation and Vibration of Conformal Antenna Arrays and Compensation Techniques*, Multifunctional Structures / Integration of Sensors and Antennas, France, 2006

[7] Schippers, H., van Tongeren J.H., Knott, P., Deloues, T., and Lacomme, P., Scherbarth, M.R., *Vibrating antennas and compensation techniques,* Research in NATO/RTO/SET 087/RTG50, 2006

[8] Tang, C.H., *Effects of Phased Array Structure Deformation and Element Outlage,* The Mitre Corporation, Bedford (MA), 1992

[9] Rüegg, M., Meier, E., and Nüesch, D., *Vibration and Rotation in Millimeter-Wave SAR,* Ieee Transactions On Geoscience And Remote Sensing, 2007

[10] Yao, W., and Wang, Y.E., *Beamforming for Phased Arrays on Vibrating Apertures,* Ieee Transactions On Antennas And Propagation, 2006

[11] Lo, Y.T., and Lee, S.W., *Antenna Handbook Vol 2: Antenna Theory*, Van Nostrand Reinhold, New York, 1993

[12] Pozar, D.M., and Schaubert, D.H., *Scan Blindness in Infinite Phased Arrayosf Printed Dipoles,* Ieee Transactions On Antennas And Propagation, 1984

[13] Milligan, T.A., *Modern Antenna Design, 2nd Ed.,* John Wiley & Sons, Inc. Publication, Canada, 2005

[14] Zhang, L., Castaneda, J.A., and Alexopoulos, N.G., *Scan Blindness Free Phased Array Design Using PBG Materials,* Ieee Transactions On Antennas And Propagation,2004

[15] Hamid Moghadas, H., Tavakoli, A., and Salehi, M., *Elimination of scan blindness in microstrip scanning array antennas using defected ground structure*, International journal of Elctronics and communications, 2007

[16] Department of Defense Test Method Standard for Environmental Engineering Considerations and Laboratory Tests, *MIL-STD-810G*, Department of Defense, USA, 2008.

[17] Nocedal, J., and Wright, S.J., *Numerical Optimization, 2nd Ed.,* Springer, USA, 2006.

[18] Rao, S.S, *Engineering Optimization Theory and Practice, 4th Ed.,* John Wiley & Sons, Inc. Publication, Canada, 2009

[19] Arora, J.S., *Optimization of Structural and Mechanical Systems,* World Scientific Publishing, Singapore, 2007

[20] Bendsøe, M.P., and Sigmund, O., *Topology Optimization : Theory, Methods and Applications*, Springer, 2004

[21] Saleem, W., Yuqing, F., and Yunqiao, W., *Application of Topology Optimization and Manufacturing Simulations - A new trend in design of Aircraft*

components, Proceedings of the International MultiConference of Engineers and Computer Scientists, 2008

[22] Kuntjoro, W., and Mahmud, J.,*Truss Structural Configuration Optimization Using The Linear Extended Interior Penalty Function Method*, Austral. Mathematical Soc., 2006

[23] Manual ANSYS, *Documentation for ANSYS*, ANSYS Inc., 2007

[24] R. Szilard, *Theories and Applications of Plate Analysis: Classical, Numerical and Engineering Methods*, John Wiley & Sons, Inc., 2004

[25] A. Joon-Ho Lee, B. Youn-Sik Park and C. Youngjin Park, *Stiffener layout optimization to maximize natural frequencies of a structure: application to HDD cover structure*, Structural Dynamics and Applied Control Laboratory, Department of Mechanical Engineering, KAIST

[26] A. Mejdi and N. Atalla, *Dynamic and acoustic response of bidirectionally stiffened plates with eccentric stiffeners subject to airborne and structure-borne excitations,* Journal of Sound and Vibration, 329 (2010), pp.4422–4439

[27] D.S. Yantek and S. Catlin, Evaluation of stiffeners for reducing noise from horizontal vibrating screen, NIOSHTIC-2 No. 20036771

[28] B. Sivasubramonian, G. V. Rao and A. Krishnan, Free Vibration of Longitudinally Stiffened Curved Panels With Cutout, Journal of Sound and vibration (1999) 226(1), pp.41-55

[29] W. Akla, A. El-Sabbagha and A. Baz, Optimization of the static and dynamic characteristics of plates with isogrid stiffeners, Finite Elements in Analysis and Design, 44 (2008), pp.513 – 523

[30] Katsumi Inoue, Masashi Yamanaka and Masahiko Kihara, Optimum Stiffener Layout for the Reduction of Vibration and Noise of Gearbox Housing, Journal of Mechanical Design,2002, Vol. 124 / 523

[31] T.R.Lin, P.O'shea, and C.Mechefske, Reducing MRI Gradient Coil Vibration with Rib Stiffeners, Concepts in Magnetic Resonance Part B (Magnetic Resonance Engineering), Vol. 35B(4), pp.198–209 (2009)

[32] O.J.O'Leary, F.W.Williams and D.Kennedy, Optimum stiffened panel design with fundamental frequency constraint, Thin-Walled Structures 39 (2001) 555–569

[33] E. Ventsel and T. Krauthammer, The Plates and Shells: Theory, Analysis and Applications, CRC Press, 1st Ed.

[34] S.Timoshenko and S.Woinowsky-Krieger, Theory of Plates and Shells, McGraw-Hill Inc, 2nd Ed.,1959

[35] F.Nicolas and S.Cervigon, Design Methodology For CRC Stiffeners Under Compression And Fuel Pressure Loads, Proceedings of ICCM-10, Whisler, B.C., Canada,1995

[36] A.Samanta and M.Mukhopadhyay, Free vibration analysis of stiffened shells by the finite element technique, European Journal of Mechanics A/Solids 23 (2004), pp.159–179

[37] B.Gangadhara Prusty, Free vibration and buckling response of hat-stiffened composite panels under general loading, International Journal of Mechanical Sciences, 50(2008), pp.1326-1333

[38] G.Qing, J.Qiu and Y.Liu, Free vibration analysis of stiffened laminated plates, International Journal of Solids and Structures, 43 (2006), pp.1357–1371

[39] K.Ghavamia and M.R.Khedmati, Numerical and experimental investigations on the compression behaviour of stiffened plates, Journal of Constructional Steel Research, 62 (2006), pp.1087–1100

[40] G.Chiandussi, I.Gaviglio and A.Ibba, *Topology optimisation of an automotive component without final volume constraint specification*, Advances in Engineering Software, 35 (2004), pp.609–617

[41] S.Kumar, *Optimization of BIW, Chasis and Casting at Mahindra&Mahindra*, Altair CAE Users Conference 2005

[42] A.Manekshaw and A,Jassal, *Optimization of Air-Conditioner Copper Tube Layout for Frequency Response*, Hypermesh Technology Conference (HTC) 2008

[43] A. Joon-Ho Lee, B. Youn-Sik Park and C. Youngjin Park, *Stiffener layout optimization to maximize natural frequencies of a structure: application to HDD cover structure*, Structural Dynamics and Applied Control Laboratory, KAIST.

[44] D.S.Yantek and S.Catlin, *Evaluation of stiffeners for reducing noise from horizontal vibrating screens,* NIOSHTIC-2, No. 20036771

[45] AH-64 Apache, http://en.wikipedia.org/wiki/Boeing_AH-64_Apache, last visited on 5th of February 2011

[46] T90 Main Battle Tank, http://www.fprado.com/armorsite/T-90S.htm, last visited on 5th of February 2011

[47] Maks 2005 Helicopters, http://www.richard-seaman.com/Aircraft/AirShows/ Maks2005/ Helicopters/index.html, last visited on 5th of February 2011

[48] Federation of American Scientists, http://www.fas.org/programs/ssp/ man/uswpns/air/attack/ah64_apache.html, last visited on 5th of February 2011